Exploring Opportunities for Ionic Liquid Capillary Columns in Petroleum Analysis

by

Brandon Michelle Weber

A thesis submitted in partial fulfillment of the requirements for the degree of

Doctor of Philosophy

Department of Chemistry

University of Alberta

ABSTRACT

Petroleum samples consist of hundreds to thousands of components and require well-designed experiments to accurately determine quality and composition. The challenges with petroleum samples in this thesis are three-fold, focusing on: alkyl phosphate contamination, group-type composition, and biodiesel content. Alkyl phosphates in petroleum samples are of great interest to refineries that process oil produced from the Western Canadian Sedimentary Basin or other water-sensitive geologies. This interest is due to the presence of residual phosphates from oil-based fracturing fluids causing premature fouling of equipment and poisoning of catalysts, leading to frequent maintenance outages.

Group-type composition is of particular importance due to the correlation with emission and performance properties for fuel. ASTM D5186 has previously been used for this purpose, and relies on supercritical fluid chromatography. Unfortunately, this instrumentation is difficult to access and is not able to perform adequate separations on samples containing biodiesel.

Our third challenge is one facing industry and consumers who operate in cold climates. Government regulations frequently mandate that industry use biodiesel in their operations to lessen the reliance on fossil fuels and decrease emissions of carbon dioxide [1]. Therefore, closer

regulation of biodiesel is possible with accurate determination of biodiesel content.

Ionic liquid capillary columns for gas chromatography provide great potential for a number of applications, due to their unique and tunable properties. They provide complex retention mechanisms that depend on multiple types of intermolecular forces, leading to unique retention properties. This thesis explores the application of ionic liquid capillary columns to these separations challenges. Retention behaviours of alkyl phosphates were studied on a number of ionic liquid gas chromatography columns. The selectivity for alkyl phosphates on ionic liquid columns were compared with selectivity on a 5% phenyl column to evaluate the potential of ionic liquids for separation of alkyl phosphates in petroleum samples. Most interestingly, separation temperature was shown to affect the elution order of a homologous series. Thermodynamic modeling was then used to predict the retention times for a series of alkyl phosphates in first- and second-dimensions. Ionic liquid columns perform best in the primary dimension for alkyl phosphates. Unknown phosphate retention coordinates were also predicted, based on the thermodynamic parameters determined by a set of standard alkyl phosphates. However, retention times of alkyl phosphates on some ionic liquid columns were unstable, due to suspected reactions between the column and analyte.

Ionic liquid columns were then compared for their ability to perform a diesel-range group-type separation providing relative abundances of saturates, mono-, di-, and polyaromatics by gas chromatography. The SLBIL-111 column provides the best resolution for the group-types of interest based on 10 model compounds. Selective detection via vacuum ultraviolet detection (VUV) was necessary for determination of saturates and monoaromatics. The optimized gas chromatography method coupled to a VUV to measure group-type composition of 10 oil sand-derived Synfuel light diesel samples, three Syncrude light gas oils, and one quality control sample. The Synfuel results using both the conventional supercritical fluid chromatography method and the new VUV method had good agreement, with an absolute error of 0.8%. The quality control sample also performed well when comparing both methods (absolute % error of 0.2) and the results agreed within error for saturate, mono- and polyaromatics.

Lastly, percent biodiesel content in diesel samples was determined using the method optimized for group-type separation. This is necessary as both biodiesel content and group-type composition results need to be collected simultaneously. Using the VUV method it was possible to determine the % biodiesel content with 0.9% error, while still maintaining our original group-type results within an error of 0.6%.

Overall, this work presents a significant step towards a method for identifying alkyl phosphates in petroleum samples. While also presenting a few of the possible challenges in using ionic liquid columns for some compounds (such as phosphates). In addition, this thesis presents a viable new method for replacement of ASTM D5186, while adding in the ability to also determine biodiesel content. This will be important to companies across North America where government regulations require specific aromatic content, as well as regulated biodiesel percentages.

PREFACE

Portions of **CHAPTER 1** and a version of **CHAPTER 2** have been published as B.M. Weber, J.J. Harynuk, "Gas chromatographic retention of alkyl phosphates on ionic liquid stationary phases", *J. Chromatogr. A* 1217 (2013) 4862. I was responsible for the operation and maintenance of the instrumentation, the data collection and analysis, as well as the manuscript composition and edits. J.J. Harynuk was the supervisory author and was involved with concept formation and manuscript composition and edits.

Portions of **CHAPTER 1** and a version of **CHAPTER 3** have been published as B.M. Weber, J.J. Harynuk, "Application of thermodynamic-based retention time prediction to ionic liquid stationary phases", *J Sep. Sci.* 37 (2014) 1460. I was responsible for the operation and maintenance of the instrumentation, the data collection and analysis, as well as the manuscript composition and edits. J.J. Harynuk was the supervisory author and helped to conceptualize the project and contributed to manuscript composition edits.

Portions of **CHAPTER 1**, **CHAPTER 4 and CHAPTER 5** have been submitted to *Analytical Chemistry* as B.M. Weber, J.J. Harynuk, "Determination of Hydrocarbon Group-Type of Diesel Fuels by Gas Chromatography with Vacuum Ultraviolet Detection". I was responsible for the operation and maintenance of the instrumentation, the data collection and analysis, as well as the manuscript composition and edits. J.J. Harynuk was the supervisory author and helped to conceptualize the project and contributed to manuscript composition edits.

“You can never be overdressed or overeducated.”

- Oscar Wilde

AKNOWLEDGEMENTS

I would like to thank my supervisor, Dr. James Harynuk, for his guidance and support throughout my degree. I am grateful for all of the conference and travel opportunities, which allowed me to travel the world and pursue my research at the same time. I would also like to thank Dr. Richard Paproski and Brenda Crickmore for their advice and support. Thank you to my committee, for your time and input into this thesis: Dr. Alex Brown, Dr. Mark McDermott, Dr. Kevin Schug, Dr. Charles Lucy and Dr. James Kariuki.

My deepest gratitude goes to my family for all the love and support they have provided during my degree. First and foremost to my wonderful husband Justin, who has celebrated my successes and loved me through all the trials and tribulations that grad school brings. To our amazing son Hudson, who has given me unconditional love and filled this journey with much needed laughter. To my parents who have supported me through every journey in my life, encouraged me and pushed me to be the best that I can be. Without all of you my life would not be so rich, or nearly as enjoyable. And of course to the incredible women who have shared this journey with me; Brianne, Nicole, Paulina, Katie and Tran Tran, you have been an incredible support system, providing endless conversation and lots of laughter.

This thesis was supported by the University of Alberta, the Natural Sciences and Engineering Council of Canada and Syncrude Canada Ltd.

Table of Contents

List of Abbreviations

2D	Two-Dimensional
AED	Atomic Emission Detector
ASTM	American Society for Testing Materials
BTEX	Benzene, Toluene, Xylene
CAPP	Canadian Association of Petroleum Producers
CCD	Charge Coupled Device
CCQTA	Canadian Crude Quality Technical Association
CFT	Capillary Flow Technology
FAEE	Fatty Acid Ethyl Ester
FAME	Fatty Acid Methyl Ester
FID	Flame Ionization Detector
GC	Gas Chromatography
HPLC	High Performance Liquid Chromatography
IL	Ionic Liquid
LMCS	Longitudinally Modulated Cryogenic System
MS	Mass Spectrometry
NMR	Nuclear Magnetic Resonance
PAH	Polyaromatic Hydrocarbon
qMS	Quadropole Mass Spectrometry
RTIL	Room Temperature Ionic Liquid

SCD	Sulphur Chemiluminescence Detector
SFC	Supercritical Fluid Chromatography
T5P	Tripentyl Phosphate
TBP	Tributyl Phosphate
TEP	Triethyl Phosphate
THP	Trihexyl Phosphate
TIP	Triisopropyl Phosphate
TMS	Trimethyl Silane
TOF-MS	Time of Flight-Mass Spectrometer
TOP	Trioctyl Phosphate
TPP	Tripropyl Phosphate
UV	Ultra Violet
VUV	Vacuum Ultraviolet
WCOT	Wall-coated Open Tubular Column
WCSB	Western Canadian Sedimentary Basin
μ-ECD	micro Electron Capture Detector

List of Symbols

A	Absorbance
AB	Biodiesel Area
AD	Diaromatic Area
ADB	Biodiesel and Diaromatic Area
AM	Monoaromatic Area
AMN	Monoaromatic and Saturate Area
AN	Saturate Area
AP	Polyaromatic Area
b	Path Length
C	Concentration
d	Diameter
d_f	Film Thickness
GC×GC	Comprehensive Two-Dimensional Gas Chromatography
K	Partition Coefficient
k	Retention Factor
L	Length
M	Mobile Phase
N	Plate Number (Efficiency)
n	Peak Capacity
n	Number of Replicates
η	Viscosity

P	Pressure
P_m	Modulation Period
R_s	Resolution
R	Gas Constant
R^2	Regression Coefficient
r_c	Radius of Column
RRf	Relative Response Factor
S	Stationary Phase
s	Standard Deviation
T	Temperature
t_m	Dead Time
t_r	Retention Time
u	Velocity
V	Volume
w_b	Baseline Peak Width
α	Selectivity Factor
β	Phase Ratio
ΔC_p	Isobaric Molar Heat Capacity
ΔH	Change in Enthalpy
ΔS	Change in Entropy
Δx	Distance
ε	Molar Absorptivity

List of Figures

List of Tables

CHAPTER ONE: Introduction

1.1 Motivation and Thesis Overview

Fossil fuels and petroleum products are the most important source of energy for today's society, providing the bulk of our global energy requirements for commercial transportation (trucking, rail, and aviation), construction, and agriculture. Crude oils (conventional or unconventional) are complex mixtures of mostly hydrocarbon-type constituents, which have a wide variety of properties. Therefore, crude oils must be carefully refined into useable products with specific quality requirements before commercial or industrial use. This thesis focuses on three specific issues that are current problems for the petroleum industry: phosphate contamination, group-type composition (saturates, mono-, di-, tri- and polycyclic aromatic compounds), and the biodiesel content of diesel blends.

The first main focus, phosphate contamination, is investigated because some of the contaminants present in crude oil come from the extraction process, and may also be formed in refining processes. In conventional oil extraction, hydraulic fracturing is commonly used to aid in the extraction of oil from reservoirs [2]. Although the mechanism is unclear, in this process the final product may be contaminated by the gellants used in the fracturing process. Despite constituting a very small percentage of the bulk content, alkyl phosphates present in a refinery environment can wreak havoc. Alkyl phosphates present in the crude oil

cause a host of problems, including refinery fouling incidents which lead to costly unplanned maintenance shutdowns [3,4]. The majority of phosphates that appear in industrial samples have retention times that do not match available standards, requiring structural determination by a new method as a first step to mitigation of this contamination issue.

Our second focus is the group-type composition of fuels, as their composition strongly impacts their performance (i.e. cetane number, pour point, smoke point, heat content) and environmental properties (i.e. particulate matter, polycyclic aromatic hydrocarbon (PAH), nitrogen oxides, carbon monoxide) [5-13]. Properties such as cetane number and exhaust emissions are linked to the total aromatic and polycyclic aromatic content of the fuel. Specifically, PAH content in diesel fuels increases particulate matter, PAH and nitrogen oxide emissions. Thus the measurement and characterization of aromatic content is necessary for quality control of diesel and to meet regulatory limits.

Our third area focuses on biodiesel, as biodiesels are increasingly important biologically derived sources of fuel that may be used on their own or blended with conventional petroleum diesel fuels. The blend of fatty acid methyl and ethyl esters (FAMEs/FAEEs) in biodiesel are produced by the trans esterification of tri-glycosides derived from biological sources [14]. In 2011, the Canadian Government introduced a

requirement to add 2% biodiesel to diesel fuels which motivates the development of a method to determine biodiesel content in diesel samples.

Petroleum samples are commonly analyzed using chromatography [15]. It involves the separation of the sample into its different components. For this work two different aims of separation are needed: it is desirable to separate the alkyl phosphate compounds from the rest of the sample and to separate the sample into different group types according to the number of aromatic rings. Once the compounds are separated, a detector is used to determine the relative amount of each in the sample, and then quantify each group or individual compound. Gas chromatography (GC) is a popular and long standing choice for the analysis of petroleum and fuel samples. Group-type separation of petroleum samples are also commonly analyzed using supercritical fluid chromatography (SFC) or high performance liquid chromatography (HPLC). A problem with SFC and HPLC methods is that insufficient resolution between the group-types in high boiling samples is often observed. This makes determination of group-types difficult, which negatively affects the quantitative results [16].

This thesis explores gas chromatographic methods for the study of alkyl phosphates, aromatic and biodiesel content in petroleum samples. Therefore, the overarching goal of this research is to develop unique gas chromatographic methods for petroleum separations. This work will be divided into two main sections; the first aimed to identify alkyl phosphates

through the study of the relationship between molecular structure and GC retention and the second was to develop a GC method capable of determining aromatic and biodiesel content in diesel-range fuels. In Chapter 2, the gas chromatographic retention of alkyl phosphates was studied on various ionic liquid stationary phases. In Chapter 3, retention times of alkyl phosphates are predicted in two-dimensional gas chromatography on ionic liquid stationary phases. In Chapter 4, a number of ionic liquid columns are tested for the separation of diesel samples, as well this chapter explores the use of a unique GC-UV-flame ionization detector system for determination of group-type composition. Chapter 5 employs a GC-vacuum UV system for analysis of diesel and biodiesel samples. Chapter 6 includes the conclusions of this thesis, as well as the future research for these topics.

1.2 Petroleum Analysis

Oil production requires the extraction of oil from underground reservoirs, which must then be processed in refineries for production of various petroleum products. These petroleum products contain an enormous amount of individual components. Interestingly, this vast number of compounds belongs to relatively few chemical classes [17]. Therefore, the overwhelming number of compounds present in petroleum samples leads to extremely complex analytical separations. There are two

main approaches to dealing with this problem in petroleum analysis; target molecule analysis and group-type separations.

Quantifying specific molecules can be extremely important, but very challenging. This leads us to the first focus of this thesis, speciation of alkyl phosphate contaminants in petroleum samples. Phosphate compounds may be introduced into crude oil samples through their use in aiding hydraulic well fracturing procedures. The presence of these compounds results in poisoning of catalysts, damage to distillation towers, and potential contamination of final products [18].

Group-type separations are also essential for petroleum analysis. The goal of these analyses is to separate specific groups of compounds rather than isolate specific components. Group-type separations are important for monitoring compositional changes of petroleum samples over time. This could be over a short period (i.e. minutes or hours) for conversion of feeds within a refinery or over a long period of time (i.e. years) to focus on changes of a product after it is released into the environment.

1.2.1 Alkyl Phosphates and Refinery Fouling

Alkyl phosphates may be introduced into petroleum samples in a variety of ways, from well fracturing additives to corrosion inhibitors. One of the most common techniques used to remove oil from the ground is

hydraulic fracturing. Hydraulic fracturing uses repetitive pumping of fracturing fluid into the well at pressures around 15,000 psi [19]. This produces a network of fractures through which the oil can be extracted. For this process to be effective the fluid must be viscous when injected, fluid when removed and compatible with the geology. To produce a fracture fluid with these qualities a gellant is added as a viscosity builder. Proppants are also added to the fluid to prevent the fractures from collapsing after the release of pressure [19]. Material such as glass beads, crushed walnuts [20] and a multitude of other material are employed as proppants to prop open the network of fractures without impeding the flow of oil.

The majority of gas and unconventional oil produced in Canada originates from the Western Canadian Sedimentary Basin (WCSB) as shown in Figure 1-1**.** The geology in the WCSB dictates the use of oil-based fracturing fluids, which typically employ phosphorus-based gellants. These phosphorus-based gellants are typically made up of alkyl phosphates, which work well in water-sensitive geologies [21]. To form the cross-linked gel hexa-coordinate metal cations (i.e. Fe^{3+}, Al^{3+}) are added along with dialkyl phosphates. A few mechanisms have been proposed for the self-assembly of these gels including a double-bridged polymer formation between the metal cations and the phosphate containing compound [22], as well as the formation of highly ordered cylindrical aggregates

[23,24,25]. After completion of the fracturing a decrease in the viscosity of the fracture fluid is required to easily remove the fluid from the well without disrupting the distribution of the proppant.

Figure 1-1. Western Canadian Sedimentary Basin (WCSB) as outlined in this map of Canada. Figure adapted from reference [26].

The gel's viscosity is greatly reduced through the addition of a breaker (i.e. water, alcohols, surfactants, or a change in pH [19]) that disrupts the self-assembly properties of the gel. Unfortunately, residues of the phosphorus-

based gellants that remain in crude oil have been implicated in fouling incidents in refineries.

Oil that is contaminated with phosphorus is pumped into refinery distillation towers. As the crude oil is fractioned off the distillation tower, trays become contaminated with a hard deposit formation compromising plant function. An example of these deposits can be seen in Figure 1-2**,** which has a clean tray depicted on the left and a fouled tray shown on the right [29].

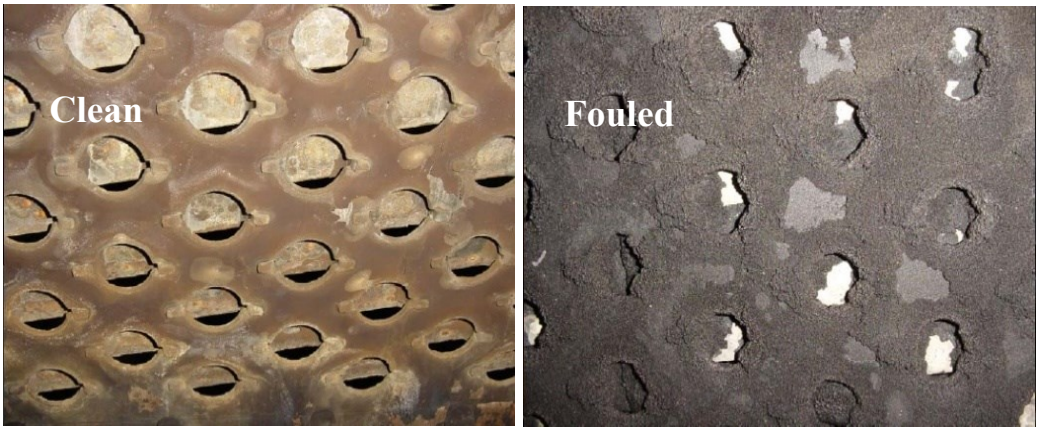

Figure 1-2. Photographs of distillation tower trays. Typical clean and operational (left) and fouled with a thick deposit (right) distillation tower trays [29].

Refineries are greatly affected by this type of fouling as it demands unscheduled plant shutdowns for cleaning, repairing or replacing affected equipment [27]. Elemental analysis of these deposits show 8-12%

phosphorus in the contaminants [28]. The remainder of the deposits consists of carbon, nitrogen, hydrogen, copper and nickel, which were anticipated, as they are either natural components of crude or added within the refinery process. The majority of the fouling occurs in equipment operating at temperatures around 400 °F (205 °C) [29], suggesting the presence of volatile phosphorus. Therefore, a solution to limit volatile phosphorus contamination is required. As a first step to mitigation of this problem it would be useful to know the composition of the deposits. A limit of 0.5 μg mL^{-1} total distillable phosphorus in feedstock [27,29] has been put in place by the Canadian Association of Petroleum Producers (CAPP) and the Canadian Crude Quality Technical Association (CCQTA). The current ICP-OES method of measuring the total volatile phosphorus concentration may not accurately represent the concentration of the relevant compounds. Speciation of the contaminating compounds could help to understand the chemistry of these compounds in a refinery environment, aiding in the effective management of the contamination.

1.2.1.1 Chemical Properties of Alkyl Phosphates

The general chemical structure of an alkyl phosphate consists of a phosphoric acid core where one or more of the hydroxyl protons have been replaced by alkyl chains, as depicted in Figure 1-3.

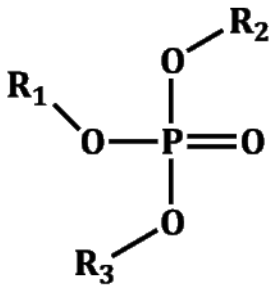

Figure 1-3. General chemical structure of an alkyl phosphate. R= hydrogen atom or alkyl chain, where at least one of R_1, R_2 and R_3 must be an alkyl chain.

If only one alkyl chain is present the structure is then referred to as a monoalkyl phosphate, while those containing two or three alkyl chains are known as di- and trialkyl phosphates, respectively. The volatility of these alkyl phosphates increases with the degree of alkylation (monoalkyl < dialkyl < trialkyl), and decreases with chain length. Dialkyl phosphates with chain lengths of approximately 2-30 carbons are typically employed in oil-based fracture fluids [30]. However, the gellants are produced as a technical mixture of mono-, di- and trialkyl phosphates, with dialkyl phosphates comprising approximately 80% of the mixture [19,31]. The compounds are formed by reaction of phosphorus pentoxide, phosphorus pentachloride or phosphorus oxychloride with selected alcohols, with the length of alcohol's alkyl chain determining the length of the alkyl phosphate chain, as well as whether it is a pure phosphate (all alkyl chains of the same length) or a mixed phosphate (differing alkyl chain lengths).

1.2.2 Group-Type Separations

Group-type separations are crucial for petroleum analysis. Group-type separations of fuels by chromatography aim to baseline separate each group-type from each other, rather than to separate individual compounds from each other. Such group-type separation allows for a more accurate determination of the distribution and type of hydrocarbon compounds present in a sample, rather than a more specific compound-wise approach. These studies can be completed over a range of time periods (i.e. minutes, days, or years), allowing for diverse analysis. As noted in Section 1.1, the distribution of saturates, mono-, di-, tri- and polyaromatic compounds influence fuel performance and emission properties [5-15]. In this thesis, the group-type resolution of particular chromatographic approaches will be assessed in Chapters 4 and 5 using model compounds representing each of these group-types.

Group-type separations of diesel samples are currently accomplished using SFC technology as outlined by ASTM [5]. Unfortunately SFC equipment that can perform this analysis properly is now very difficult to access. Very few suppliers offer SFC instrumentation with the required flame ionization detector (FID), and those SFC-FID instruments that are available suffer from poor reliability. Group-type separation of these types of samples utilizing GC separations often require two-dimensional (2D) separations or mass spectrometric detectors that give non-uniform

responses [32,16] making them less practical for routine analysis. Introduction of the Canadian requirement to add 2% biodiesel content to diesel fuel in 2011 has further complicated the SFC protocol as the biodiesel component does not readily elute from the SFC column. This problem has led to incorrect analytical results and fouling of the SFC column. For these reasons, this thesis pursued the use of ionic liquid stationary phases for hydrocarbon group-type separation, and additionally to determine the percent of biodiesel that has been added.

1.2.3 Biodiesel

Increasing energy demands necessitate the need for diverse fuel sources. Biodiesels are increasingly important biologically derived sources of fuel that may be used on their own or blended with conventional petroleum diesel fuels (petrodiesel). Renewable biological sources are used to produce biodiesel, which is a blend of fatty acid alkyl esters [33]. Biodiesel is produced by the trans-esterification of oils and fats as outlined in Figure 1-4, where a vegetable oil or animal fat is reacted with an alcohol (i.e. methanol, ethanol) in the presence of a catalyst to produce fatty acid alkyl esters (biodiesel) and glycerol [34]. The oil or fat can come from a number of sources such as: rapeseed, sunflower, coconut, peanut, and animal fats [35].

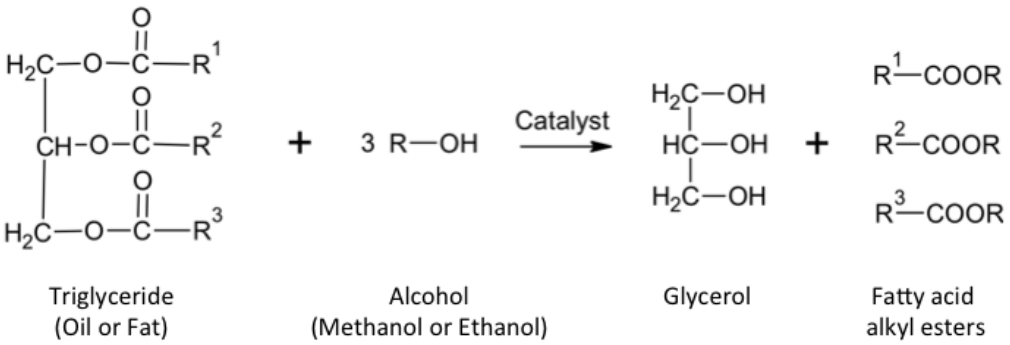

Figure 1-4. Production of biodiesel by trans-esterification.

The mixture of fatty acid alkyl esters that are produced are referred to as 100% biodiesel (B100). B100 biodiesel can then be blended with petrodiesel in varying proportions and are designated as BX fuels where X corresponds to the percentage of B100 added [36]. Biodiesel blends generate lower emission compared to petrodiesel [1], making them an attractive alternative. Canadian government regulations require 2% renewable diesel (i.e. biodiesel) content be blended [37]. Therefore, a technique that can determine BX content will be especially beneficial for customers making their own blends.

1.3 Chromatography

Chromatography is a broad term referring to the separation of samples into their various components. The first published use of chromatography was by Mikhail Tswett in 1903; his research employed liquid-adsorption chromatography for the separation of plant pigments

[38]. Martin and Synge won the Nobel Prize in 1952 for their development of partition chromatography [39], and separations have only advanced since then. Martin and James introduced gas-liquid partition chromatography in 1952 with the use of a gaseous mobile phase for the separation of volatile fatty acids, and GC was born [40]. GC has come a long way since this first separation, with the introduction of fused silica capillary columns in 1979 [41], all the way to current comprehensive two-dimensional chromatography [42].

1.3.1 Chromatography Theory

Chromatographic separations are based on the equilibrium of an analyte (A) between the stationary phase (S) and the mobile phase (M). This equilibrium is expressed as:

$$A_M \leftrightarrow A_S \qquad \textbf{(Equation 1-1)}$$

This equilibrium equation shows that as the equilibrium shifts to the right, the analyte is more strongly retained in the column. Therefore, as analytes are transported along the column they are separated based on their distribution between the stationary and mobile phase expressed by:

$$K = \frac{C_s}{C_M} \qquad \textbf{(Equation 1-2)}$$

where C_s and C_M are the concentration of the analyte in the stationary and mobile phases, respectively. A more convenient way of expressing the retention is to use the retention factor, k:

$$k = \frac{K}{\beta} \qquad \textbf{(Equation 1-3)}$$

where K is defined in Equation 1-2 and β is the phase ratio. The phase ratio is the ratio of the volume of the mobile phase to the volume of the stationary phase:

$$\beta = \frac{V_M}{V_S} \qquad \textbf{(Equation 1-4)}$$

where V_M and V_S are the volume in the mobile phase and the stationary phase respectively. It is however more convenient to define β in terms of column dimensions, where it is approximated as:

$$\beta \approx \frac{r_C}{2d_f} \qquad \textbf{(Equation 1-5)}$$

where r_c is the radius of the column and d_f is the film thickness. The benefit of using retention factor, k, is that retention may then be easily calculated by:

$$k = \frac{t_R - t_M}{t_M} \qquad \textbf{(Equation 1-6)}$$

where t_R is the retention time of the analyte and t_M is the time it takes an unretained compound to elute from the column (dead time). Hence, if two or more compounds are introduced onto the column at the same time, but under the conditions of the experiment they have different k values, they will be

separated on the column and may be detected individually. The distribution coefficient, *K*, is temperature dependent, where *K* becomes smaller at high temperatures, meaning the analyte is less retained. Careful selection of oven temperature throughout the run can greatly affect the separation of compounds, and most chromatographers routinely use temperature programming. In a temperature-programmed experiment the temperature increases during the run, meaning that *K* for the later eluting compounds begins to decrease until these compounds are eluted from the column. In this way temperature programming facilitates the timely separation of compounds within a sample having a wide range of retention factors.

To determine how well separated two compounds may be, selectivity is calculated. The selectivity factor quantifies the difference in retention between two compounds, α:

$$\alpha_{i,j} = \frac{k_j}{k_i} \qquad \textbf{(Equation 1-7)}$$

where k_j is the retention factor of the later eluting compound, and k_i is the retention factor for the earlier eluting compound.

The sharpness of the peak is also imperative to how well two peaks will be separated, and is usually represented as a measure of plate number, *N*:

$$N = 16\left(\frac{t_R}{w_b}\right)^2 \qquad \textbf{(Equation 1-8)}$$

where w_b is the peak width at the baseline.

How well two analytes are separated on a column can be expressed in terms of resolution, R_S:

$$R_S = \left(\frac{\sqrt{N}}{4}\right)\left(\frac{\alpha - 1}{\alpha}\right)\left(\frac{k_2}{k_2 + 1}\right) \qquad \textbf{(Equation 1-9)}$$

This equation demonstrates how resolution can be improved by increasing efficiency (N), increasing separation factor (α), or by increasing the retention factor. Increasing the length of the column, narrowing the column diameter, or decreasing the film thickness can increase efficiency. However, as can be seen in Equation 1-9 the square root dependence means that for a 2-fold increase in resolution a 4-fold increase in efficiency is required. This kind of increase is very difficult to achieve without excessively long columns and analysis times. Changing the chemistry of the stationary phase and therefore changing the analyte-stationary phase interactions can increase selectivity factor. Lastly, increasing the retention factor requires lowering the temperature of the column. As can be seen in Equation 1-9, as k increases the retention term of the equation approaches a value of one, leading to diminishing gains as retention is increased.

1.3.2 One-Dimensional Separations

The primary goal of chromatography is to separate sample mixtures into their individual components. When analyzing a mixture of volatile or semi-volatile chemicals, GC is most commonly used to perform the

separation, identification and quantification of components. In GC, a sample is volatilized in the injector and introduced onto the column, where it is transported by carrier gas. The column contains a stationary phase, which is typically a thin layer of liquid coated on the wall of a fused silica capillary referred to as a wall-coated open tubular column (WCOT). These WCOT columns typically vary in length from 1-100 m, with inner diameters between 0.1-0.53 mm and have film thicknesses ranging from 0.08-5.0 μm. Inert carrier gas carries the sample through this column as the analytes partition between the stationary and mobile phases to different extents. While interacting with the stationary phase, the analytes are immobile. Analytes in the mobile phase travel through the column with the velocity of the mobile phase. If the analytes do not interact with the stationary phase at all, they elute from the column quickest and are said to be unretained. The greater the compound's interaction with the stationary phase, the longer it will take to elute from the column; these types of analytes are said to be retained by the column. The amount of interaction that an analyte has with the stationary phase depends on the structural and chemical characteristics of each analyte, and as a result their retention is different. Thus, the components in a sample can be separated based on the amount of time it takes them to elute from the column (retention time). The temperature at which the column oven is kept can also affect the extent to which the analytes are retained in the column. Once the analytes have

travelled from the injector and through the heated column they arrive at the detector, as is depicted in Figure 1-5.

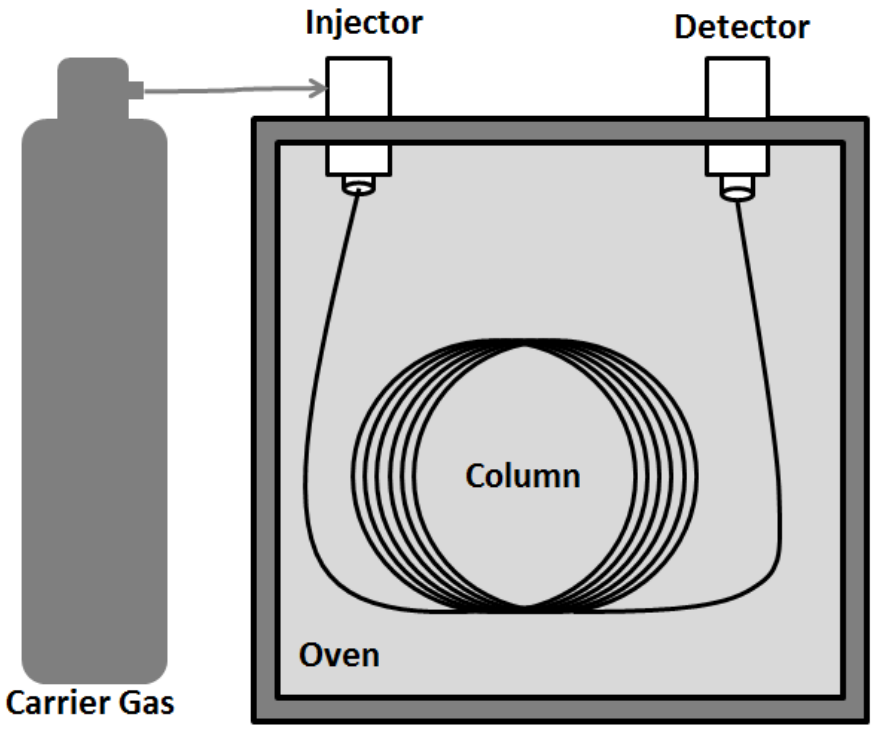

Figure 1-5. Schematic of one-dimensional gas chromatograph.

Problems may arise if two or more components of the sample reach the detector at the same time, meaning that they are not resolved. This happens when the partition coefficients of the compounds are very similar, because their interactions with the stationary phase occur in a similar manner. If the sample is composed of a simple mixture it is generally easy

to solve this problem by changing the stationary phase being used in the separation. Where more complicated mixtures are involved, this problem is not easily solved by changing the stationary phase and requires more complex problem solving. System efficiency may be described in part by peak capacity (n), the theoretical number of peaks that can be resolved in the separation time:

$$n = \frac{t_{R\_max} - t_M}{w_b R_s} \qquad \textbf{(Equation 1-10)}$$

where t_{R_max}, is the maximum retention time of the system. It is not statistically possible to achieve this due to the probability of peaks overlapping, as in real samples only ~20% of the calculated peak capacity is achieved. Increasing the separation power of a chromatographic system is possible, such as in the case of two-dimensional separations, as discussed in Section 1.3.3.

1.3.3 Two-Dimensional Gas Chromatography

Two-dimensional gas chromatography is employed for use with complex mixtures that cannot be separated using a one-dimensional GC instrument. The most common use of two-dimensional GC is comprehensive two-dimensional GC (GC×GC). This technique was first implemented by Liu and Phillips in 1991 [42]. GC×GC allows the separation and analysis of highly complicated mixtures by subjecting them to multiple

separation mechanisms, with the assumption that anything not separated by the first mechanism will be separated by the second. When compared with one-dimensional chromatography, this setup increases the peak capacity from that of single column (n) to the product of the individual peak capacities for both columns ($n_1 \times n_2$). This two-dimensional setup is also advantageous because the sensitivity increases due to the compression of the effluent band by the modulator separating the two columns [43,44]. Chemical noise from the injector and primary column may also be reduced by the focusing provided by the modulator.

To maximize the two-dimensional separation space, it is important for the two dimensions to operate with different retention mechanisms. Comprehensive techniques such as GC×GC require that the entire sample is separated by all dimensions, in a way that preserves the separation achieved in the previous dimension. Figure 1-6 shows the configuration of a GC×GC system, where two columns are coupled together by a modulator. The primary column is traditionally the type of column you would use in a 1D experiment, usually 15-30 m in length, 0.25-0.32 mm in diameter and 0.08-1 μm in film thickness. Most commonly a non-polar stationary phase is employed in the first dimension. A fraction is collected by the modulator and then released in a short pulse to the second dimension. A modulator works to collect a fraction of sample and focus it before releasing it onto the second column. It is the focusing in the second dimension that provides

the increased sensitivity for two-dimensional systems, and allows co-eluting compounds to be separated.

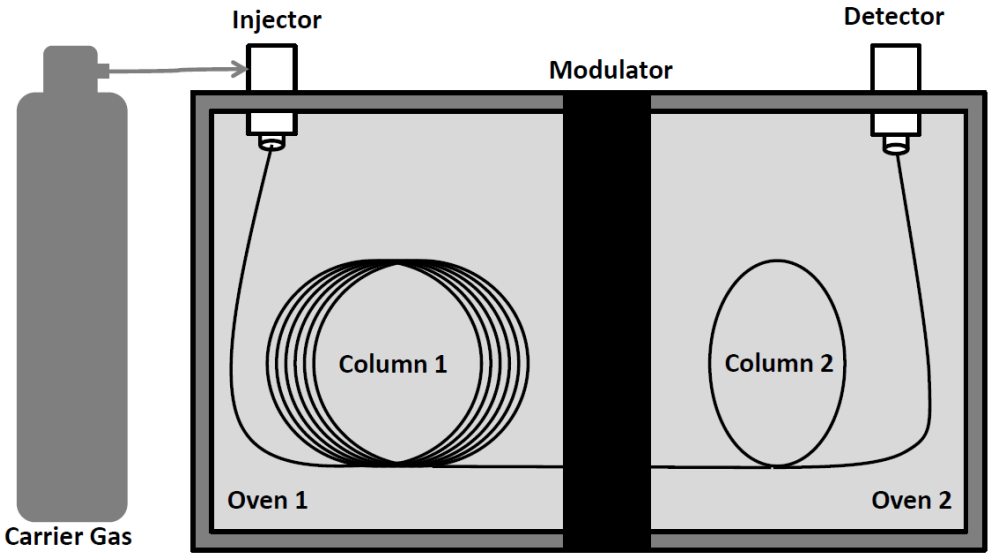

Figure 1-6. Schematic of a two-dimensional GC system.

The second-dimension column is usually a short polar column, usually 0.5-2 m in length. It is best practice to match the diameters in the first and second dimensions or have the second dimension slightly larger, for example if a 0.25 mm diameter column is used in the first dimension it should be coupled to a 0.25 mm diameter column. Since the length of the column is so short the second-dimension separation is very fast and considered to be isothermal. Having a short retention time in the second dimension prevents wraparound, which occurs when the second

dimension retention time is longer than the modulation period, resulting in the elution of a peak over successive modulation periods. This wraparound can be a large problem if the peak elutes in occupied retention space.

The modulator is the heart of a two-dimensional separation, because connecting two columns in series without an interface only achieves a one-dimensional separation. There are a number of modulators that are currently available, but they fall into to two major categories: thermal and valve-based modulators. Thermal modulation is more commonly used, as the first commercially available modulator was the rotating thermal modulator developed by Phillips and coworkers [45,46]. As modulator technology advanced, these types of modulators were replaced by cryogenic modulators, due to the disadvantages of moving parts and temperature limits instilled by requiring the modulator to exceed the oven temperature by 100 °C. The first cryogenic GC×GC modulator developed by Marriott and coworkers was the longitudinally modulated cryogenic system (LMCS) [47]. However, this approach still had drawbacks, such as moving parts, and the use of liquid CO_2. Liquid CO_2 only allows the trap to be cooled to approximately -50 °C, which is not sufficiently low to trap more volatile analytes. This led to the development of other non-moving cryogenic modulators that use cold jets of liquid CO_2 or liquid nitrogen to trap analytes [48,49,50]. Modulators that rely on this cold jet system trap effluent from the first dimension by using cryogen to

cool the column, causing an increase in retention factor trapping the eluting material in the cold spot. Once the cryogen jet is turned off and/or the hot jet is turned on, the trapped analytes begin to move. This process is depicted in Figure 1-7.

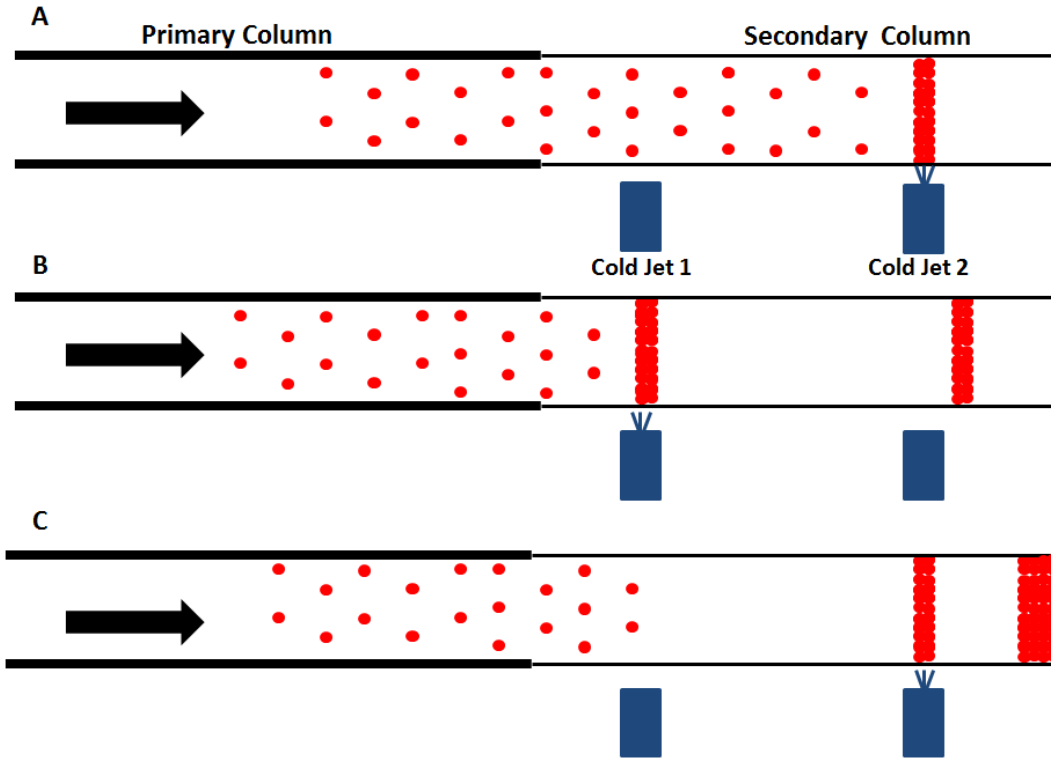

Figure 1-7. Thermal modulator process. When cold jet 2 is on and cold jet 1 is off (A) effluent is focused in a narrow band within the ^{2}D column. When cold jet 1 is on, it traps effluent from the ^{1}D column while the downstream jet is off to launch an injection pulse to ^{2}D (B). This process repeats (D) as cold jet 1 turns off and effluent passes to cold jet 2 which is now turned on.

The other group of modulators is valve-based interfaces. Valve-based modulators aim to overcome some of the disadvantages of thermal

modulators such as the high cost of cryogen and the difficulty in trapping very volatile analytes. Initial valve-based modulators connected a valve to the primary column, secondary column, auxiliary gas flow and a restricted vent line. This style of modulation is less sensitive and is not comprehensive because not all of the primary column effluent is passed to the second dimension. To overcome some of these disadvantages Seeley developed a valve-based interface that employed the use of sample loops, allowing the entire sample to be transferred to the second column [51]. This setup has the added advantage that the valve is outside of the oven and not in the flow path, allowing for increased temperatures [51]. This configuration is depicted in Figure 1-8.

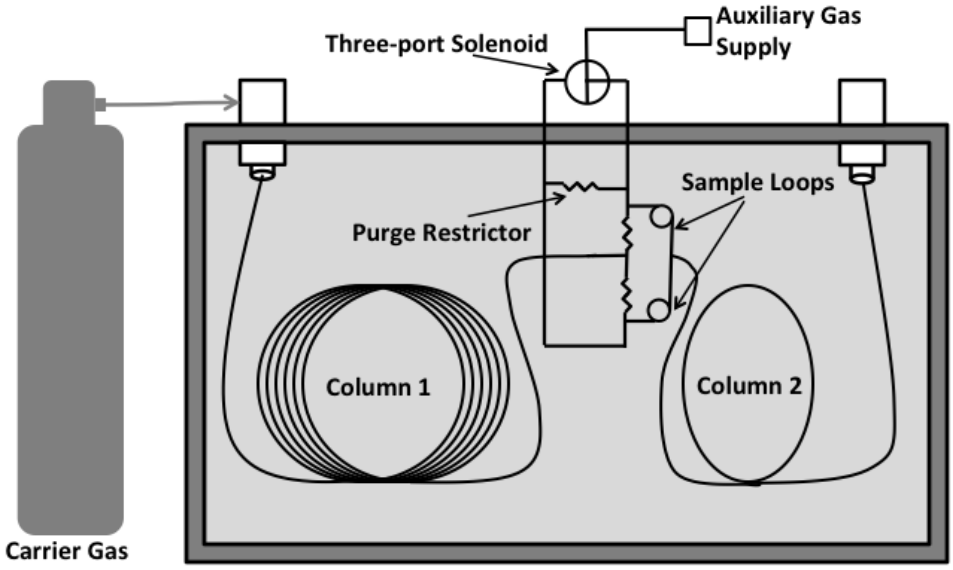

Figure 1-8. Schematic of a valve based two-dimensional GC system.

When the solenoid valve is in the position indicated in Figure 1-8, the auxiliary gas flow forces effluent through the upper sample loop and onto the second-dimension column. In this position the auxiliary gas is also supplying a small flow that directs the primary column effluent to the lower sample loop. When the position of the solenoid valve is switched, the flows are switched and the primary column effluent collects in the upper sample loop while the sample that was in the lower loop is separated on the second column.

The main advantage of valve-based techniques is that even with the most volatile analytes, there is no possibility of breakthrough (assuming that the loops are not over-filled) and no need for cryogenics. Valve-based modulators are also advantageous in very fast second-dimension separations due to fast switching times, which make very narrow injection bands possible. The major disadvantage of valve-based systems is that they are inflexible because if the flow rate or modulation period is changed, the two sample loops must also be changed. The sample loops also limit this type of system to very short modulation periods.

Using either the thermal or valve-based modulators produces very narrow peaks in the second dimension. Therefore, the peaks that elute the GC×GC systems are narrow; typically with widths at the base on the order of 100-400 ms. A minimum of 10 points per peak is required for accurate quantification. Thus, detectors must collect data at a rate of at least 50 Hz.

Detailed information on detectors for GC×GC may be found in [52] and [53]. Generally speaking, this limits GC×GC to the flame ionization detector (FID), micro electron capture detectors (μ-ECD), atomic emission detectors (AED), sulphur chemiluminescence detectors (SCD), quadropole mass spectrometers (qMS), nitrogen phosphorus detectors (NPD), and time-of-flight mass spectrometers (TOF-MS). Most GC×GC users employ the use of an FID, as it has negligible internal volume, responds to most hydrocarbons and is insensitive to non-hydrocarbons such as noble gases, N_2, O_2, CO, CO_2, and NO, while allowing acquisition rates up to 300 Hz. As an alternative, μ-ECDs are fairly insensitive to hydrocarbons and sensitive to halogen and nitrogen containing molecules, while allowing adequate acquisition rates. Coupling GC×GC instrumentation to a TOF-MS provides simultaneous detection of all mass-to-charge ratios, along with structural information for identification while still providing necessary acquisition rates. Although there are other available detectors that have been studied, the FID, μ-ECD and TOF-MS are the three most commonly used for GC×GC.

In GC×GC, the detector observes a series of second-dimension chromatograms that elute one after another from the secondary column. Looking at the data in this manner is very cumbersome. Therefore, the data is usually converted into a three-dimensional plot characteristic of this technique. Software accomplishes this by aligning all of the second-

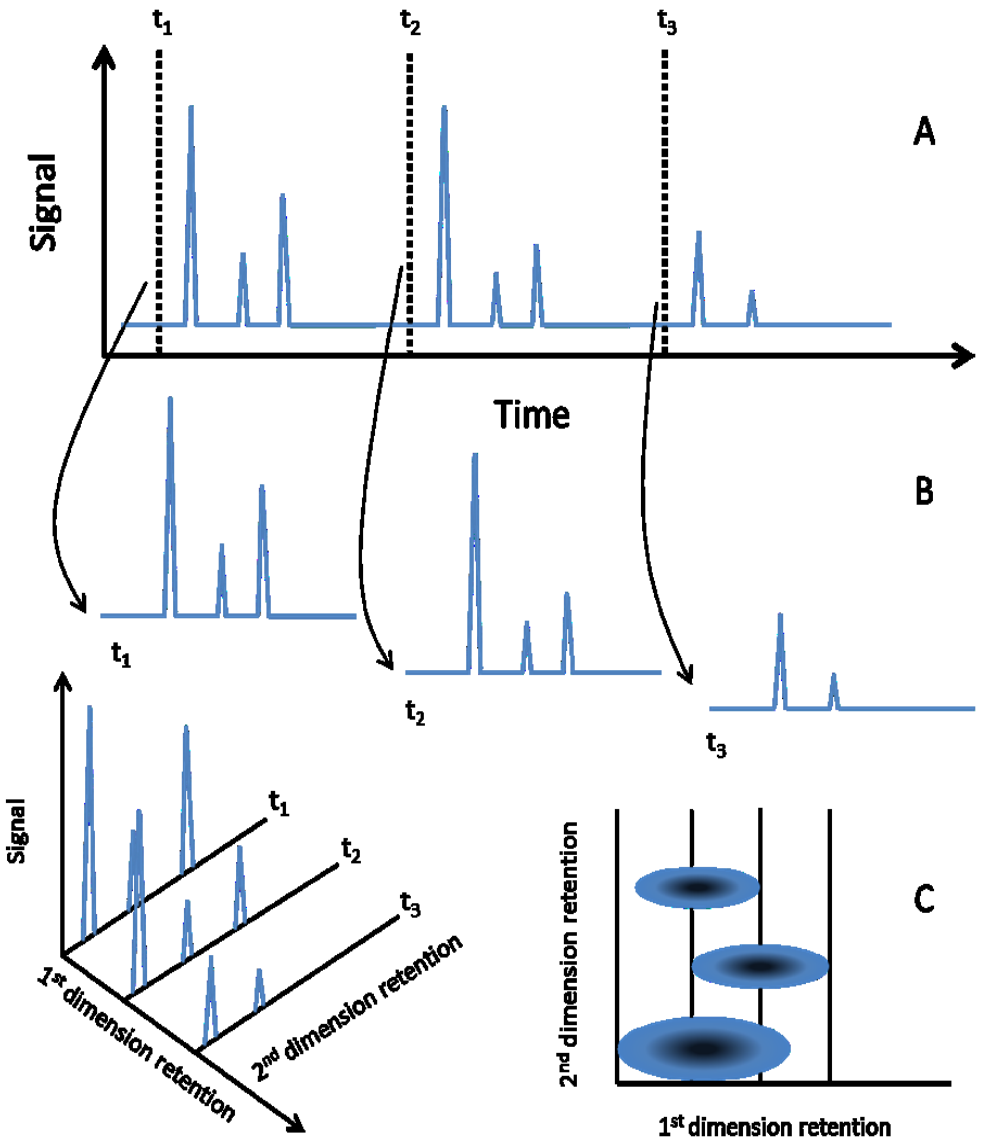

Figure 1-9. Use of raw GC×GC data. Raw GC×GC data (A) consisting of a series of short second dimension chromatograms. Injections onto the second dimension occurred at t_1, t_2, and t_3. The injection times are used to slice the original signal into a number of individual chromatograms (B). Primary and secondary retention are then plotted as the *x* and *y* axes, where signal intensity is then plotted on the *z*-axis (C). If this plot is then viewed from above, the peaks appear as color coded spots (D). Adapted from Figure 4 in reference [50].

dimension chromatograms side-by-side with the primary retention plotted along an *x*-axis and secondary retention plotted on the *y*-axis. The peaks appear as spots of varying color or contour lines on the *z*-axis. The data may then be most easily viewed in the form of a contour plot. The process of generating the user-friendly contour plots is depicted in Figure 1-9.

GC×GC is a widely used technique, with far reaching applications. It has been used extensively in petroleum [54,54,15], environmental analysis [55,56], fragrance analysis [57,58], forensics [59,60,61] and metabolomics [62,63]. There is continued interest in applying this comprehensive chromatography to many different sample sets, as well as exploring further principles of multidimensional chromatography. There have been a number of review articles that outline interesting applications and developments in this field [15,64-69]. The review articles [15,64-69] highlight the versatility and power of two-dimensional gas chromatography.

1.3.4 Detection

In this thesis, two modes of detection are used. The first, and most common for GC is flame ionization detection (FID). FID is a universal detector that responds to all analytes that contain reduced carbon. At the end of the column is a hydrogen-air flame, where reduced carbon is burned. The burning of this reduced carbon produces CHO^+ ions, in a side

reaction during combustion in the flame. Electrodes continuously measure the conductivity of the flame to determine the concentration of CHO^+ ions. An FID is an ideal detector for hydrocarbons because it provides an approximately uniform signal to carbon. This type of uniform response makes the FID a reasonable choice for our petroleum analyses.

The second mode of detection employed in this work is ultraviolet absorbance (UV). UV detection has also been used sporadically since 1962 when it was first reported by Kaye [70]. GC-UV systems have since been used for analysis of wine, indoor dust and for functional group analysis [71,72,73]. Most recently there has been work performed to determine PAH and other organic compounds using GC-UV [74]. With monochromatic UV detectors any analyte that possesses a chromophore provides a signal that is proportional to concentration. UV light shines through a flow cell, which contains the column effluent as it exits the column, and analytes absorb some of the UV light. The amount of light absorbed is described by Beer's Law:

$$A = \varepsilon b C \qquad \textbf{(Equation 1-11)}$$

where A is absorbance, ε is the molar absorptivity (varies with different wavelengths and structure of analytes), b is the path length of the detector cell, and C is the concentration of the analyte. The majority of GC instruments currently available only allow a single wavelength to be monitored at one time, with a select few being capable of a range of

wavelengths. The main disadvantage to UV detection is that saturates (i.e. alkanes) do not appreciably absorb UV light. However, the work discussed in Chapter 4 will be taking advantage of this property to differentiate between saturates and unsaturates that cannot be separated in 1D GC. The first UV instrument used in Chapter 4 of this thesis operates at a set wavelength of 254 nm, allowing for operation at one wavelength of light to be monitored in the flow cell. At this wavelength only compounds containing Pi-bonds will absorb, allowing us to differentiate between saturated and aromatic compounds.

More complex multiwavelength UV detectors have recently been introduced and allow a range of wavelengths (125-240 nm) to be monitored. This region contains what is referred to as the vacuum ultraviolet region, where nearly every chemical compound has a response. This occurs because in the range of 115-185 nm both $\pi \rightarrow \pi^*$ and $\sigma \rightarrow \sigma^*$ transitions can be probed [75]. In this instrument, the detector response is proportional to the amount of analyte per unit time, operating as a mass-sensitive detector [75]. Since this detector also collects the gas phase absorption spectra it provides qualitative information along with quantitative information, making it useful for our studies. Since the extinction coefficients vary for different analytes, quantification can be more difficult for UV detection. Therefore, where possible for the work in this thesis, FID will be used.

1.3.5 Ionic Liquid Stationary Phases

In gas chromatography, there are a number of commonly used stationary phases that have a range of polarities. The most recent advancement in GC stationary phases is the use of ionic liquids. Ionic liquid stationary phases have complex retention mechanisms that depend on multiple types of molecular forces, leading to unique retention properties [76]. 'Ionic Liquid' (IL) is used to describe a broad class of salts which melt at or below 100 °C. There is a specific class referred to as room temperature ionic liquids (RTIL) that are liquid at room temperature (~25 °C). Most RTILs have organic cations and inorganic ions, which are depicted in Figure 1-10.

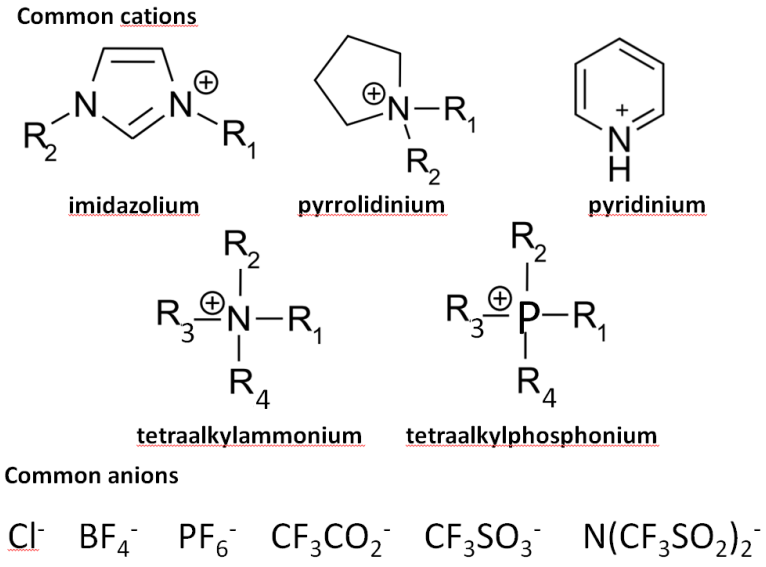

Figure 1-10. Structures of common cations and anions for ionic liquid capillary columns. Adapted from Figure 1 in reference [77].

Varying the combinations of these anions and cations alters the physical and chemical properties of the ionic liquid. The most interesting thing about these ionic liquids is their unique properties, such as: wide liquid ranges; good thermal stability; a wide range of viscosities, non-flammability; and low volatility. Of these, the most important factors making them useful in GC are low volatility, high viscosity, thermal stability and variable polarities.

Ionic liquids as stationary phases are extremely interesting because they display an unusual dual-nature retention behavior, separating a wide range of polar and non-polar compounds [77]. This allows these types of stationary phases to be used for a number of applications because of their efficient separation of a wide variety of analyte mixtures including alkanes, alcohols and polycyclic aromatic hydrocarbons to name a few. By using a different cation or anion, the separation performance of these stationary phases may be affected. Supelco (Bellefonte, PA, USA) has made a number of these IL stationary phases commercially available, which is the first new class of stationary phases that have become available in decades [78]. Ionic liquid stationary phases show great potential for petroleum separations, including unique selectivity for polar and polarizable molecules (such as PAHs) over aliphatic compounds, and much higher thermal stability than conventional “polar” phases [79,80,81]. By using IL columns, we strive to develop relatively simple methods for complex petroleum separations.

1.4 Thermodynamic Modeling

Mathematical relationships can describe some of the physical properties that are important in gas chromatography. Therefore, models can be developed to describe and predict chromatographic behavior. Predictive modeling allows the prediction of analyte behavior and separations without physical experimentation. There are several approaches to predicting retention in GC, including retention indices [82-86] and thermodynamic models [87-93]. Thermodynamic methods are based on modeling the thermodynamic equilibrium established between the stationary and mobile phases when an analyte is at or near infinite dilution. Our preferred approach uses a three-parameter thermodynamic model, works well for a series of different molecules, regardless of the phase chemistry or the chemistry of the compounds [91,15]. This model employs the three-parameter linearized equation, where the natural logarithm of the partition coefficient at a specific temperature is regressed against the inverse of temperature and natural logarithm of that temperature:

$$\ln(K) = A + B\frac{1}{T} + C\ ln(T) \qquad \textbf{(Equation 1-12)}$$

The three terms A, B and C are related to entropy $\Delta S(T_0)$, enthalpy $\Delta H(T_0)$ at some reference temperature, T_0, and the isobaric molar heat capacity

ΔC_p of the analyte during its transition between the mobile and stationary phases through Equations 1-13 – 1-14:

$$A = \frac{\Delta S(T_0) - \Delta C_p \ln(T_0) - \Delta C_p}{R} \qquad \textbf{(Equation 1-13)}$$

$$B = -\frac{\Delta H(T_0) - \Delta C_p T_0}{R} \qquad \textbf{(Equation 1-14)}$$

$$C = \frac{\Delta C_p}{R} \qquad \textbf{(Equation 1-15)}$$

T_0 was set to 90 °C for this work. The three-parameter model also assumes ΔC_p remains constant even though ΔC_p is actually a temperature-dependent term. However, because of the relatively small contribution this term has in determination of the partition coefficient, this discrepancy is of little importance.

Predictions are made using these equations where ΔH, ΔS and ΔC_p are determined from experiment and used to calculate A, B and C in Equation 1-13 – Equation 1-15. A partition coefficient for a given temperature was then calculated using Equation 1-12. Once the partition coefficient has been obtained, the retention factor and retention time in an isothermal separation can then be predicted using Equations 1-16 – 1-18:

$$\beta = \frac{r_c}{2d_f} \qquad \textbf{(Equation 1-16)}$$

$$k = \frac{K}{\beta} \qquad \textbf{(Equation 1-17)}$$

$$k = \frac{t_r - t_m}{t_m} \qquad \textbf{(Equation 1-18)}$$

To use these equations accurately the dead time (t_m) and phase ratio (β) for the column must be precisely known.

One of the significant advantages of thermodynamic models is that when thermodynamics are modeled precisely, the analytes' retention times can be predicted independent of operating conditions. This is of utmost importance because properties such as retention index vary with oven temperature and temperature-programming rate. As well, thermodynamic parameters may be easily collected on any gas chromatograph, and can be modeled for many different classes of compounds.

The discussion so far has focused on the use of thermodynamics in 1D GC, but with the increased use of GC×GC, modeling in two-dimensions is also required. Again thermodynamics are advantageous for this set-up because they can easily account for changes in operating conditions, as long as the model accounts for the temperature dependence of the thermodynamic parameters over the range of temperatures studied [91]. The basis of the 2D GC model is the same as for 1D GC as outlined in Equations 1-12 – 1-15, where a time summation model is then applied. The time summation procedure was developed by Snijders et al. [94], and predicts the distance traveled by an analyte during an interval of time

which is sufficiently small for both the carrier gas velocity and retention factor of the analyte to be assumed constant.

To predict the retention time of an analyte in GC×GC, two sets of iterative calculations must be performed. The first iterative process is used to calculate time required for an analyte to travel the length of the primary column, and the second to determine the time required for the analyte to travel from the modulator and through the length of the secondary column. For this process to work accurately with a temperature ramped run in 1D or 2D, the velocity of the carrier gas (u_x) must be calculated:

$$u_x = \sqrt{\frac{u_0}{P^2 - (\frac{x}{L})(P^2 - 1)}} \qquad \textbf{(Equation 1-19)}$$

$$u_0 = \frac{d_c^2}{32}\frac{P^2 - 1}{2\eta L}P_0 \qquad \textbf{(Equation 1-20)}$$

where the outlet velocity (u_0) is calculated for a given length (L), distance along the column (x), diameter (d_c), viscosity (η), outlet pressure (P_0) for the column, and the inlet to outlet pressure ratio (P).

The distance (Δx) that an analyte will travel in a time interval (Δt) is calculated:

$$\Delta x = u_x \frac{1}{(1 + k)}\Delta t \qquad \textbf{(Equation 1-21)}$$

where retention factor (k) is calculated from the thermodynamic parameters in conjunction with the phase ratio of the column as outlined in Equation 1-16 – Equation 1-17.

The total distance traveled by the analyte over the iterations is compared to the length of the column until distance travelled exceeds the length of the column, as seen below:

$$L \leq \sum_{i=1}^{n} \Delta x_i \qquad \textbf{(Equation 1-22)}$$

$$t_r = n\Delta t \qquad \textbf{(Equation 1-23)}$$

This process is then repeated to determine the ^2t_r. However, care must be taken to use the proper geometric and thermodynamic parameters as well as inlet and outlet pressures for the two columns.

1.5 Summary

This thesis uses gas chromatography in conjunction with ionic liquid capillary columns to develop unique separation methods for analytes of interest in petroleum samples. The three main areas of focus are alkyl phosphates, aromatic and biodiesel content in petroleum. Chapter 2 and 3 focus on the relationship between GC retention and the molecular structure of alkyl phosphates, utilizing ionic liquid columns. Chapter 4 focuses on the development of a GC method capable of determining aromatic content in diesel fuels. Chapter 5 deals with the use of a unique

VUV detector for quantification of aromatic and biodiesel content. Developing methods for a number of analyte types is accomplished using ionic liquid columns to provide unique separations. This will enable mitigation strategies in the case of alkyl phosphates, and readily available techniques for determination of aromatic content. In doing so, it is hoped that these methods will enable future technology to more effectively produce petroleum products.

CHAPTER TWO: Gas Chromatographic Retention of Alkyl Phosphates on Ionic Liquid Stationary Phases[1]

2.1 Introduction

As discussed in Section 1.1 petroleum is a complex mixture made up of thousands of mostly hydrocarbon-type constituents. Major issues can be caused by contaminants present in petroleum products. Refinery performance can be negatively affected when alkyl phosphates are present in small percentages. Previous research in our group has focused on the chromatographic analysis of alkyl phosphates in petroleum samples [95]. One industrial use of alkyl phosphates is as components of gellants used to increase the viscosity of oil-based fluids used in the hydraulic fracturing of oil and gas wells in water-sensitive geologies. Although the fracturing fluid is removed prior to extraction of oil, traces of gellant remain in the well and contaminate the oil. These residual phosphates present challenges for refineries handling the oil, including premature fouling of equipment and poisoning of catalysts. Frequent maintenance outages and unpredictable life spans of equipment/catalysts are the major problems caused by phosphate contamination.

[1] Portion of this chapter published as B.M. Weber, J.J. Harynuk, *J. Chromatogr. A* 1217 (2013) 4862.

Nominally, dialkyl phosphates with alkyl chains ranging from 2 to 30 carbons in length are used in fracture fluids [96,97]. However, they are manufactured as technical mixtures and the number of alkyl chains, position of attachment to the phosphate core, and extent of branching are not controlled, presenting challenges for speciation. Our group introduced a method for the separation and quantification of alkyl phosphates using comprehensive two-dimensional gas chromatography-time-of-flight mass spectrometry (GC×GC-TOFMS) [98]. This work demonstrated that electron impact-TOFMS spectra of alkyl phosphates were of limited value for elucidating the structures of unknown members of the family due to the combined instability of the molecular ions and the slight bias in the response of the TOFMS against higher mass ions. Additionally, in studies of industrial samples, the vast majority of phosphate and suspected phosphate peaks have retention times that do not match those of available standards. With only a limited library of alkyl phosphates, we have undertaken a study of the retention behaviours of alkyl phosphates in GC as a route toward tools to predict the structures of unknown alkyl phosphates based on retention in GC or GC×GC.

As outlined in Section 1.5, retention can be predicted using several different approaches including retention indices [82] and thermodynamic models [99,88,89,90,91,92,93]. Our preferred approach uses the three-parameter model discussed in Section 1.5 using Equations 1-12 – 1-15,

which model the interaction between a compound and the stationary phase and works well for a series of different molecules, regardless of the phase chemistry or the chemistry of the compounds [92,93].

Ionic liquid stationary phases have complex retention mechanisms that depend on multiple types of intermolecular forces, leading to unique retention properties [100]. This has been particularly notable for compounds containing phosphorus [101]. Consequently, it was decided to investigate the retention of a suite of alkyl phosphates on a variety of commercially available ionic liquid columns. Determining a stationary phase with a unique selectivity for alkyl phosphates and reduced retention of hydrocarbons would be ideal. This type of column would be an excellent candidate for one of the separation dimensions in a multidimensional GC analysis of alkyl phosphates in a petroleum hydrocarbon sample.

2.2 Experimental

2.2.1 Chemicals

Analytes consisted of triethyl phosphate (TEP), tripropyl phosphate (TPP), triisopropyl phosphate (TIP) (Sigma-Aldrich, Oakville, ON, Canada), tributyl phosphate (TBP) (VWR, Mississauga, ON, Canada), trihexyl phosphate (THP), and trioctyl phosphate (TOP) (Alfa Aesar, Ward Hill, MA, USA). ACS grade hexane (Sigma-Aldrich) and decane (Acros Organics, Bridgewater, NJ, USA) were used as solvents for all of the mixtures.

2.2.2 Instrument

Initial experiments were conducted on a HP5890 GC (HP, Mississauga, ON, Canada) using helium as carrier gas at a linear velocity of ~30 cm s^{-1}. All injections were performed manually in triplicate using split mode (50:1) with simultaneous injection of methane as a dead-time marker. Due to the diversity of retention characteristics across the phases tested, it was not practical to study all molecules over the same temperature range. Therefore, samples were analyzed over a temperature range of 60 °C in 10 °C increments. The injector temperature was 250 °C, and detection was done via flame ionization detection (FID). The raw FID signal was monitored directly at 100 Hz and collected by a computer using Galaxie software (Version: 1.9.3.2, Varian, Saint-Laurent, QC, Canada) to bypass the internal digitization electronics of the 5890 GC, which limit the data rate to 20 Hz. To confirm the observed retention patterns, an Agilent Technologies 7890A GC with a 5975 quadrupole MS, electron impact ionization source, and 7683 auto sampler (Agilent Technologies) was used. Data acquisition and automation in this case were accomplished using MS ChemStation (Version 03.00.611; Agilent).

2.2.3 Stationary Phases

A column having dimensions of 30 m × 250 µm and a 0.25 µm film thickness of 5% phenyl, 95% methyl phase (Rtx-5; Restek, Bellefonte, PA, USA) was used as a reference column to evaluate the relative selectivities of the IL phases. The IL columns studied were all 30 m × 250 µm with 0.2 µm films provided by Supelco (Oakville, ON, Canada). Phases are detailed in Table 2-1, and their structures are depicted in Figure 2-2**.**

Table 2-1. Ionic liquid stationary phase names, compounds and maximum temperatures.

Column Identifier	Stationary Phase	Maximum Temperature °C
SLBIL-61	1,12-Di(tripropylphosphonium)dodecane bis(trifluoromethylsulfonyl)imide trifluoromethylsulfonate	290
SLBIL-82	1,12-Di(2,3-dimethylimidazolium)dodecane bis(trifluoromethylsulfonyl)imide	270
SLBIL-100	1,9-Di(3-vinylimidazolium)nonane bis(trifluoromethylsulfonyl)imide	230
SLBIL-111	1,5-Di(2,3-dimethylimidazolium)pentane bis(trifluoromethylsulfonyl)imide	270

SLB

IL-61

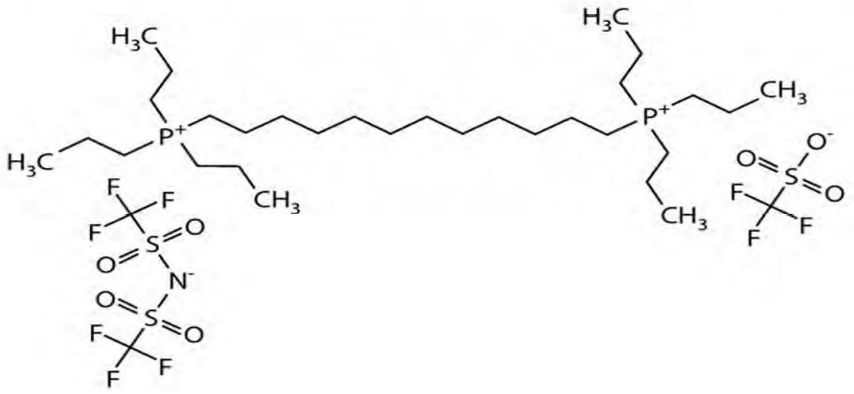

SLB

IL-82

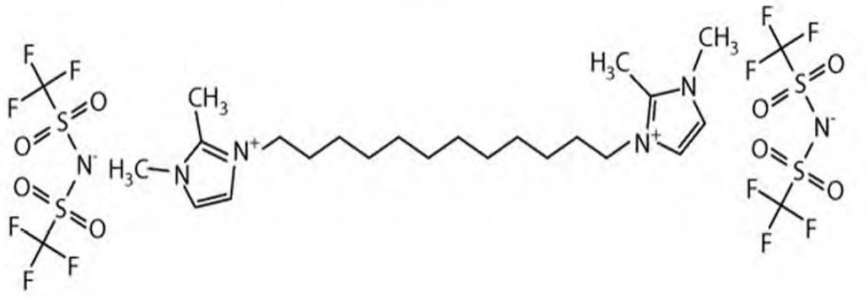

SLB

IL-100

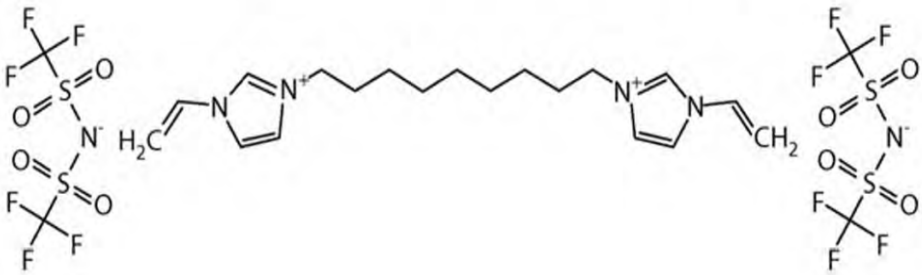

SLB

IL-111

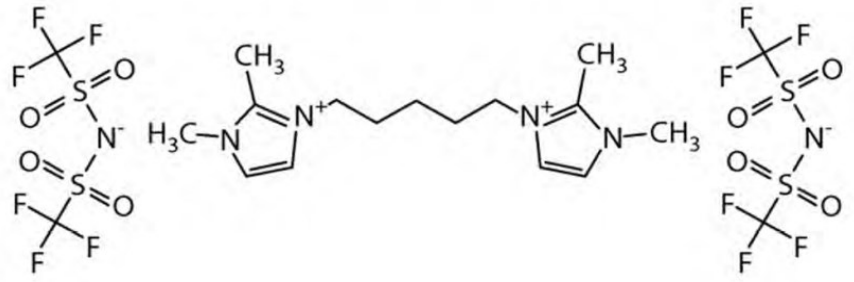

Figure 2-1. Structures of ionic liquid stationary phases.

2.2.4 Procedure

Isothermal runs were conducted at temperatures that ensured a reasonable retention time for the compounds (1 min < t_R < 35 min) providing retention factors in the range of 0.5 < k < 15. Samples were injected in split mode to an injector held at 250°C. The injection volume was 1 µL with a split ratio of 50:1. When the experiments were completed on the GC-MS these same conditions were used. In addition, the transfer line and source temperatures were 230 and 185°C, respectively and the EI voltage was 70 V. Mass spectral searching was performed against the 2005 edition of the NIST MS Database (NIST, Gaithersburg, MD, USA).

2.3 Results and discussion

Alkyl phosphates are a class of contaminants that pose a problem for refineries that process crude oil derived from water-sensitive geologies where the use of oil-based fracturing fluid is required [102]. Technical mixtures of alkyl phosphates exhibit a variety of chain lengths and degrees of branching. To study the chemistry of these compounds in a refinery environment, and thus assess the fouling potential of individual phosphates, the identification of these phosphates is required. It is possible to identify trialkyl phosphates where all three alkyl chains are identical using GC-quadropole mass spectrometer (qMS) and analyzing authentic standard mixtures, as we did for this research. However, due to the large

number of compounds in real samples, GC×GC is the preferred method for conducting the separation. The assignment of GC×GC-TOFMS spectra of trace alkyl phosphates in real samples difficult due to the relative stability of the molecular ion for the alkyl phosphate (or phosphate-trimethyl silane (TMS)) [98].

One potential route toward the identification of alkyl phosphates is through the study of the relationship between molecular structure and GC retention. Additionally, for practical analyses of alkyl phosphates in real samples, any column that offered a unique selectivity for alkyl phosphates over petroleum hydrocarbons could provide a route to a simpler analytical approach (e.g. targeted multidimensional GC *vs.* comprehensive multidimensional GC) that would be more easily adapted to field or routine industrial plant use.

Thus the retention of commercially available alkyl phosphates on a suite of commercially available ionic liquid columns was surveyed; retention on a 5% phenyl/95% dimethyl polysiloxane film was also investigated as a reference. The elution order on the reference 5% phenyl column was unsurprising, with retention time increasing with increasing chain length and the branched TIP eluting before the straight chain TPP. During initial experiments it was discovered that the IL-100 phase was very selective for the alkyl phosphates so the column was cut and a 10 m length was used for the remainder of the experiments on this phase. Table

2-2 provides retention times of the trialkyl phosphates on the series of ionic liquid columns at a range of isothermal temperatures.

Table 2-2. Adjusted alkyl phosphate retention times collected on ionic liquid GC columns.

Retention Times for Tri-alkyl Phosphates (min)							
Column	**Temp (°C)**	**Ethyl**	**Propyl**	**Isopropyl**	**Butyl**	**Hexyl**	**Octyl**
IL-61	110	-	-	28.95	-	-	-
	120	-	-	19.30	-	-	-
	130	-	-	13.06	-	-	-
	140	-	-	9.25	-	-	-
	150	7.80	15.87	6.86	38.55	-	-
	160	6.02	11.17	5.31	24.87	-	-
	170	4.84	8.19	4.29	16.68	-	-
	180	4.02	6.25	-	11.65	-	-
	190	3.44	4.96	-	8.46	-	-
	200	3.03	4.08	-	6.41	22.46	28.25
	210	-	-	-	-	15.17	18.26
	220	-	-	-	-	10.66	12.32
	230	-	-	-	-	7.79	8.69
	240	-	-	-	-	5.93	6.41
	250	-	-	-	-	4.70	4.94

Retention Times for Tri-alkyl Phosphates (min)							
Column	**Temp (°C)**	**Ethyl**	**Propyl**	**Isopropyl**	**Butyl**	**Hexyl**	**Octyl**
	260	-	-	-	-	3.86	3.97
IL-82	180	4.19	5.81	3.33	-	-	-
	190	3.53	4.61	2.89	6.97	22.55	23.24
	200	3.07	3.80	2.59	5.35	14.90	14.87
	210	2.74	3.24	2.37	4.28	10.27	9.98
	220	2.50	2.84	2.21	3.55	7.40	7.05
	230	2.31	2.56	-	3.05	5.57	5.24
	240	2.18	2.35	-	2.70	4.38	4.08
	250	3.07	3.80	-	2.44	3.59	3.35
IL-100 (10 m)	180	3.90	5.37	2.66	8.46	28.01	28.55
	190	2.97	3.71	2.06	5.49	16.18	15.83
	200	2.18	2.72	1.56	3.82	10.02	9.52
	210	1.73	2.07	1.28	2.75	6.40	5.89
	220	1.39	1.59	1.06	2.01	4.15	3.73
	230	1.20	1.33	-	1.60	2.95	2.61
IL-111	150	7.70	11.06	5.12	18.90	-	-
	160	5.87	7.91	4.07	12.58	-	-
	170	4.65	5.93	3.37	8.80	-	-
	180	3.83	4.63	2.90	6.42	-	-

Retention Times for Tri-alkyl Phosphates (min)							
Column	**Temp (°C)**	**Ethyl**	**Propyl**	**Isopropyl**	**Butyl**	**Hexyl**	**Octyl**
	190	3.25	3.77	2.57	4.90	11.55	11.40
	200	2.85	3.19	2.34	3.91	7.96	7.63
	210	2.56	2.78	2.17	3.26	5.78	5.44
	220	-	-	-	-	4.42	4.12
	230	-	-	-	-	3.55	3.29
	240	-	-	-	-	2.97	2.77
	250	-	-	-	-	2.59	2.42

The behavior of the phosphates on the IL-61 phase follows a similar elution order to the 5% phenyl column, with the exception that the branched TIP is poorly retained on the phase to the point where it is the first compound to elute. A similar trend for TIP was observed for the remainder of the IL columns tested in this research.

On the IL phases other than IL-61, very surprising retention behavior was observed. At lower temperatures, the elution order for THP and TOP was as expected; however, at elevated temperatures, the elution order was reversed, with TOP eluting prior to THP. The temperature where this elution reversal occurred varied with the phase, but it was observed on all of the IL phases tested other than IL-61 (though the two peaks were

eluting closer together and it is likely that their elution order would reverse if the column was heated above the maximum temperature for this column). Elution order reversals with changes in temperature are known in the literature [103], and unexpected elution patterns have been observed previously on IL columns (for example with fatty acid methyl esters [100,104,105]). However, to the best of our knowledge, this is the first documented case of elution order reversal within a homologous series of compounds.

To confirm the identities of the compounds and the qualities of the standards, each column was installed into a GC-qMS so that mass spectra of the compounds could be obtained. The identity of each trialkyl phosphate was confirmed by MS, a library search against the NISTMS 2005 database, and manual assignment of major ions. The molecular ions were often weak or entirely absent in the spectra; however, ions for $H_3PO_4R^+$ and $H_2PO_4R^+$ (where R is an alkyl chain) were present and useful for compound identification. In addition, all of the alkyl phosphate spectra also contained the m/z = 99 $H_4PO_4^+$ ion. Annotated spectra for all alkyl phosphates are shown in Figure 2-2.

A)

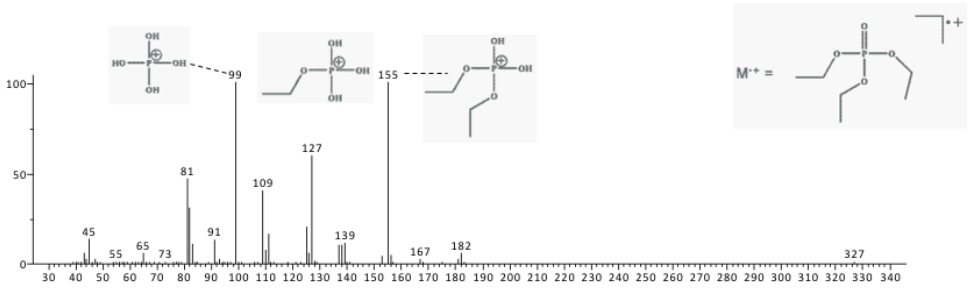
99
155
127
81
109
91
139
45
55
65
73
167
182
327
M·+ =

B)

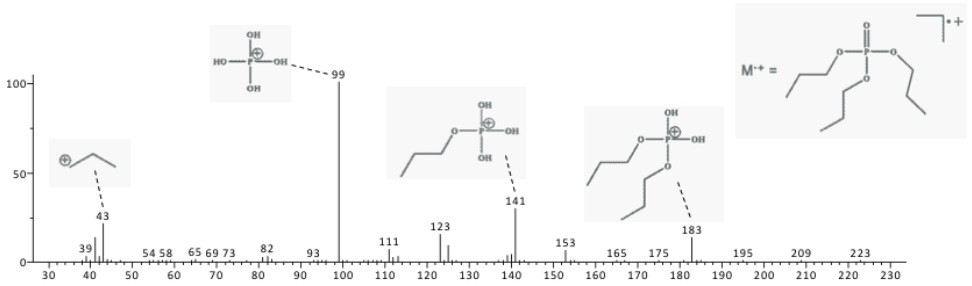
99
43
141
183
123
39
54 58
65 69 73
82
93
111
153
165
175
195
209
223
M·+ =

C)

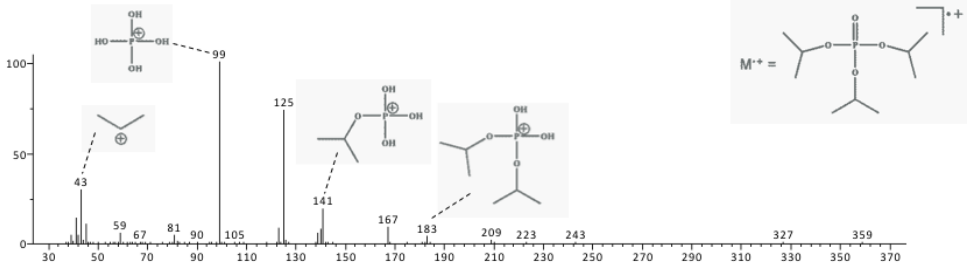
99
125
43
141
59
67
81
90
105
167
183
209
223
243
327
359
M·+ =

D)

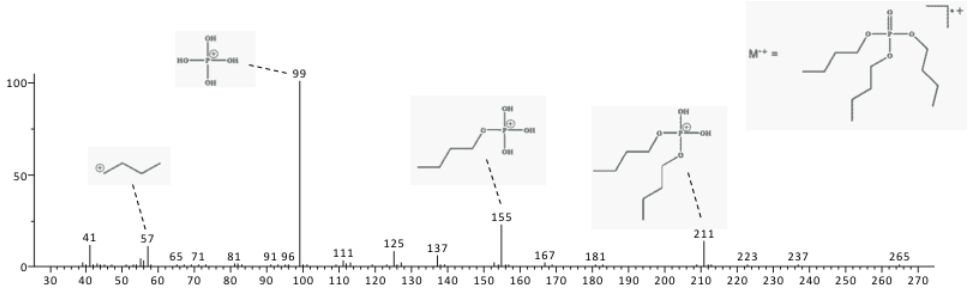
99
155
211
41
57
65 71
81
91 96
111
125
137
167
181
223
237
265
M·+ =

E)

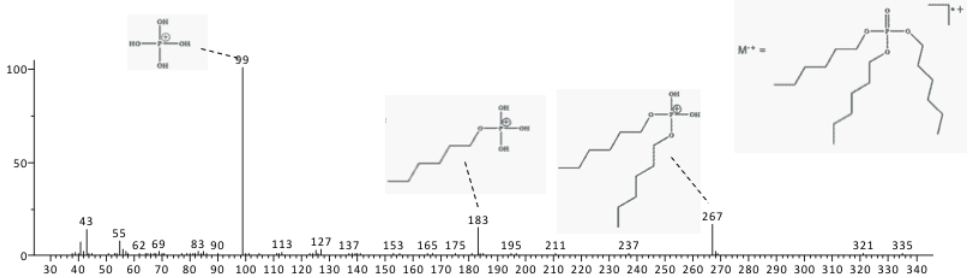
99
183
267
43
55
62 69
83 90
113
127
137
153
165 175
195
211
237
321
335
M·+ =

F)

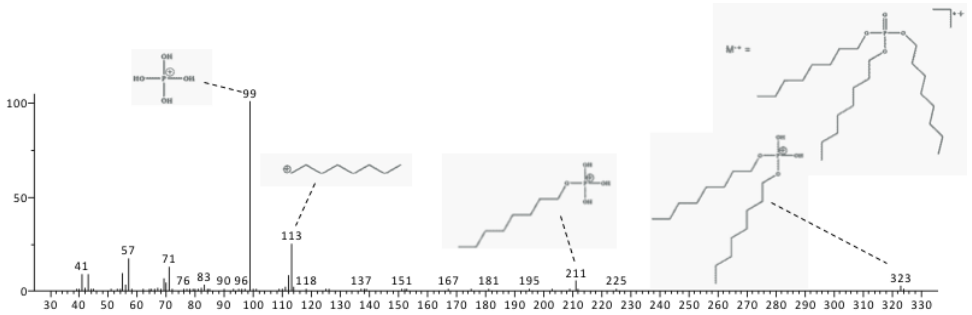

Figure 2-2. Example experimental EI mass spectra of model compounds and possible fragment ions. (A) triethyl phosphate (B) tripropyl phosphate (C) triisopropyl phosphate (D) tributyl phosphate (E) trihexyl phosphate (F) trioctyl phosphate.

Currently, we can only speculate as to the reason for this elution behavior for THP and TOP on the IL phases, and future work will need to include a more in-depth study of the interaction of these compounds with the phases will be required. Additionally, triheptyl, trinonyl, and tridecyl phosphates are not commercially available so we cannot study their behavior. One possible hypothesis is that this is a shape-selective effect and that the phases contain a pocket-like domain into which alkyl phosphates with hexyl (possibly heptyl) or shorter chains can fit, but which is too small to accommodate the trioctyl chain at high temperatures. It is also possible that this is due to a phase-change phenomenon in the polymeric stationary phase. To study this, simulations of the dipole moment of the anion and cation for IL-60 were completed. The dipole moment of the anions remains relatively constant, while there are large fluctuations in the dipole moments of the dication. This indicates that the cation is changing

conformation with temperature, which is consistent with the shape-selectivity we observe.

By collecting retention data for all of our compounds isothermally at a series of temperatures for each phase, it was possible to extract thermodynamic parameters governing the retention of the molecules using an approach described in Section 1.4 [93]. The values for the coefficients A, B, and C (Equations 1-12 – 1-15) that were determined for our compounds are compiled in Table 2-3.

Table 2-3. Calculated Parameters A,B, and C for tested phosphate compounds.

Compound	Column	C	B	A
TEP	Rtx-5	1.01E+01	9.50E+03	-7.88E+01
	IL-61	1.06E+01	1.09E+04	-8.30E+01
	IL-82	8.65E+00	1.03E+04	-6.95E+01
	IL-100	9.22E+00	1.17E+04	-7.48E+01
	IL-111	1.02E+01	1.08E+04	-8.03E+01
TIP	Rtx-5	1.19E+01	1.05E+04	-9.14E+01
	IL-61	1.12E+01	1.14E+04	-8.77E+01
	IL-82	9.67E+00	1.09E+04	-7.75E+01
	IL-100	-3.84E+00	5.74E+03	1.79E+01
	IL-111	1.10E+01	1.12E+04	-8.71E+01
TPP	Rtx-5	1.20E+01	1.15E+04	-9.38E+01

Compound	Column	C	B	A
	IL-61	1.16E+01	1.24E+04	-9.17E+01
	IL-82	1.10E+01	1.22E+04	-8.77E+01
	IL-100	6.84E+00	1.16E+04	-5.95E+01
	IL-111	1.11E+01	1.20E+04	-8.85E+01
TBP	Rtx-5	1.40E+01	1.36E+04	-1.09E+02
	IL-61	1.25E+01	1.38E+04	-9.96E+01
	IL-82	1.39E+01	1.45E+04	-1.10E+02
	IL-100	1.39E+01	1.57E+04	-1.12E+02
	IL-111	1.23E+01	1.34E+04	-9.84E+01
THP	Rtx-5	1.74E+01	1.76E+04	-1.36E+02
	IL-61	1.32E+01	1.61E+04	-1.07E+02
	IL-82	1.81E+01	1.84E+04	-1.43E+02
	IL-100	1.43E+01	1.78E+04	-1.17E+02
	IL-111	3.33E+01	2.54E+04	-2.52E+02
TOP	Rtx-5	2.08E+01	2.04E+04	-1.63E+02
	IL-61	1.72E+01	1.89E+04	-1.37E+02
	IL-82	2.29E+01	2.15E+04	-1.79E+02
	IL-100	1.86E+01	2.07E+04	-1.50E+02
	IL-111	4.62E+01	3.27E+04	-3.46E+02

From these values, and using the manufacturer designated phase ratio for each column, it was possible to predict the retention factor for each

compound on each phase as a function of temperature. Figure 2-3 depicts plots of the natural logarithm of predicted retention factor vs. temperature for each compound on each phase tested, providing the elution orders for the compounds at a given temperature. The dots indicated on each curve are the actual measured values for ln (*k*) for each compound on each column. Each point represents three individual measurements, which were for all intents and purposes identical. In these figures, elution order reversal temperature is observed, where the lines gross over, at temperatures that correspond to Table 2-2. Further, by inspecting the curves for THP and TOP on IL-61 (the only phase for which these two compounds were not observed to reverse their elution pattern), one would expect that the two compounds would reverse their elution order at a temperature of about 300 °C, which is above the maximum temperature of the column (290 °C) [106]. It is worth noting that these retention factors were predicted on the basis of thermodynamic parameters and retention data spanning a 60 °C range and then extrapolated to temperatures for which obtaining experimental data was impractical or impossible. However, even with this limitation, our experience with the thermodynamic modeling approach [95,96] used in this work suggests that the predicted values are a good approximation of the true values.

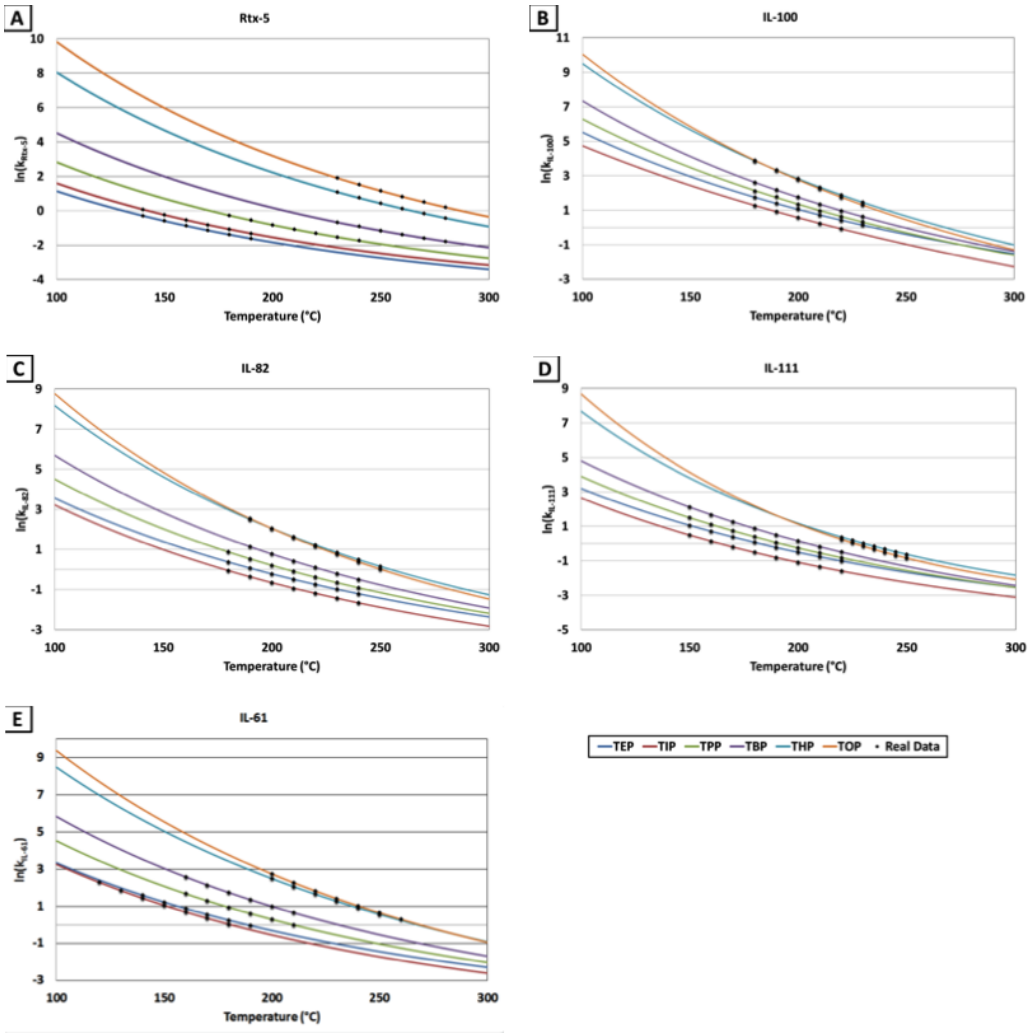

Figure 2-3. Comparison of retention factors for alkyl phosphates as a function of temperature on the columns studied. (A) Rtx-5 (B) IL-100 (C) IL-82 (D) IL-111 (E) IL-61.

The relative selectivities that the phases exhibited for the alkyl phosphates across a range of temperatures is also informative, as this comparative analysis of stationary phases can be useful for guiding column choices in GC or multidimensional GC method development. Figure 2-4 depicts the relative selectivities of the ionic liquid columns versus Rtx-5 for

the test alkyl phosphates across a range of temperatures, plotted as k_{IL}/ $k_{5\%}$, where k_{IL} is the predicted retention factor for the compound on the IL phase and $k_{5\%}$ is the predicted retention factor on the 5% phenyl phase. It is apparent in Figure 2-4 that IL-100 is the most selective column tested for the alkyl phosphates, with all of the alkyl phosphates having significantly higher retention factors on this phase than the 5% phenyl phase, with the exception of TOP, which had approximately the same retention factor on both phases. The other phases were moderately more selective for shorter-chain alkyl phosphates while for TOP the 5% phenyl column was more retentive. The trends in relative selectivities are explained by the fact that as the chain lengths of the phosphates increase, the hydrophobic nature of the molecules increases, and thus their affinity for the 5% phase.

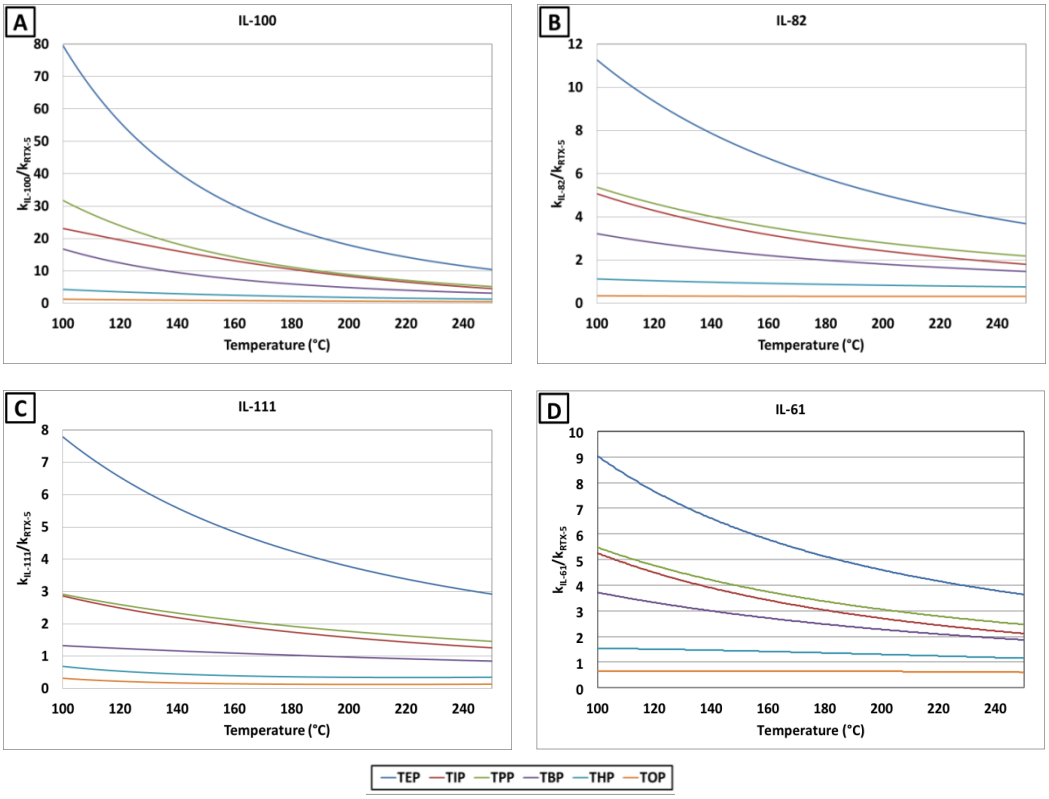

Figure 2-4. Relative selectivities of ionic liquid columns vs. Rtx-5 for alkyl phosphate compounds as a function of temperature. (A) IL-100 (B) -111 (C) IL-IL-82 (D) IL-61.

On the basis of these plots, a 5% phenyl × IL-100 column combination could be very interesting for a multidimensional GC separation. However, if one were to attempt this column combination for a GC×GC separation, one would undoubtedly require either independent temperature control of the two columns, or would need to put the IL-100 column in the primary dimension. The reason being that all of the phosphates except for TOP have retention factors (and thus elution

temperatures) on the 5% phenyl column that are significantly lower than those observed for the IL-100 phase. Consequently, with the traditional apolar/polar column coupling used in GC×GC, extreme wraparound would be expected for the alkyl phosphates if both columns were in the same oven.

2.4 Conclusions

Ionic liquid capillary columns for use in gas chromatography provide chromatographers with a host of new and interesting selectivities to address challenging separations. However, as we have demonstrated, one cannot assume that conventional wisdom with respect to elution behavior will hold true, even within a homologous series of compounds. In the case of the alkyl phosphate standards it was shown that the retention behavior of the entire suite of compounds could not be easily rationalized, but could still be reliably predicted using a thermodynamic model.

Retention studies such as these, especially for ionic liquid columns can be useful in guiding column choices for method development. Based on the results presented in this research, the IL-100 column is the most selective for short-chain alkyl phosphates and would be a likely candidate for the selective separation of these compounds from petroleum hydrocarbons in a 1D GC application. It would also be a good candidate for use as one of the dimensions in a multidimensional GC separation of alkyl

phosphates from other analytes. The analysis of alkyl phosphates in petroleum samples by GC×GC using ionic liquid columns along with the synthesis and study of an expanded suite of alkyl phosphates remain for future study.

CHAPTER THREE: Analysis of Alkyl Phosphates in Comprehensive Two-dimensional Gas Chromatography on Ionic Liquid Stationary Phases[2]

3.1 Introduction

Gaining an understanding of the contaminants present in petroleum helps make the refining process more efficient, reducing time and product loss. Due to the complexity of petroleum samples, innovative techniques are needed to better understand their behavior in refineries. By using selective gas chromatography capillary columns, such as ionic liquids, in conjunction with powerful prediction techniques, it can help to determine important contaminants in refineries. Identification and monitoring of phosphorus compounds would be very useful in predicting and/or preventing refinery fouling.

As in Chapter 2, the goal of this chapter is to use ionic liquid columns to positively identify phosphates in petroleum samples based on their retention behavior. Chapter 2 showed that some commercially available ionic liquid columns provide selectivity for alkyl phosphates [107]. Therefore, we continued our work to use ionic liquid columns for

[2] Portions of this chapter published as B.M. Weber, J.J. Harynuk,, *J Sep. Sci.* 37 (2014) 1460.

one of the separation dimensions in multidimensional GC analysis of alkyl phosphates. In this chapter four different column setups are tested to evaluate the possibility of an ideal candidate for one of the separation dimensions in multidimensional GC analysis of alkyl phosphates in petroleum hydrocarbon samples. Ideally this ionic liquid column setup will provide unique selectivity for alkyl phosphates and reduced retention of hydrocarbons. The phosphates can be positively identified in the petroleum samples based on their multidimensional separation pattern, as well as matching with the predicted retention times in both dimensions.

With only a limited library of alkyl phosphates, a study of the retention behaviors of alkyl phosphates in GC as a route towards tools that can be used to predict the structures of unknown alkyl phosphates based on retention in GC or GC×GC, was undertaken. As outlined in Section 1.3.6, prediction of retention times can be accomplished using several different approaches including retention indices [82] and thermodynamic models [108,109,110,89,111,92,93]. Our preferred approach uses the three-parameter model discussed in Section 1.4 using Equations 1-12 – 1-15, which models the interaction between a compound and the stationary phase. The three-parameter model works well for a series of different molecules, regardless of the phase chemistry or the chemistry of the compounds [82,93]. To extend this model to two-dimensions for the current work, the three-parameter model is used in conjunction with the

time summation model detailed in Section 1.4 using Equations 1-19 – 1-21 [94]. This is done to predict both the primary and secondary retention times of our analytes. The other important consideration in using this method is that there is now also a modulator through which the sample passes. The instrumentation used for this work employs a pneumatic modulator, as discussed in Section 1.3.3. This becomes an important consideration because these modulators do not contain stationary phase, which means that there are only two chromatographic zones. Because there is no retention in the modulator, chromatographic retention only needs to be considered in the primary and secondary dimension. If a thermal modulator was used, it would contain stationary phase for which the model would likely need to account, by also modeling the separation in the modulator.

Based on the results obtained in Chapter 2, four different column setups were tested to determine the effectiveness of our prediction method, using these unique columns on our alkyl phosphate samples. The column set-ups were chosen from their relative alkyl phosphate retention, employing IL-100 as a selective choice for alkyl phosphate comparison, and IL-61 as a 'well-behaved' comparison. The experimental 2D retention times were collected, and compared to our predicted retention times. In taking this one step further, the thermodynamic parameters for our standards were used to predict the thermodynamics of a test compound. The

thermodynamics for the test compound were then used to predict its retention in both dimensions, and was then compared to the experimental results. By successfully predicting 2D retention of standards and unknown compounds, more extensive identification of contaminant phosphates in petroleum samples may be completed.

3.2 Prediction of Retention Times in Comprehensive Two-dimensional Gas Chromatography on Ionic Liquid Stationary Phases

3.2.1 Overview

Herein, four different combinations of capillary columns are used for the prediction of alkyl phosphate retention times in two-dimensional GC. By employing ionic liquid capillary columns, unique selectivity for alkyl phosphates is achieved. To test the capabilities of our prediction methods, two different ionic liquid columns were used, and were employed in both the first and second dimensions of our chromatography to determine which setup would be most useful for future samples.

3.2.2 Experimental

3.2.2.1 Chemicals

Analytes consisted of triethyl phosphate (TEP), tripropyl phosphate (TPP), triisopropyl phosphate (TIP) (Sigma-Aldrich, Oakville, ON, Canada), tributyl phosphate (TBP) (VWR, Mississauga, ON, Canada), trihexyl phosphate (THP), and trioctyl phosphate (TOP) (Alfa Aesar, Ward Hill, MA, USA). ACS grade hexane (Sigma-Aldrich) and decane (Acros Organics, Bridgewater, NJ, USA) were used as solvents for all of the mixtures.

3.2.2.2 Instrument

Initial experiments were conducted on a HP5890 GC (HP (Agilent Technologies), Mississauga, ON, Canada) and a Varian 3800 (Varian Inc., Mississauga, ON) using helium as a carrier gas at a linear velocity of ~30 $cm \cdot s^{-1}$. All injections were performed manually in triplicate using split mode (50:1) with simultaneous injection of methane as a dead-time marker. Due to the diversity of retention characteristics across the phases tested, it was not practical to study all molecules over the same temperature range so samples were analyzed over a temperature range of 60 °C in 10 °C increments. The injector temperature was 250 °C. Detection was via flame ionization detection (FID). For the HP5890 the raw FID signal was monitored directly at 100 Hz and collected by a computer using

Galaxie software (Version: 1.9.3.2, Varian, Saint-Laurent, QC, Canada) to bypass the internal digitization electronics of the 5890 GC which limit the data rate to 20 Hz.

For the two-dimensional work an Agilent 7890A gas chromatograph (Agilent Technologies, Missisauga, ON) equipped with a split/splitless injector, flame ionization detector, and a capillary flow technology (CFT) GC×GC modulator. Injections were performed in split mode with a split ratio of 50:1 and an inlet temperature of 250 °C. The flame ionization detector was maintained at a temperature of 250 °C with a data-sampling rate of 200 Hz. 99.999% Hydrogen (Praxair, Edmonton, AB) was used as a carrier gas. The modulation period was 1.5 s with a flush time of 0.15 s for all experiments.

Raw data files were exported from Chemstation (Agilent) as text files and then converted using a custom script written in MATLAB 7.10.0 (The Mathworks, Natick, MA) into a format that was imported into ChromaTOF 4.33 (Leco Corporation, St. Joseph, MI) for GC×GC processing.

3.2.2.3 Stationary Phases

The IL columns used for collection of thermodynamic information in one dimension were all 30 m x 250 μm with 0.2 μm films of the following phases: SPB-5MS, SLBIL-61, SLBIL-82, SLBIL-100 and SLBIL-111 (Supelco,

Oakville, ON, Canada), as detailed in Chapter 2 [107]. For the two-dimensional work, the primary dimension columns were IL-61, IL-100 (15 m × 0.1 mm × 0.08 μm) and SLB5ms (15 m × 0.1 mm × 0.1 μm), and secondary dimension columns were IL-61, IL-100 (3 m × 0.25 mm × 0.2 μm) and SLB5ms (3 m × 0.25 mm × 0.25 μm). These short secondary columns were made by cutting 30 m columns down to 3 m segments, to have second-dimension separation times close to the length of the modulation period.

3.2.2.4 Procedure

Previously determined thermodynamic parameters for the alkyl phosphates of interest from Chapter 2 were used to demonstrate the prediction of retention time for compounds in GC×GC. This was accomplished using the thermodynamic model outlined in Section 1.3.6. All two-dimensional separations were performed under constant flow conditions, where the flow in the first dimension was set to 0.5 mL/min, and in the second dimension to 22 mL/min. The separations were started at 50 °C, with a temperature programmed rate of 15 °C/min to a final temperature 20 °C under the maximum temperature for the column set, with a hold time of a period long enough to elute all analytes by the end of

the run. GC×GC retention time predictions were calculated using a custom script written in MATLAB.

3.2.3 Results and Discussion

3.2.3.1 ^{2}D Predictions of standard compounds

In this chapter, we demonstrate the prediction of retention times for compounds in GC×GC with the use of a pneumatic modulator. Based on the results presented in Chapter 2 [15], the IL-100 column is the most selective for alkyl phosphates, especially for short chain alkyl phosphates, and would be a good candidate for use as one of the dimensions in a multidimensional GC separation of alkyl phosphates from other analytes. Therefore, we have completed predictions of the alkyl phosphates in two dimensions using the IL-100 column in both the primary and secondary dimensions. As a test for this method the same predictions were also completed using an IL-61 column in both primary and secondary dimensions. In both cases, a 5% phenyl phase column was used as the complementary column.

The retention times in GC×GC were initially predicted for all compounds using the measured length and nominal values for the inner diameter and film thickness. Previous work indicated that both the inner diameter and film thickness of the stationary phase vary from column to

column [92], so for each column these parameters are estimated. In this work the inner diameter of the column is estimated by collecting triplicate chromatograms of methane at 100 °C at constant pressure, and using HP flow calculator (Agilent Technologies) to determine the diameter of the column, based on the holdup time. This was completed for both the first- and second-dimension. For the 3 m columns, this diameter was determined by the remainder of the 30 m length of column (~27 m) that the 3 m segment was taken from. Next, the experimental results were used to estimate the film thickness, using the estimated column diameter and measured length. This was accomplished by adjusting the film thickness while keeping everything else constant until the predicted $^{1}t_r$ of the compounds gave the smallest error when compared with experimental values. Again this process was repeated in the second dimension. The values for the length, estimated inner diameter and estimated film thickness are tabulated in Table 3-1.

The second consideration for making these types of GC×GC predictions is the effect of wraparound. In this work wraparound peaks are those having $^{2}t_r > 1.5$ s (P_M), meaning that a peak will elute during a modulation pulse. Consequently, to compare the predicted and experimental values, the experimental $^{1}t_r$ must be decreased, and the experimental $^{2}t_r$ must be increased.

Table 3-1. Values for length, estimated inner diameter and estimated film thickness for each column used.

Column	Length (m)	Inner Diameter (mm)	Film Thickness (μm)
Equity 5ms	16.50	0.104	0.105
	3.00	0.250	0.210
IL-61	16.82	0.097	0.072
	3.00	0.250	0.180
IL-100	10.64	0.097	0.110
	3.00	0.240	0.200

As an example, with a modulation period of 1.5 s and a predicted ^2t_r of 13.86 s, the peak would be plotted 13.86÷1.5 = 9.24 modulation periods after injection. Thus the experimental ^1t_r would appear to be 9 × 1.5 s = 13.5 s longer than its actual value. To calculate the ^2t_r, a similar process is used, where the peak would appear experimentally at 0.36 s, and its actual value would be 0.36 s + (9 × 1.5 s) = 13.86 s. The number of wraparound times must be known to complete this unwrapping process, and will provide a peak table with true values for the retention coordinates of the peaks, such as the data shown in this chapter.

To determine the number of times that an analyte had wrapped around under experimental conditions, the method developed by Micyuse et al; may be used [112]. Using this method, the experiment is performed

twice with the modulation period changed slightly in the two experiments (Run 1 was 1.5 s and Run 2 was 1.6 s). Peaks that do not wrap around will not experience a shift in retention between the two runs, and those peaks that do wrap around will have a shift in ^2t_r that corresponds to the number of times that they have wrapped around. However, it is also possible to determine the number of wraparounds that occur by using our predicted ^2t_r. If the value is greater than the modulation period you can divide ^2t_r by P_M, and round to the nearest integer. This is the method that was used to present the "unwrapped" retention values for this work.

Once the column dimensions and wraparound were accounted for, both the predicted and experimental retention times were plotted as peak apexes as seen in Figure 3-1 (A-D). This figure illustrates two experimental set-ups where the ionic liquid column is in the second dimension (A and B), and two where the ionic liquid column is in the first dimension (C and D). Examining A and B it can be seen that the early eluting compounds in the primary dimension are then significantly retained on the second dimension column. This leads to large amounts of wraparound, where in the most extreme case as seen in B for TEP the ^2t_R is ~41 s, meaning that with a modulation period of 1.5 s this compound is wrapped around 27 times. It may also be noted from A and B that for the early eluting compounds the experimental data do not agree well with predicted data which is mostly likely due in large part to the fact that these compound are

highly polar and chromatograph poorly (i.e. extreme tailing) on this 5% phenyl (non-polar) phase.

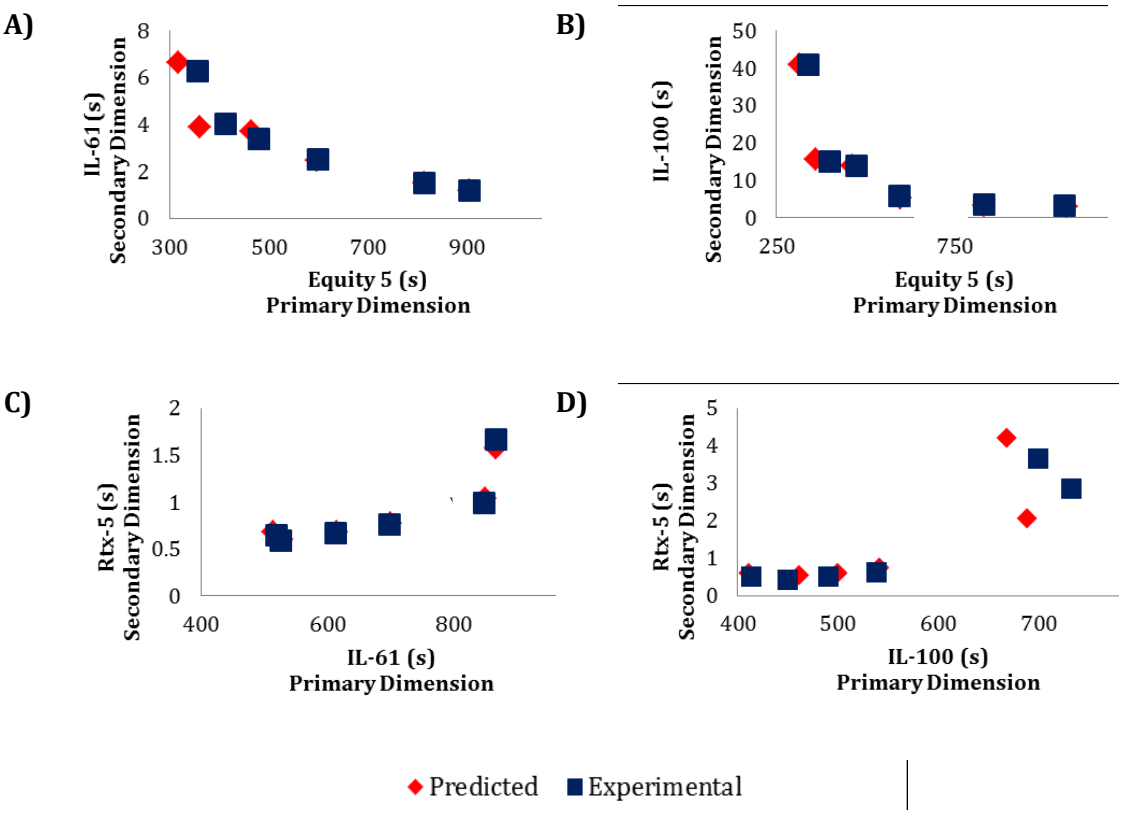

Figure 3-1. Peak apex plots of both experimental and predicted retention times. A) Equity-5ms × IL-61 B) Equity-5ms × IL-100 C) IL-61 × Rtx-5 D) IL-100 × Rtx-5. 'unknown' T5P is shown with the hollow markers.

Predictions with the ionic liquid column in the first dimension as shown in Figure 3-1 (C and D) were done because of the poor chromatography that was observed with our other set-up, together with the unique selectivity that the ionic liquid columns have for alkyl phosphates as shown in our previous work [107]. With this column setup, the chromatography of the

early eluting alkyl phosphates is greatly improved, and it is observed that the wraparound is also largely decreased. The most extreme case now being ~4 s secondary retention or 2 wraparounds as opposed to the 27 as observed in B. Table 3-2 contains the raw retention data for all of the compounds in all of the setups, the actual differences in predicted and experimental retention times are calculated.

Table 3-2. Retention times of each compound on each column, corresponding to those in Figure 3-1.

		Predicted		Measured		Difference	
	Compound	1D (s)	2D (s)	1D (s)	2D (s)	1D (s)	2D (s)
A (Equity 5 × IL-61)	TEP	317.80	6.65	357.00	6.26	39.20	-0.39
	TIP	360.65	3.90	412.50	4.04	51.85	0.14
	TPP	464.90	3.70	480.00	3.41	15.10	-0.30
	TBP	598.25	2.45	598.50	2.50	0.25	0.05
	THP	813.70	1.50	813.00	1.51	-0.70	0.01
	TOP	906.00	1.20	906.00	1.17	0.00	-0.03
B (Equity 5 × IL-100)	TEP	317.75	40.90	339.00	40.79	21.25	-0.11
	TIP	360.45	15.55	400.50	15.11	40.05	-0.44
	TPP	464.40	13.85	475.50	13.99	11.10	0.15
	TBP	597.40	5.45	597.00	5.90	-0.40	0.45
	THP	833.80	3.40	834.00	3.69	0.20	0.30

		Predicted		Measured		Difference	
	Compound	1D (s)	2D (s)	1D (s)	2D (s)	1D (s)	2D (s)
	TOP	1065.55	3.05	1059.00	3.34	-6.55	0.29
C (IL-61 × Rtx5)	TEP	513.70	0.68	519.00	0.65	5.3	-0.03
	TIP	528.53	0.60	526.50	0.59	-2.03	-0.01
	TPP	615.17	0.68	613.50	0.68	-1.67	-0.01
	TBP	699.94	0.78	697.50	0.77	-2.44	-0.02
	THP	848.72	1.04	847.50	0.99	-1.22	-0.05
	TOP	865.56	1.58	865.50	1.67	-0.06	0.09
D (IL-100 × Rtx5)	TEP	411.40	0.60	414.00	0.50	2.60	-0.100
	TIP	461.55	0.55	450.00	0.44	-11.55	-0.12
	TPP	500.25	0.60	490.50	0.50	-9.75	-0.09
	TBP	542.25	0.75	538.50	0.63	-3.75	-0.12
	THP	669.35	4.20	700.50	3.66	31.15	-0.54
	TOP	689.35	2.05	733.50	2.88	44.15	0.82

Based on the differences observed in Table 3-2, it is clear that with better chromatography as in cases C and D, the agreement between experimental and predicted results is vastly improved. In setups A and B the ^{1}D error is much worse, where for A the average absolute error is 17.9 s, and for B is 13.3 s, with the largest error coming from the three early

eluting compounds. In comparison to C and D where the average ^{1}D 2.1 s in case C and 17.1 s in D. This difference in absolute error is important because the error between runs may be ±1 modulation period, or ±1.5 s, so as seen in case C, reasonable values for predicted retention time can be obtained. In the second dimension similar results are seen where the average absolute error for setup A is 0.15 s, B is 0.29 s, C is 0.03 s and D is 0.3 s. However, in the case of the second dimension a larger error is expected when there is larger error in the first dimension. As a result retention is predicted at a lower temperature at that point in time than compound actually elutes from the column. In case C since there is a small error in ^{1}D retention times we expect to see a small error in ^{2}D retention times, and this is in fact what we see. In the experimental data an error of ~±0.5 s in run-to-run variance, so for experimental results to agree with predicted values at ±0.03 s shows the power of these types of predictions. Results similar to those seen in C were also expected for setup D, so further investigation into this retention behavior was undertaken.

3.2.3.2 Prediction of Unknowns

With the success of predicting these types of compounds in two dimensions, the concept of predicting an unknown compound from the thermodynamics of known compounds was then tested. For this portion of

the research tri-n-pentyl phosphate (T5P) was treated as an unknown. The thermodynamics for this compound were not previously determined and instead were estimated based on the thermodynamics of the standard compounds (TEP, TPP, TBP, THP and TOP), which are also composed of linear alkane chains. In order to predict our unknown compound we first compiled the thermodynamic parameters of our known compounds. A linear regression of each of our thermodynamic properties is then performed where the thermodynamic parameter values are used in the *y*-axis and carbon number is the *x*-axis, as shown in Figure 3-2.

Thermodynamic parameters of the unknown 15 carbon T5P were then predicted from the linear regression equation, where x is equal to 15. These predicted thermodynamics are used in the same manner as the collected thermodynamics for our standards, as outlined in the introduction, and imported into our MATLAB model to predict the retention times on the columns of interest. The T5P was then also run using the same method as the rest of the standards in two dimensions and its experimental retention time was compared to its predicted retention time in Figure 3-3**.**

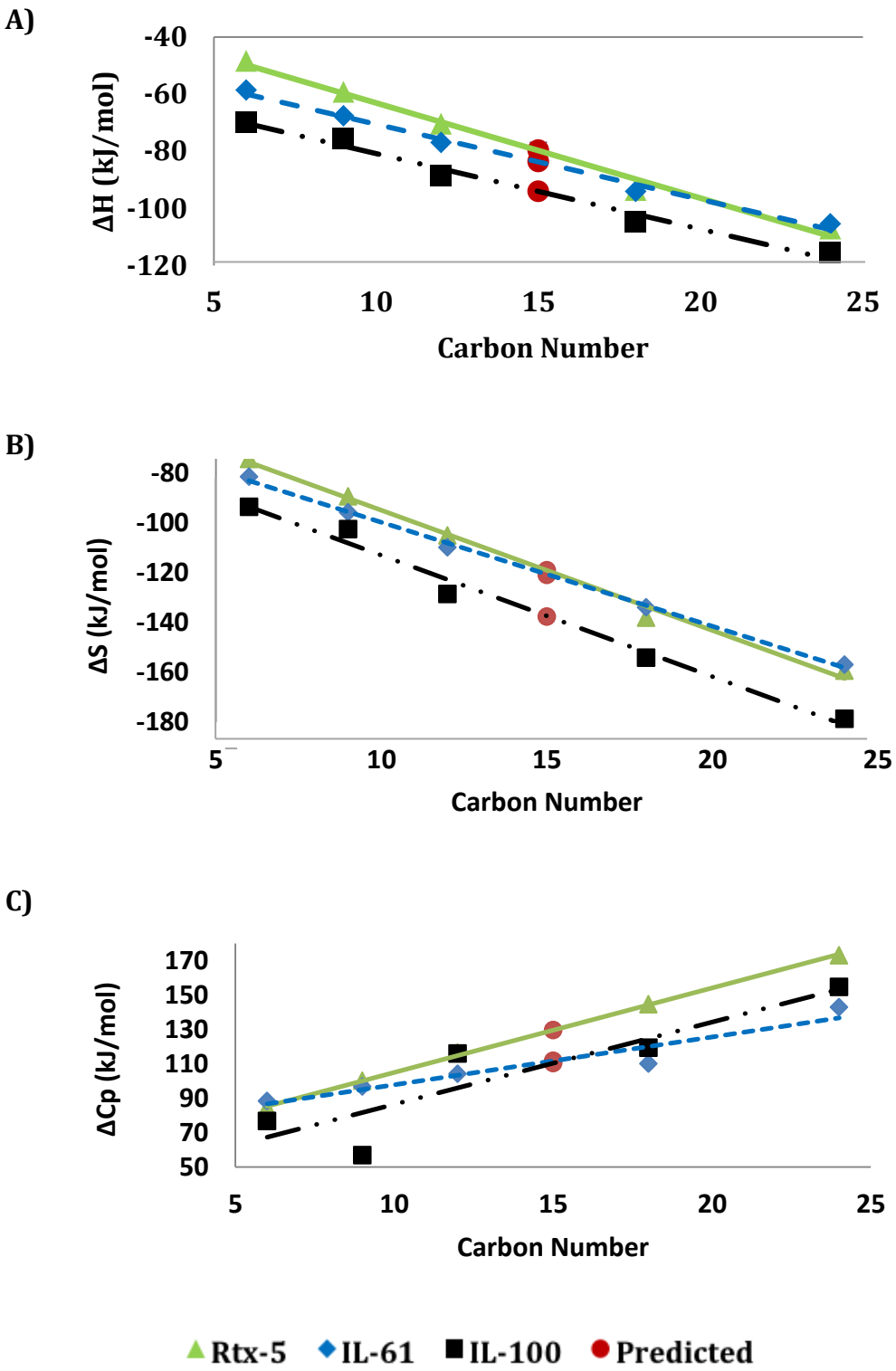

Figure 3-2. Linear regression of each thermodynamic parameter on three different columns. A) $\Delta H(T_0)$ B) $\Delta S(T_0)$ C) ΔC_p.

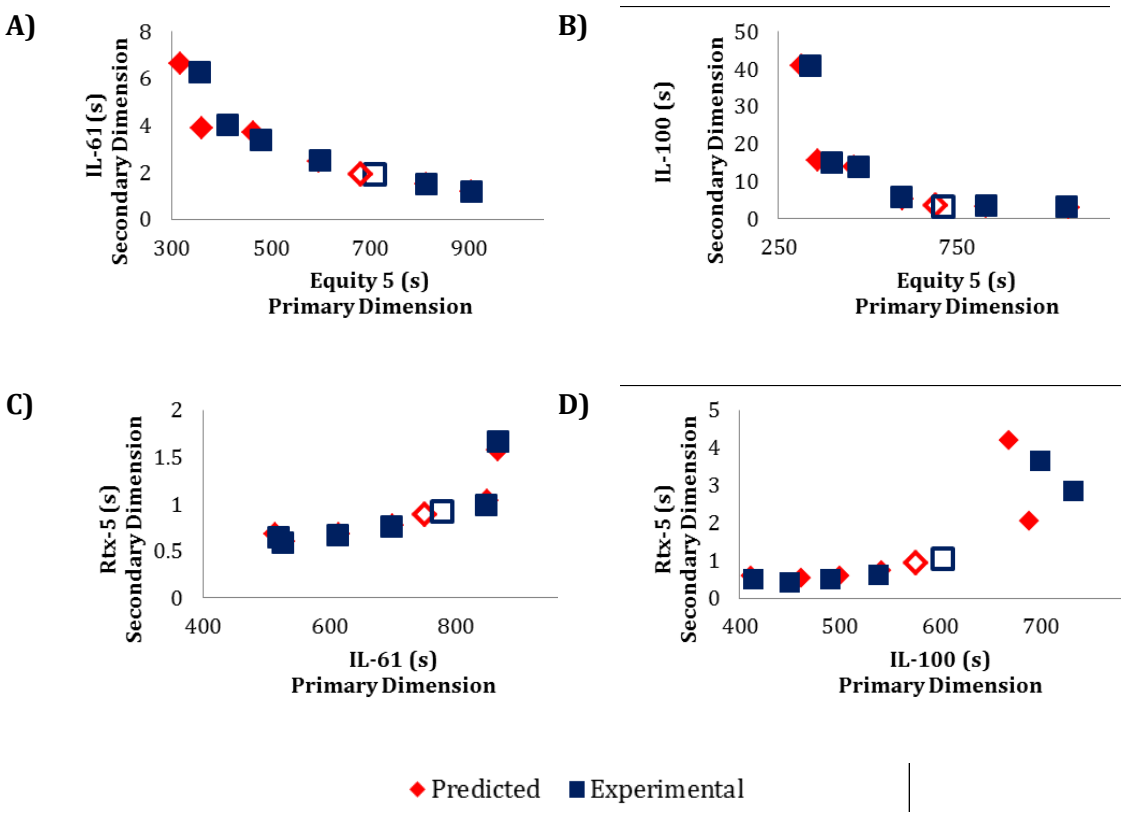

Figure 3-3. Peak apex plots of both experimental and predicted retention times. A) Equity-5ms × IL-61 B) Equity-5ms × IL-100 C) IL-61 × Rtx-5 D) IL-100 × Rtx-5. 'unknown' T5P is shown with the hollow markers.

In this figure it may be noted that in all of the different setups this simple prediction method is capable of giving an approximate retention region for the unknown compound. Although it is clearly not predicted as well as the standard compounds, it can give a chromatographer an idea of which region of the chromatogram needs to be considered. Especially since this method works for two dimensional gas chromatography where the

retention pattern may also be scrutinized. The experimental and predicted retention times are in Table 3-3**.**

Table 3-3. Predicted and measured retention times for tri-pentyl phosphate in four different 2D column set-ups.

		Predicted		**Measured**		**Difference**	
	Compound	1D (s)	2D (s)	1D (s)	2D (s)	1D (s)	2D (s)
A (Equity 5 × IL-61)	T5P	681.90	1.90	711.00	1.90	29.10	0.00
B (Equity 5 × IL-100)	T5P	690.70	3.70	714.00	3.34	33.35	0.36
C (IL-61 × Rtx5)	T5P	750.30	0.89	777.00	0.93	26.70	0.04
D (IL-100 × Rtx5)	T5P	576.70	0.95	603.00	1.07	26.35	0.12

To have more accurate predictions of unknown compounds a model that includes more descriptors for the unknown will be required. Relating the unknown compound to only the carbon number does not give enough information about the compound to give an accurate prediction of retention time.

3.3 Investigation of Alkyl Phosphate Behavior on IL-100 Columns

3.3.1 Retention Time Drift on IL-100

3.3.1.1 Overview

Typical errors for predicting experimental retention times using this method are less than 1 s in the first dimension and less than 0.1 s in the second dimension [113]. Larger errors in predicting experimental retention times for alkyl phosphates on the IL-100 column as in Table 3-2 led to a more in-depth study of this phase. During this investigation it was observed that the retention times of alkyl phosphates were gradually increasing as more and more injections were performed. To determine how much variability was seen over injections, further study was completed on new IL-100 columns. Experiments were also completed as an attempt to determine the cause of such behavior on these columns.

3.3.1.2 Experimental

3.3.1.2.1 Chemicals

Analytes consisted of triethyl phosphate (TEP), tripropyl phosphate (TPP), triisoproyl phosphate (TIP) (Sigma-Aldrich, Oakville, ON, Canada), tributyl phosphate (TBP) (VWR, Mississauga, ON, Canada), trihexyl phosphate (THP), and trioctyl phosphate (TOP) (Alfa Aesar, Ward Hill, MA, USA), docosane (Sigma Aldrich), undecane (Sigma Aldrich), octadecane

(Sigma Aldrich), ethyl toluene (Sigma Aldrich), tetralin (Caledon), naphthalene (Fisher Scientific), dibenzothiophene (Sigma Aldrich), anthracene (Eastman), pyrene (Sigma Aldrich) toluene (Fisher Scientific), ethyl benzene (Fisher Scientific) and para-xylene (Fisher Scientific). ACS grade hexane (Sigma-Aldrich), decane (Acros Organics, Bridgewater, NJ, USA) and carbon disulfide (Fisher Scientific) were used as solvents.

3.3.1.2.2 Instrumentation

Experiments were conducted on a HP6890 GC (HP Agilent Technologies, Missisauga, ON, Canada) using helium as a carrier gas at a linear velocity of ~30 cm s^{-1}. This instrument was equipped with an Agilent 7683 (Agilent Technologies) autosampler. For all experiments, the injection port and detector temperatures were set to 220°C. These compounds were analyzed in a temperature-programmed format with a start temperature of 50°C, ramping at 15°C/min to a maximum temperature of 210°C with a hold time of 30 minutes.

3.3.1.3 Results and Discussion

When running samples of trialkyl phosphates on the IL-100 columns for this thermodynamic study, retention times were gradually increasing. A study was conducted using brand new 30 m IL-100 columns

to investigate this discrepancy. After conditioning according to manufacturer settings (provided with the column), a series of injections alternating multiple runs of individual trialkyl phosphate standards with multiple injections of a mixture of hydrocarbon standards was run repeatedly. The analyses of the hydrocarbon standards are depicted in Figure 3-4, where the vertical black lines indicate a set of phosphate runs. Further conditioning of the column can be seen by the dramatic decrease in retention time in approximately the first 25 runs, which were completed after manufacturer indicated conditioning. Therefore, two sets of points will be considered separately: 1-25 because they were run in the conditioning phase, and 26-41 after conditioning was complete.

Sets of an individual tri-alkyl phosphate were run between the hydrocarbon standards to see if phosphate injections changed the retention of the hydrocarbon standards. If the slope of a plot of injection number *vs.* retention time is different than zero this would indicate that the retention characteristics of the column are changing over time. To test if these values were different than zero a Student's t-test was used, as outlined in Equation 3-1.

$$t_{calculated} = \frac{|\bar{x} - known\ value|}{s}\sqrt{n} \qquad \textbf{(Equation 3-1)}$$

where $\bar{x}$ is the mean, s is the standard deviation and n is the number of measurements. Using Equation 3-1, if $t_{calc} > t_{table}$ the difference is significant.

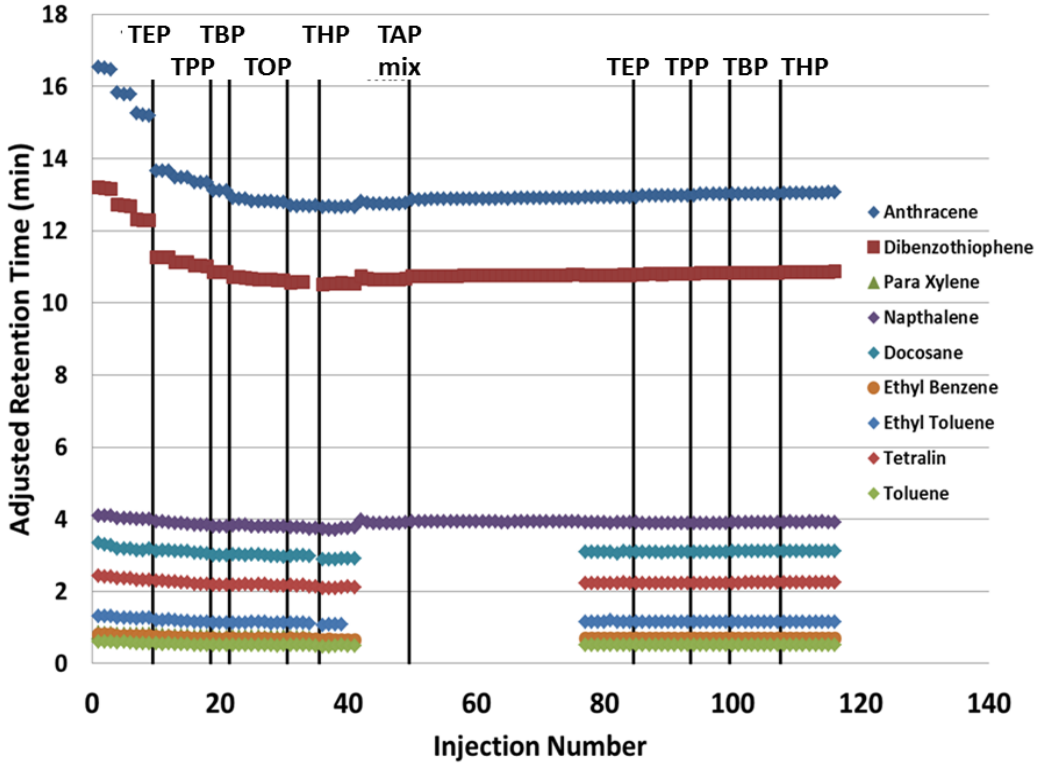

Figure 3-4. Retention time drift of non-phosphate standards on a new IL-100 column. Vertical black lines indicate the replicate injection of a phosphate standard.

As outlined in Table 3-4, in the case of all trialkyl phosphates for runs 1-25 and 26-41, $t_{calc} > t_{table}$(at 99.9%), meaning that the slopes of their respective lines are significantly different than zero. For runs 26-41, they are also trending in a positive manner, meaning that the runs are getting gradually longer. This is unusual as in gas chromatography we would generally expect that run time would decrease as the column ages.

Table 3-4. t-test results from slope of replicate tri-alkyl phosphate injections on a new IL-100 column.

Compound	Sample Range	t_{calc}	DF	t_{table} @ 99.9 %	$t_{calc} > t_{table}$
TEP	1 to 25	20.963	23	3.850	YES
	26-41	91.751	14	4.073	YES
TPP	1 to 25	474.500	23	3.850	YES
	26-41	77.498	14	4.073	YES
TBP	1 to 25	25.972	23	3.850	YES
	26-41	63.293	14	4.073	YES
THP	1 to 41	255.127	23	3.850	YES
	26-41	403.154	14	4.073	YES

The slopes of the line in the region of runs 26-41 were then used to calculate the difference in retention time per injection, as outlined in Table 3-5, where degrees of freedom (DF) is defined by *n-2*.

Table 3-5. Retention time drift over replicate injections for alkyl phosphate standards.

Compound	Sample Range	Slope (min per injection)	Intercept (min)	R^2	Retention difference per injection (s)
TEP	26-41	0.0039	10.11	0.97	0.20
TPP	26-41	0.0044	11.84	0.97	0.26
TBP	26-41	0.0035	15.12	0.95	0.21
THP	26-41	0.0173	25.26	0.998	1.04

Positive slopes indicate that the all of the phosphates tested here have an increasing retention time with replicate injections. The smaller

trialkyl phosphates TEP, TPP and TBP seem to have less of an impact (~0.2 s/injection) as opposed to the longer chain THP that has a relatively large retention difference per injection. If that increase in retention continues over the course of 100 runs for THP, it would have a 1.73 minute difference in retention from run 1 to 100. This makes our careful predictions unreliable over replicate injections.

Further testing was then completed on the hydrocarbon sample runs collected after conditioning of the column to determine if it was specifically the phosphates increasing retention on this column. In Table 3-5 the shaded portion for each compound includes runs 77-116, the separations of runs in groups of 77-82, 84-93, 94-99, 100-107 and 108-116 are the groups of runs that were collected between injections of phosphates, as outlined in Figure 3-4. The slopes of injection number *vs.* retention time of these smaller groups were also tested to see if they were significantly different than 0.

Table 3-6. t-test results for replicate injections of hydrocarbon compounds on a new IL-100 column.

Compound	Sample Range	t_{calc}	DF	t_{table} @ 99.9 %	$t_{calc} > t_{table}$
Anthracene	77-116	142.58	38	3.646	YES
	77-82	3.99	4	8.610	NO
	84-93	8.06	6	5.959	YES
	94-99	4.77	4	8.610	NO
	100-107	9.08	6	5.959	YES/Reverse Trend

Compound	Sample Range	t_{calc}	DF	t_{table} @ 99.9 %	$t_{calc} > t_{table}$
	108-116	19.35	7	5.408	YES
Dibenzothiophene	77-116	188.60	38	3.646	YES
	77-82	3.87	4	8.610	NO
	84-93	7.70	6	5.959	YES
	94-99	5.84	4	8.610	NO
	100-107	-3.87	6	5.959	NO
	108-116	12.69	7	5.408	YES
Napthalene	77-116	32.41	38	3.646	YES
	77-82	2.76	4	8.610	NO
	84-93	3.23	6	5.959	NO
	94-99	7.37	4	8.610	NO
	100-107	15.75	6	5.959	YES
	108-116	2.71	7	5.408	NO
Docosane	77-116	40.32	38	3.646	YES
	77-82	4.00	4	8.610	NO
	84-93	3.45	6	5.959	NO
	94-99	8.60	4	8.610	NO
	100-107	6.25	6	5.959	YES
	108-116	0.57	7	5.408	NO
Ethyl Benzene	77-116	20.68	38	3.646	YES
	77-82	3.46	4	8.61	NO
	84-93	4.01	6	5.959	NO
	94-99	2.31	4	8.610	NO
	100-107	9.45	6	5.959	NO
	108-116	-4.01	7	5.408	NO
Ethyl Toluene	77-116	4.25	38	3.646	YES
	77-82	1.82	4	8.610	NO
	84-93	4.99	6	5.959	NO
	94-99	1.84	4	8.610	NO
	100-107	5.12	6	5.959	NO
	108-116	10.62	7	5.408	YES/Reverse Trend
Tetralin	77-116	29.68	38	3.646	YES
	77-82	2.63	4	8.610	NO
	84-93	5.98	6	5.959	YES/Reverse Trend

Compound	Sample Range	t_{calc}	DF	t_{table} @ 99.9 %	$t_{calc} > t_{table}$
	94-99	4.19	4	8.610	NO
	100-107	12.12	6	5.959	YES
	108-116	8.37	7	5.408	YES/Reverse Trend
Toluene	77-116	15.89	38	3.646	YES
	77-82	3.54	4	8.610	NO
	84-93	6.19	6	5.959	YES/Reverse Trend
	94-99	0.29	4	8.610	NO
	100-107	1.90	6	5.959	NO
	108-116	-6.19	7	5.408	NO

In Table 3-6 it should be noted that the trend for the total set (77-116) of hydrocarbon runs was significantly different than zero for all compounds. The smaller sets of runs (those run between phosphate injections) were subsequently examined. The majority (29/40) of these smaller sets are not significantly different than zero, indicating that the hydrocarbon runs themselves are not contributing to the increase in retention time on the column. If subsequent injections of hydrocarbons were contributing significantly to the change in retention over time we would also expect these slopes to be positive. In the 11 cases that are different than zero, five of them are significantly different than zero but in the opposite direction, meaning that their retention actually decreases over time. The remaining six sections that are significantly different than zero have much smaller t_{calc} values than their total run, as expected. Following this trend, it is inferred that the majority of the increase in

retention time over all of the runs was due to the injection of phosphates onto the column.

In an attempt to confirm the significance of the change after injection of phosphate compounds, t-tests were performed to determine whether the difference between the means of each set of runs was significant using **(Equation 3-2)**.

$$t_{calculated} = \frac{|\overline{x_1} - \overline{x_2}|}{\sqrt{\frac{s_1^2}{n_1} + \frac{s_2^2}{n_2}}} \qquad \textbf{(Equation 3-2)}$$

where $\bar{x}$ is the mean, s is the standard deviation and n is the number of measurements. Using Equation 3-2, if $t_{calc} > t_{table}$ the difference is significant. If the difference in means were significant this would indicate that the injection of phosphate samples between sets of hydrocarbon runs is significantly changing the retention time of the hydrocarbon standards. The degrees of freedom for this calculation are found using Equation 3-3, and the results of these calculations are summarized in Table 3-7.

$$Degrees\ of\ Freedom = \left\{ \frac{\left(\frac{s_1^2}{n_1} + \frac{s_2^2}{n_2}\right)^2}{\frac{\left(\frac{s_1^2}{n_1}\right)^2}{n_1 + 1} + \frac{\left(\frac{s_2^2}{n_2}\right)^2}{n_2 + 1}} \right\} - 2 \qquad \textbf{(Equation 3-3)}$$

Table 3-7. Between set t-test results for replicate injections of hydrocarbon standards on an IL-100 column.

Compound	Sample Range	t_{calc}	DF	t_{table} @ 99 %	Significantly Different
Anthracene	(77-82) vs (108-116)	52.10	10	3.169	YES
	(77-82) vs (84-93)	27.94	10	3.169	YES
	(84-93) vs (94-99)	6.62	6	3.707	YES
	(94-99) vs (100-107)	0.89	5	4.032	NO
	(100-107) vs (108-116)	13.12	10	3.169	YES
Dibenzothiophene	(77-82) vs (108-116)	55.72	11	3.105	YES
	(77-82) vs (84-93)	28.08	12	3.054	YES
	(84-93) vs (94-99)	6.97	6	3.707	YES
	(94-99) vs (100-107)	5.51	5	4.032	YES
	(100-107) vs (108-116)	14.75	9	3.250	YES
Napthalene	(77-82) vs (108-116)	14.72	13	3.012	YES
	(77-82) vs (84-93)	7.45	11	3.106	NO
	(84-93) vs (94-99)	0.42	11	3.106	NO
	(94-99) vs (100-107)	17.18	12	3.054	YES
	(100-107) vs (108-116)	3.00	14	2.977	YES
Docosane	(77-82) vs (108-116)	44.34	12	3.054	YES
	(77-82) vs (84-93)	0.21	5	4.032	NO
	(84-93) vs (94-99)	4.05	8	3.355	YES

Compound	Sample Range	t_{calc}	DF	t_{table} @ 99 %	Significantly Different
	(94-99) vs (100-107)	7.37	7	3.450	YES
	(100-107) vs (108-116)	4.71	10	3.169	YES
Tetralin	(77-82) vs (108-116)	27.60	12	3.054	YES
	(77-82) vs (84-93)	9.66	8	3.355	NO
	(84-93) vs (94-99)	0.42	11	3.106	NO
	(94-99) vs (100-107)	26.53	11	3.106	YES
	(100-107) vs (108-116)	4.83	14	2.977	YES
Ethyl Toluene	(77-82) vs (108-116)	18.06	11	3.106	YES
	(77-82) vs (84-93)	8.60	10	3.169	NO
	(84-93) vs (94-99)	0.27	11	3.106	NO
	(94-99) vs (100-107)	24.14	9	3.250	YES
	(100-107) vs (108-116)	5.15	15	2.947	YES
Ethyl Benzene	(77-82) vs (108-116)	16.12	11	3.106	YES
	(77-82) vs (84-93)	8.82	10	3.169	NO
	(84-93) vs (94-99)	0.42	12	3.054	NO
	(94-99) vs (100-107)	15.30	7	3.495	YES
	(100-107) vs (108-116)	4.21	15	2.947	YES

Compound	Sample Range	t_{calc}	DF	t_{table} @ 99 %	Significantly Different
Toluene	(77-82) vs (108-116)	11.24	10	3.169	YES
	(77-82) vs (84-93)	8.78	12	3.054	NO
	(84-93) vs (94-99)	0.29	10	3.169	NO
	(94-99) vs (100-107)	13.23	8	3.355	YES
	(100-107) vs (108-116)	2.54	14	2.977	NO

The results of these t-tests show that after multiple injections of phosphates, as evidenced by the t-test of the first set of runs (77-82) versus the last set of runs (108-116), in every case there was significant change in retention time. It is also interesting that in the case of (77-82 *vs.* 84-93) there is no significant change in retention for all but the two most retained compounds. This comparison (77-82 vs 84-93) was performed before and after running tri-ethyl phosphate, our smallest phosphate standard, which was expected to have less of an impact on the column. However, in the case of THP between sets (100-107) and (108-116) significant change was noted for all but the least retained compound (toluene). The toluene runs do not show significant drift, but this is expected as it elutes from the column extremely quickly. It may also be noted in this table that the magnitude of the drift was greater for more-retained compounds such as anthracene and dibenzothiophene. Therefore, THP has the greatest impact

on changing retention, and standard compounds that are more retained are affected more by this change.

3.3.2 Calibration Curve Consistency

3.3.2.1 Overview

After observing significant changes in retention over repeat injections on the IL-100 phase, further investigation into the phenomenon of alkyl phosphate interaction with the ionic liquid columns was explored. Based on results in the previous section, it was hypothesized that a reaction is happening between the alkyl phosphates and the ionic liquid phase in such a way that the entire phosphate sample is not reaching the detector. To examine this further the following section will focus on the slope of the calibration curves on ionic liquid columns versus conventional 5% phenyl columns.

3.3.2.2 Experimental

3.3.2.2.1 Chemicals

Analytes consisted of triethyl phosphate (TEP), tripropyl phosphate (TPP), triisoproyl phosphate (TIP) (Sigma-Aldrich, Oakville, ON, Canada), tributyl phosphate (TBP) (VWR, Mississauga, ON, Canada), trihexyl phosphate (THP), and trioctyl phosphate (TOP) (Alfa Aesar, Ward Hill, MA, USA), undecane (Sigma Aldrich), octadecane (Sigma Aldrich), and

naphthalene (Fisher Scientific). Carbon disulfide (Fisher Scientific) was used as solvent.

3.3.2.2.2 Instrumentation

Experiments were conducted on a HP6890 GC (HP Agilent Technologies, Mississauga, ON, Canada) using helium as a carrier gas at a linear velocity of ~30 cm s^{-1}. This instrument was equipped with an Agilent 7683 (Agilent Technologies) auto sampler. For all experiments, the injection port and detector temperatures was 220°C. These compounds were analyzed in a temperature-programmed format with a start temperature of 50°C, ramping at 12.5°C/min to a maximum temperature of 210°C with a hold time of 30 minutes. IL-100, IL-111 and IL-61 Supelco ionic liquid columns were compared with a 5% methyl/95% dimethyl polysiloxane column, as outlined in Section 2.2.3.

3.3.2.3 Results and Discussion

From the behavior of the alkyl phosphates on the IL-100 column we hypothesized from the structure shown in Figure 2-1 that a reaction is occuring between the alkyl phosphates and the imidazolium ring of the stationary phase. To test the plausibility of this theory, calibration curves were made for the phosphate compounds and two alkane standards on a 5% methyl/95%

dimethyl polysiloxane column as a reference. The calibration curves were then repeated on both an IL-100 and IL-111, which both have imidizolium rings in their cation, as well as on an IL-61 column which employs a phosphonium cation in place of an imidizolium ring. In order to ensure that the ionic liquid column and the 5% methyl/95% dimethyl polysiloxane column were compared as precisely as possible, the 5% methyl/95% dimethyl polysiloxane column was run immediately after each ionic liquid calibration curve, resulting in three different 5% methyl/95% dimethyl polysiloxane column calibrations. The IL-100 and IL-111 runs were run in sequence, while the IL-61 was run at a later date with new solutions. For this reason it is imperative that the IL runs must be compared to their corresponding 5% methyl/95% dimethyl polysiloxane column runs.

A)

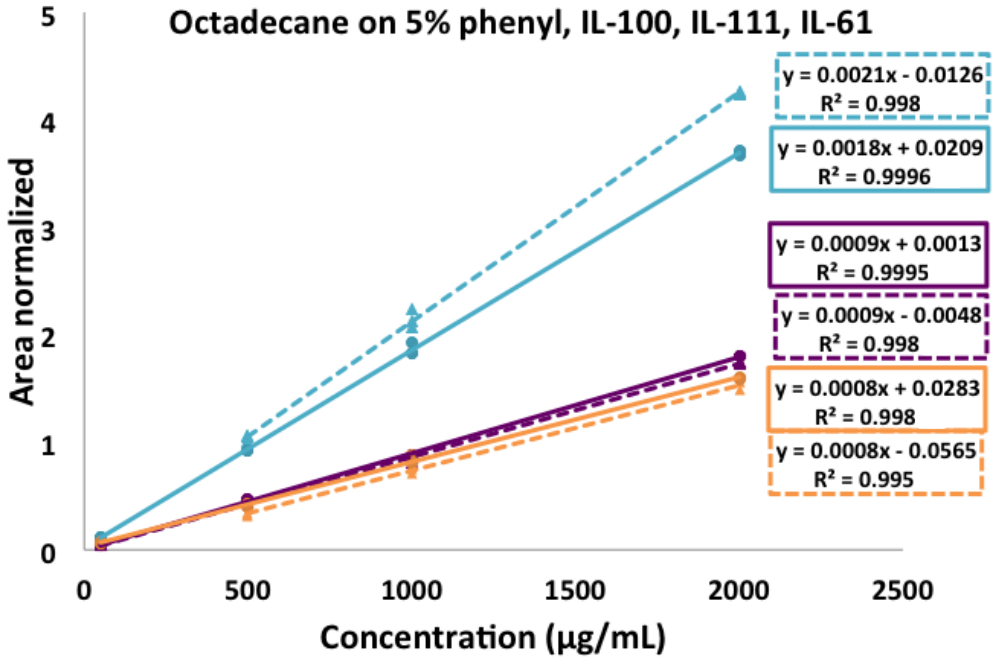
Octadecane on 5% phenyl, IL-100, IL-111, IL-61
Area normalized
Concentration (µg/mL)
0
1
2
3
4
5
0
500
1000
1500
2000
2500
y = 0.0021x - 0.0126
R² = 0.998
y = 0.0018x + 0.0209
R² = 0.9996
y = 0.0009x + 0.0013
R² = 0.9995
y = 0.0009x - 0.0048
R² = 0.998
y = 0.0008x + 0.0283
R² = 0.998
y = 0.0008x - 0.0565
R² = 0.995

B)

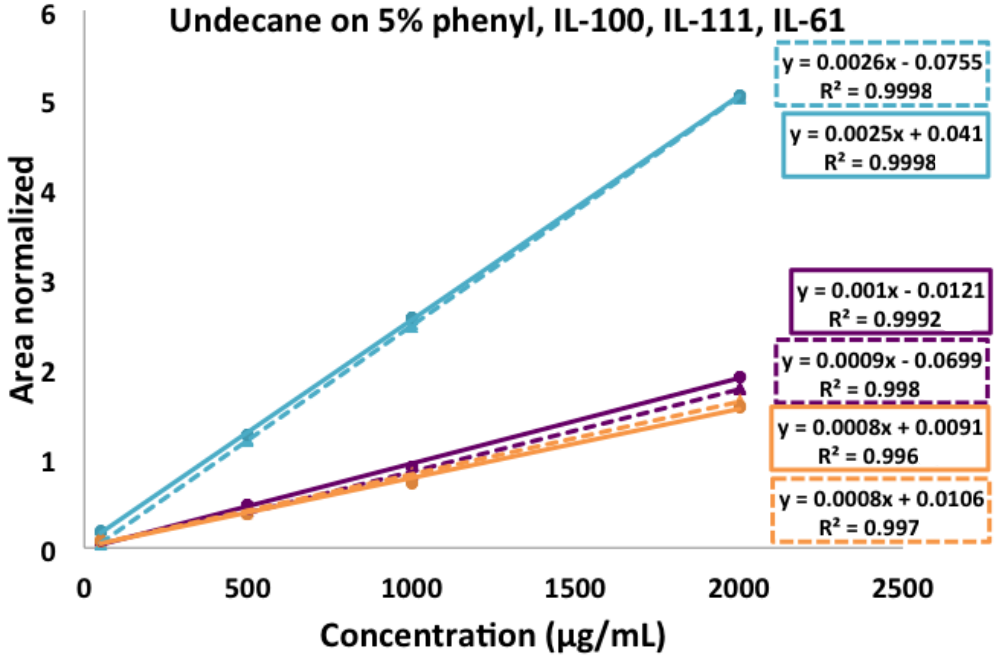
Undecane on 5% phenyl, IL-100, IL-111, IL-61
Area normalized
Concentration (µg/mL)
0
1
2
3
4
5
6
0
500
1000
1500
2000
2500
y = 0.0026x - 0.0755
R² = 0.9998
y = 0.0025x + 0.041
R² = 0.9998
y = 0.001x - 0.0121
R² = 0.9992
y = 0.0009x - 0.0699
R² = 0.998
y = 0.0008x + 0.0091
R² = 0.996
y = 0.0008x + 0.0106
R² = 0.997

C)

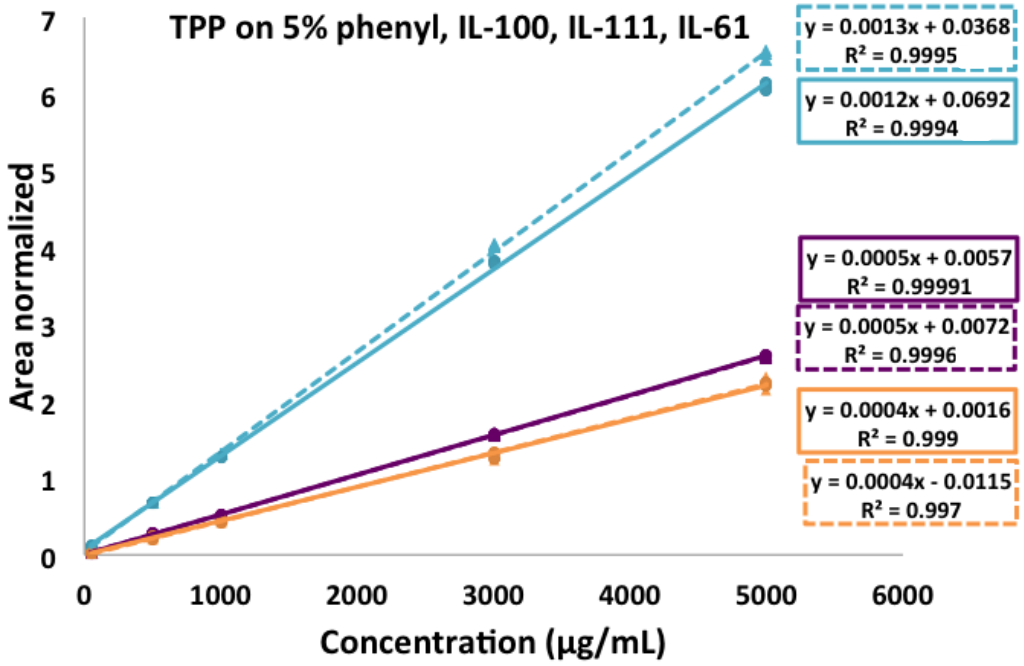
TPP on 5% phenyl, IL-100, IL-111, IL-61
Area normalized
Concentration (µg/mL)
y = 0.0013x + 0.0368
R² = 0.9995
y = 0.0012x + 0.0692
R² = 0.9994
y = 0.0005x + 0.0057
R² = 0.99991
y = 0.0005x + 0.0072
R² = 0.9996
y = 0.0004x + 0.0016
R² = 0.999
y = 0.0004x - 0.0115
R² = 0.997

D)

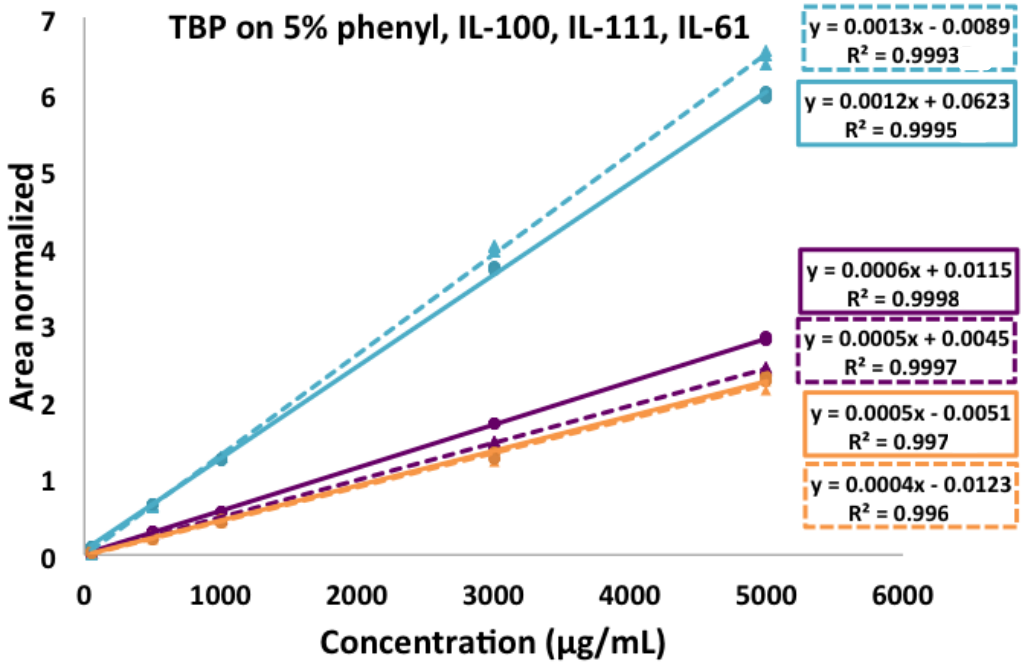
TBP on 5% phenyl, IL-100, IL-111, IL-61
Area normalized
Concentration (µg/mL)
y = 0.0013x - 0.0089
R² = 0.9993
y = 0.0012x + 0.0623
R² = 0.9995
y = 0.0006x + 0.0115
R² = 0.9998
y = 0.0005x + 0.0045
R² = 0.9997
y = 0.0005x - 0.0051
R² = 0.997
y = 0.0004x - 0.0123
R² = 0.996

E)

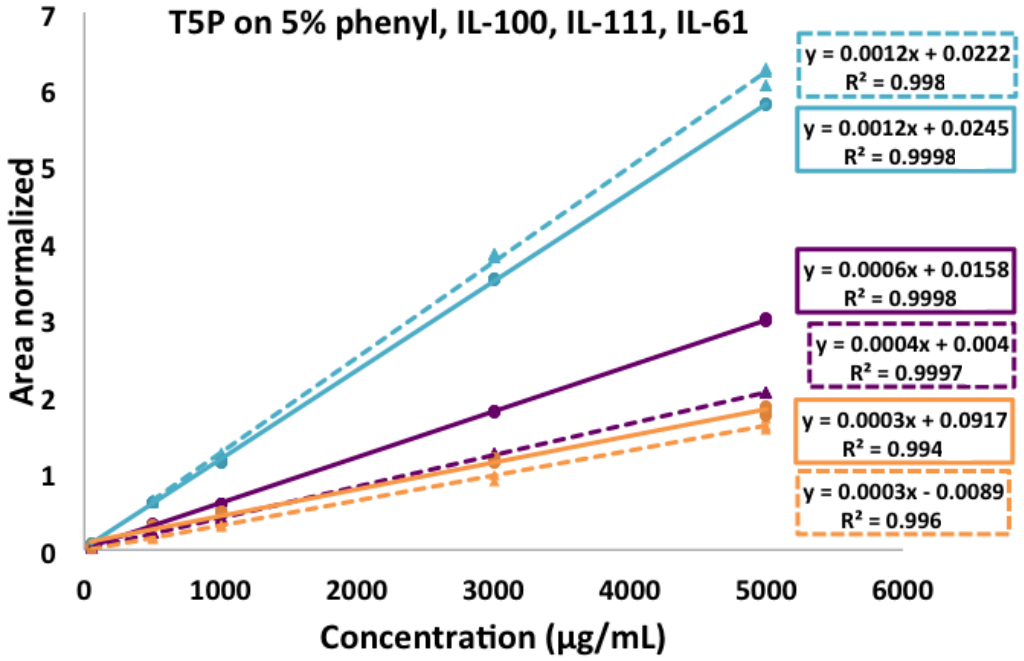
T5P on 5% phenyl, IL-100, IL-111, IL-61
Area normalized
Concentration (µg/mL)
y = 0.0012x + 0.0222
R² = 0.998
y = 0.0012x + 0.0245
R² = 0.9998
y = 0.0006x + 0.0158
R² = 0.9998
y = 0.0004x + 0.004
R² = 0.9997
y = 0.0003x + 0.0917
R² = 0.994
y = 0.0003x - 0.0089
R² = 0.996

F)

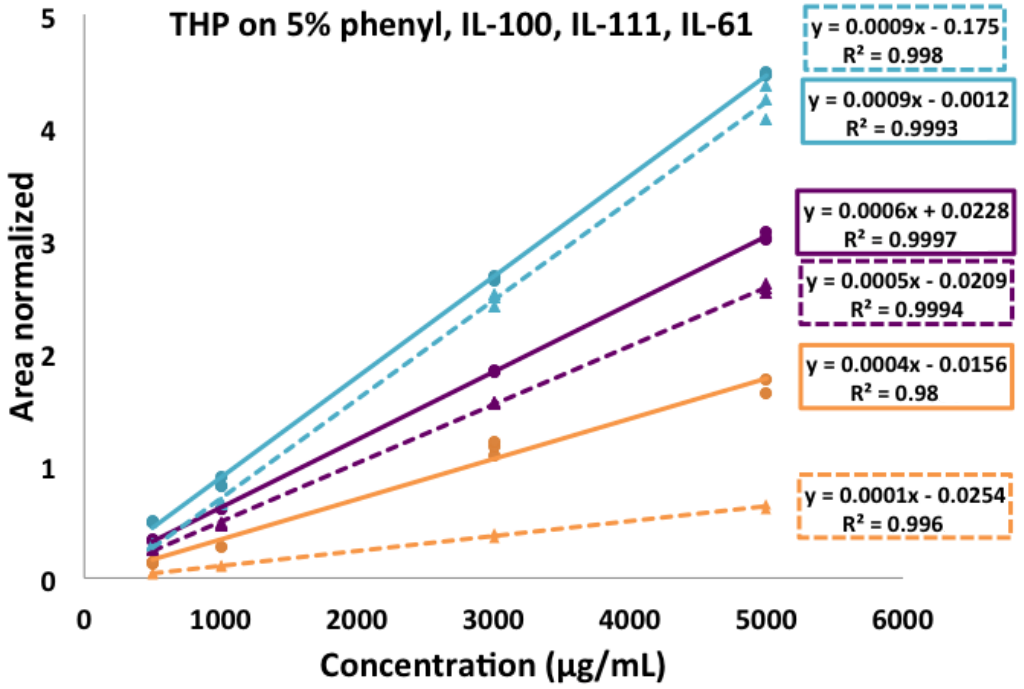
THP on 5% phenyl, IL-100, IL-111, IL-61
Area normalized
Concentration (µg/mL)
y = 0.0009x - 0.175
R² = 0.998
y = 0.0009x - 0.0012
R² = 0.9993
y = 0.0006x + 0.0228
R² = 0.9997
y = 0.0005x - 0.0209
R² = 0.9994
y = 0.0004x - 0.0156
R² = 0.98
y = 0.0001x - 0.0254
R² = 0.996

G)

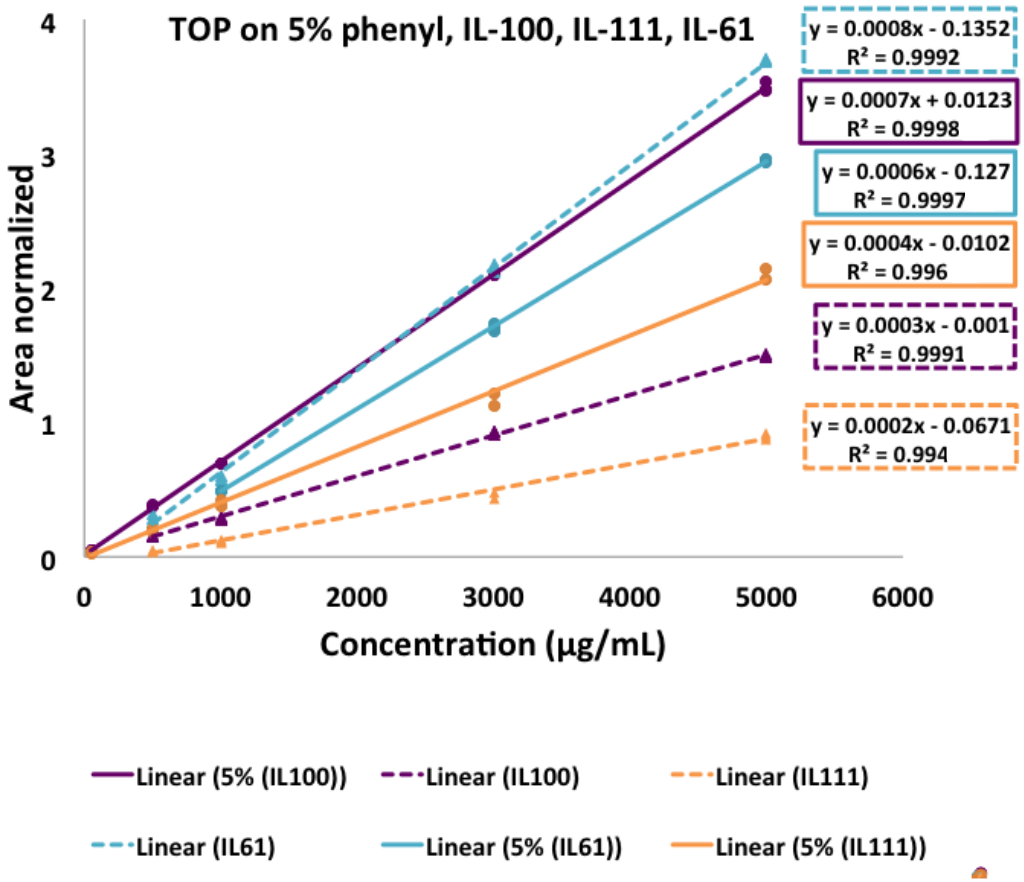

Figure 3-5. Calibration curve comparison for IL-100, IL-111, IL-61 and %5 phenyl. Completed using Napthalene as an internal standard. A) Octadecane B) Undecane C) TPP D) TBP E) T5P F) THP G) TOP.

Figure 3-5 A and B, the calibration curves for the ionic liquid column and its corresponding 5% phenyl curve have very similar slopes (ration of ~1.0). In the case of undecane the ratio of the slopes on IL vs. 5% phenyl are between 1.0 and 1.1. However, as we look at the comparison of curves in Figure 3-5 C-G we note that for IL-100 and IL-111 the slope of the curve is decreased. This trend is more significant the larger the alkyl phosphate, so the largest effect is seen for TOP (G), where the slope of the curve on IL-

100 and IL-111 is drastically smaller than slope for the comparable 5% phenyl curve. The ratio of the slopes on IL-100 and IL-111 vs. 5% phenyl are 2.3 and 2.0 respectively, while IL-61 vs. 5% phenyl is 1.3. The decrease in slope is also more significant for the IL-100 column than for the IL-111. Although, for the IL-61 curves, the slopes match well with their corresponding 5% phenyl phase for all of the compounds. All of this indicates that the phosphates are not quantitatively eluting from the column, with the IL-100 column being affected the most. This non-quantitative elution is also observed on the IL-111 to a lesser extent, and is not observed for the IL-61 column.

To examine whether this non-quantitative elution is due to a reaction occurring between the column and the alkyl phosphate compounds, nuclear magnetic resonance (NMR) was performed. NMR was performed on a pure sample of IL-100, pure sample of trioctyl phosphate and a mixture of IL-100 and TOP heated together in an oil bath at 180°C for 1 hour under a nitrogen atmosphere.

A)

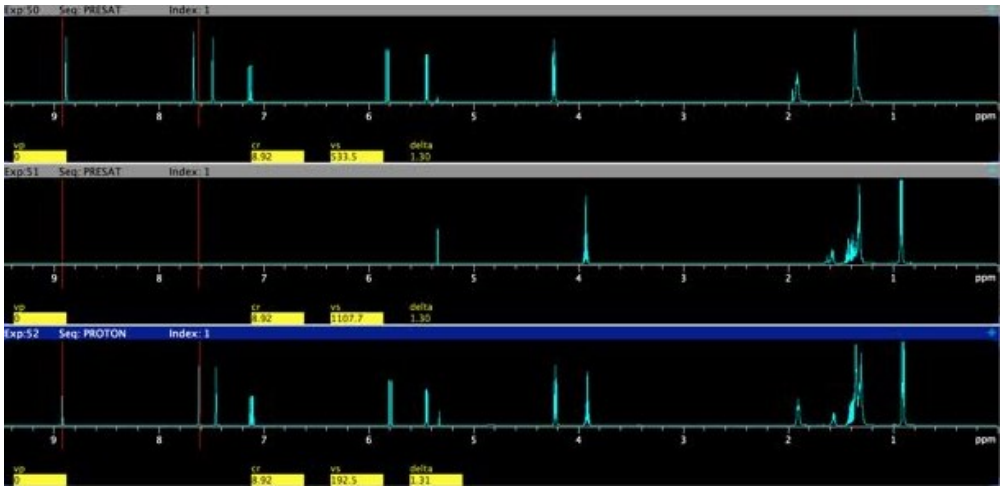
Exp:50 Seq: PRESAT Index: 1
ppm
vp cr vs delta
0 8.92 533.5 1.30
Exp:51 Seq: PRESAT Index: 1
ppm
vp cr vs delta
0 8.92 1107.7 1.30
Exp:52 Seq: PROTON Index: 1
ppm
vp cr vs delta
0 8.92 192.5 1.31

B)

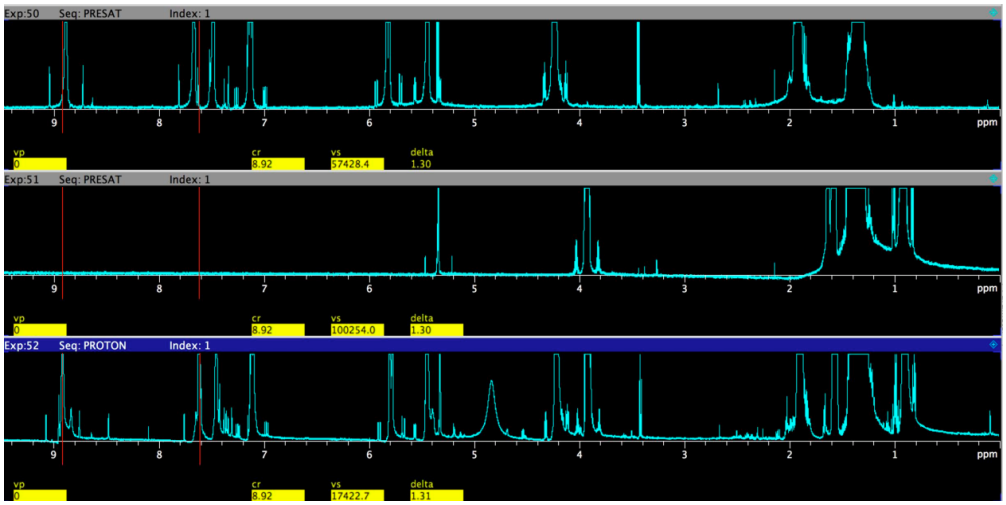
Exp:50 Seq: PRESAT Index: 1
ppm
vp cr vs delta
0 8.92 57428.4 1.30
Exp:51 Seq: PRESAT Index: 1
ppm
vp cr vs delta
0 8.92 100254.0 1.30
Exp:52 Seq: PROTON Index: 1
ppm
vp cr vs delta
0 8.92 17422.7 1.31

C)

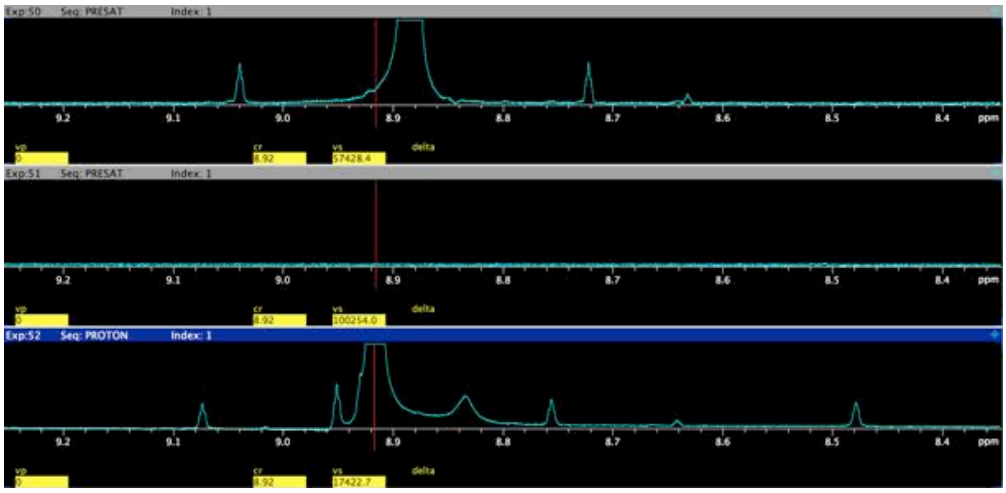
Exp:50 Seq: PRESAT Index: 1
9.2 9.1 9.0 8.9 8.8 8.7 8.6 8.5 8.4 ppm
vp 0
cr 8.92
vs 17428.4
delta
Exp:51 Seq: PRESAT Index: 1
9.2 9.1 9.0 8.9 8.8 8.7 8.6 8.5 8.4 ppm
vp 0
cr 8.92
vs 100254.0
delta
Exp:52 Seq: PROTON Index: 1
9.2 9.1 9.0 8.9 8.8 8.7 8.6 8.5 8.4 ppm
vp 0
cr 8.92
vs 17422.7
delta

D)

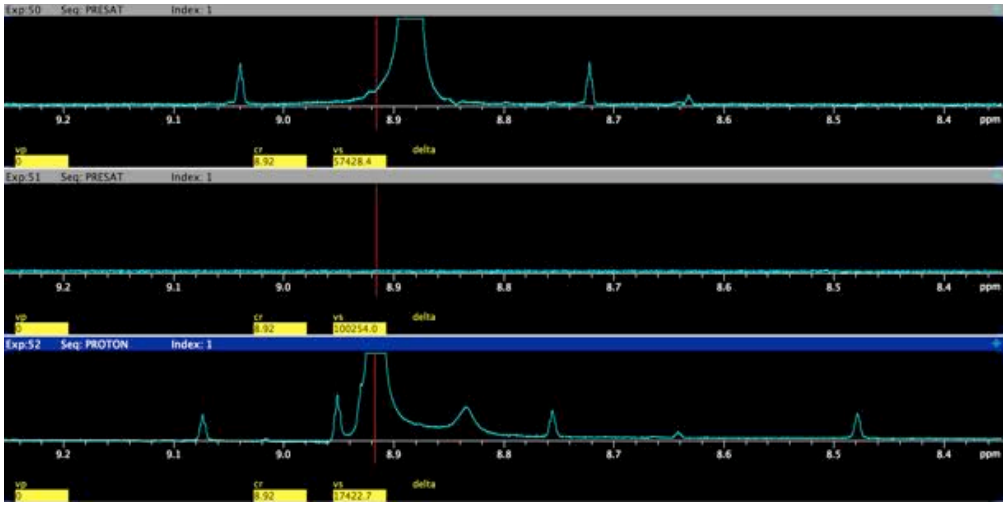
Exp:50 Seq: PRESAT Index: 1
9.2 9.1 9.0 8.9 8.8 8.7 8.6 8.5 8.4 ppm
vp 0
cr 8.92
vs 17428.4
delta
Exp:51 Seq: PRESAT Index: 1
9.2 9.1 9.0 8.9 8.8 8.7 8.6 8.5 8.4 ppm
vp 0
cr 8.92
vs 100254.0
delta
Exp:52 Seq: PROTON Index: 1
9.2 9.1 9.0 8.9 8.8 8.7 8.6 8.5 8.4 ppm
vp 0
cr 8.92
vs 17422.7
delta

E)

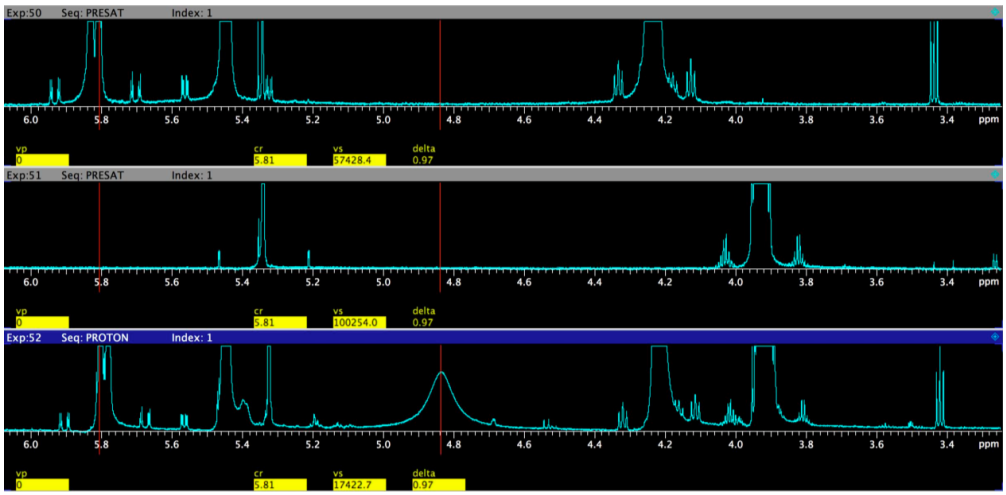

F)

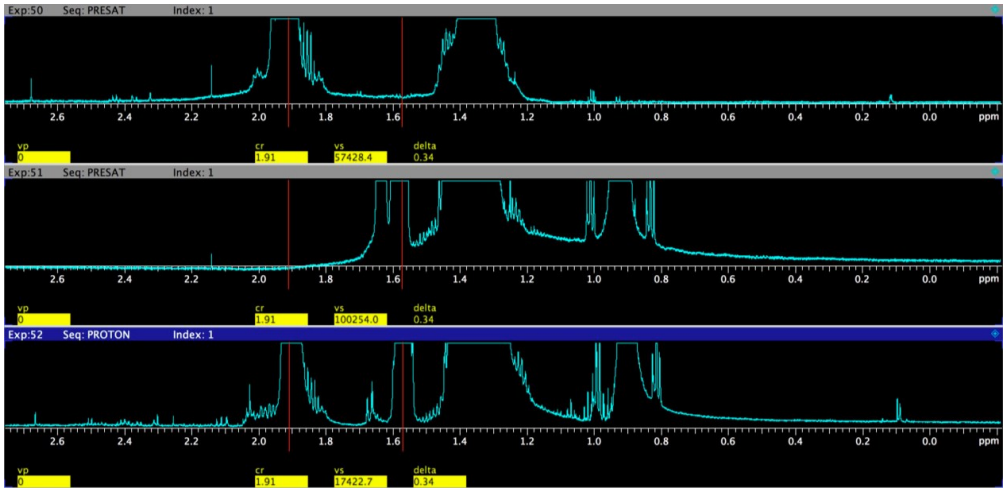

Figure 3-6. ^{1}H NMR Experiments. In A-F Top = SB-IL-100 by itself Middle = TOP Bottom = SB-IL-100 with TOP cooked. A) Full Experiment B) Vertical scale expansion C) Downfield expansion D) Expansion of 6.8 to 8ppm E) Expansion 3.3 to 6ppm F) Up field region

Figure 3-6 A-F show the results for both the ionic liquid phase and alkyl phosphate separately, as well as the result of the two of them being heated at 180°C for 1 hour. Figure 3-6 B is a substantial vertical scale expansion of all three samples to better observe the small peaks near the baseline, two peaks in the downfield/aromatic region do not line up

perfectly. The vertical scale was arbitrarily chosen with the ^{13}C satellite peaks (~60-75 Hz either side of the main peak) at about 50% of the vertical height. These are ~0.5% natural abundance and indicate how small the amount of change is before and after heating. While there are a few peaks not present in either of the starting materials, they have very low abundance having peaks substantially below or close to the 0.5% ^{13}C satellite peaks. While there are small changes occurring after mixing and heating, only a small fraction of total material is changing. Figure 3-6 C-D show various expansion regions where subtle shifts can be noted, but cannot be positively identified at this point in time.

Although we are currently unsure of the exact reaction taking place, the NMR results suggest that there is a reaction taking place. Based on this evidence in conjunction with the fact that there was a noted decrease in calibration slope for the columns with an imidizolium ring it is most likely that the imidizolium ring is the source of reaction. Previous research has documented similar reactions of imidazole groups [114,115,116,117]. Based on this information, Figure 3-7 outlines our proposed mechanisms of reaction.

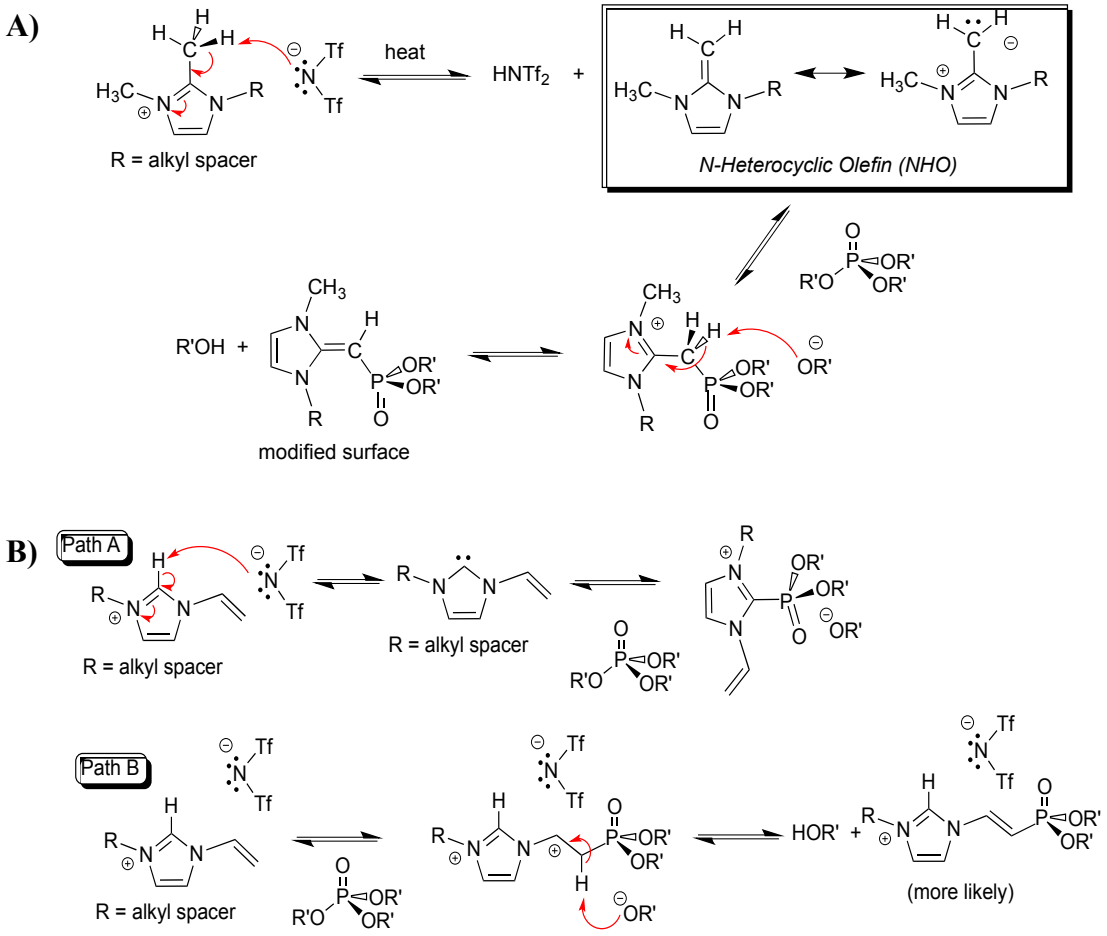

Figure 3-7. Proposed mechanism for reaction of alkyl phosphates with a capillary column. A) IL-111 and B) IL-100.

The reaction mechanisms are slightly different for the two columns because there are different substituents on the imidizolium rings. In the case of IL-111, the reaction is happening on the imidizolium ring at the position of the methyl substituent. The phosphate forms a bond with the methyl carbon on the imidizolium ring. However, in the case of the IL-100 the substituent on the imidizolium ring is a vinyl group, leading to two

different possibilities. Either the phosphate can react at the vinyl group or on the imidizolium group itself. Since the vinyl group is a fairly reactive group, path B is most likely the pathway the compounds are taking. Coupled with the information from our calibration curves, where we noted that the extent of reaction was higher on the IL-100 versus IL-111, it seems likely that pathway B or a combination of A and B are used on the IL-100 column.

3.4 Conclusions

3.4.1 Prediction Capability

Prediction of alkyl phosphate compounds in GC and GC×GC can be a useful tool for identification of unknowns. By using a prediction model in conjunction with the selectivity of an ionic liquid capillary column challenging separations and identifications become possible. However, these prediction models need to be used carefully and with reliable gas chromatographic data. In the case of the alkyl phosphate standards retention behavior could be reliably predicted when the chromatography was performing well (i.e. non-tailing peaks, repeatable retention times).

Prediction of retention behavior of alkyl phosphates in GC is a possible route towards tools that may be used to help predict the structures of unknown alkyl phosphates based on retention in GC or GC×GC. This was demonstrated by the prediction of T5P (unknown) in the

column setups used in this chapter. Further work will be required to fine-tune the prediction of unknowns based on more molecular descriptors (e.g., number of bonds, polarity of molecule, size of molecult, etc.). However, current work proves that even using a minimum of descriptive values a reasonable prediction can be made. This type of unknown predictive model on these unique columns will be a good candidate for aiding in the identification of unknown phosphates in petroleum samples by GC or GC×GC.

3.4.2 IL-100 Investigation

In the study of a new IL-100 column, a set of non-phosphate compounds (e.g., hydrocarbons) were analyzed to test the column between sets of phosphates. There were significant drifts in retention time for both the phosphates and the hydrocarbon samples. These drifts in retention time over replicate injections make discrepancies between the predicted and experimental values plausible. Further study, including reaction kinetics and phosphorus NMR, as well as collaboration with Supelco (Bellefonte, PA) will be necessary to determine why this behavior is observed on the IL-100 columns.

3.4.3 Calibration Curve Investigation

Calibration curve investigations were completed by comparing slopes of three different ionic liquid columns with 5% phenyl column slopes indicated non-quantitative elution from IL-100 and IL-111, but not IL-61. The two ionic liquid columns with decreased calibration curve slopes, compared to the 5% phenyl curve, employ imidizolium rings in the cations of their stationary phase. It was inferred that a reaction is occurring between the ionic liquid column and the alkyl phosphate compounds. Our theory is further confirmed by changes in the NMR spectra when the column compound and our phosphate are heated together. Reaction with the phase creates problems for both predictions of retention time (as it is not constant) and quantitative measurements (due to reaction with the column). Further work will need to be completed to precisely confirm our hypothesized reaction.

CHAPTER FOUR: Development and Optimization of a Method for Separating Diesel Fuels According to Hydrocarbon Group-Type by Gas Chromatography.

4.1 Introduction

The American Society for Testing Materials (ASTM) method D-5186-03 is used to determine the aromatic and polycyclic aromatic hydrocarbon (PAH, two or more aromatic rings) content of diesel and aviation turbine fuels in North America [118]. This ASTM method employs Supercritical Fluid Chromatography (SFC) with a carbon dioxide mobile phase and a flame ionization detector (FID) to separate and detect diesel fuel components according to compound class (i.e. group-type separation). Unfortunately, the SFC equipment used to perform this analysis is now very difficult to access. Very few suppliers offer SFC-FID instrumentation, and those SFC-FID instruments that are available suffer from poor reliability. In addition there are a limited number of companies who are able to service these instruments when they fail. As a result, few labs are equipped to perform this analysis, and therefore a replacement method is required.

Group-type separations of diesel fuel have been reported in the literature using gas chromatography (GC) [119-122], high performance

liquid chromatography (HPLC) [123-127] and a number of hyphenated techniques including LC-GC [128,129], SFC-GC [130], and SFC-mass spectrometry (MS) [131]. Many of which have been reviewed recently [132,133,134]. Most commonly HPLC (i.e. UV) detectors yield a non-uniform response for saturates and aromatics [120, 135, 136, 137], mandating the use of complex calibrations. However, the use of an FID provides reliable mass quantification of the different hydrocarbon group-types [120,135,136,137]. When more complex hyphenated techniques are used, reliable quantitation becomes more difficult, especially when mass spectrometric detectors are employed. These detectors have non-uniform responses in group-type separations [120], making these more complex techniques less practical for routine analysis.

4.2 Comparison of Ionic Liquid Stationary Phases

4.2.1 Overview

Ionic liquid (IL) stationary phases for GC exhibit several properties that show great potential for petroleum separations, including: unique selectivity for polyaromatic hydrocarbons over aliphatic compounds, and much higher thermal stabilities than conventional polar phases [138,139,140]. Therefore, determining which IL stationary phase exhibits the greatest selectivity for aromatic group-types versus saturated compounds is of utmost importance. The preferred setup was tested using

a GC-FID system, as this is the least expensive, most robust option with very easy detector calibration for hydrocarbon samples.

To have accurate diesel group-type determination, high aromatic group-type resolution is necessary, while maintaining the resolution of saturates and aromatics [120]. To achieve the best separation possible, several IL columns offering different phase chemistries are studied in this chapter. The columns are assessed primarily on the basis of whether they can achieve high resolution between the different hydrocarbon groups: saturates, mono-, di-, tri- and polyaromatics.

4.2.2 Experimental

4.2.2.1 Chemicals

Initial testing was performed using seven model compounds: docosane (Sigma Aldrich), ethyl toluene (Sigma Aldrich), tetralin (Caledon), naphthalene (Fisher Scientific), dibenzothiophene (Sigma Aldrich), anthracene (Eastman) and pyrene (Sigma Aldrich). For method development a further three compounds were added: toluene (Fisher Scientific), ethyl benzene (Fisher Scientific), and para-xylene (Fisher Scientific). Model compound samples were prepared by dissolving each compound in ACS grade carbon disulfide (Fisher Scientific) at a concentration of 1000 μg/mL.

4.2.2.2 Instrument

Experiments were conducted on a HP6890 GC-FID (Agilent Technologies, Mississauga, ON, Canada) using helium as a carrier gas at a linear velocity of ~30 cm s^{-1}. This instrument was equipped with an Agilent 7683 auto sampler (Agilent Technologies). The injector and detector temperature were set to 10 °C below the maximum operating temperature for each column.

4.2.2.3 Stationary Phases

The IL columns studied were all 30 m × 250 μm with 0.2 μm films provided by Supelco (Oakville, ON, Canada). The columns used are listed in Table 4-1.

Table 4-1. Ionic liquid stationary phases.

Column Identifier	Stationary Phase	Maximum Temperature °C
SLBIL-59	1,12-di(tripropylphosphonium)dodecane bis(trifluoromethylsulfonyl)imide	300
SLBIL-61	1,12-Di(tripropylphosphonium)dodecane bis(trifluoromethylsulfonyl)imide trifluoromethylsulfonate	290

Column Identifier	Stationary Phase	Maximum Temperature °C
SLBIL-76	Tri(tripropylphosphoniumhexanamido)triethyl amine bis(trifluoromethylsulfonyl)imide	270
SLBIL-82	1,12-Di(2,3-dimethylimidazolium)dodecane bis(trifluoromethylsulfonyl)imide	270
SLBIL-100	1,9-Di(3-vinylimidazolium)nonane bis(trifluoromethylsulfonyl)imide	230
SLBIL-111	1,5-Di(2,3-dimethylimidazolium)pentane bis(trifluoromethylsulfonyl)imide	270

4.2.2.4 Procedure

To Each IL column was tested using a number of starting temperatures, ramp rates, and initial hold times to determine if different conditions significantly affected the resolution. All of the columns were then compared using the same method on each column. Once the best column was chosen based on the group-type separation results, a Box-Behnken design of experiment was used to optimize the analytical method [141,142]. Box-Behnken for three parameters requires the use of a high, low and medium level for each parameter to determine the optimal conditions based on maximized resolution. Using this method, 12 different

experiments and one control were created to test three ramp rates, three start temperatures and three initial hold times, as outlined in Table 4-2.

Table 4-2. List of Box-Behnken experiments performed.

Experiment	Ramp (°C/min)	Start T (°C)	Hold Time (min)
1	3	60	3
2	20	60	3
3	3	120	3
4	20	120	3
5	3	90	0
6	20	90	0
7	3	90	6
8	20	90	6
9	10	60	0
10	10	120	0
11	10	60	6
12	10	120	6
Control	10	90	3
Control	10	90	3
Control	10	90	3
Control	10	90	3

4.2.2.5 Calculations

Determining the resolution between the latest eluting model compound of one group-type versus the earliest eluting model compound of the next group-type is one way of quantifying the degree of separation between two group-types. Resolution, R_S, between two group-types such as mono- and diaromatics was calculated based on:

$$R_S = \frac{2(t_{r2} - t_{r1})}{(W_2 + W_1)} \qquad \textbf{(Equation 4-1)}$$

where t_{r1} and t_{r2} are the retention times of the latest eluting monoaromatic and the earliest eluting diaromatic model compounds studied, respectively. W_1 and W_2 are the baseline peak widths of the latest eluting monoaromatic and the earliest eluting diaromatic model compound studied, respectively. A resolution ≤0 indicates that model compounds from the respective group-types were eluting in the wrong order. For example, docosane is a saturate model compound and naphthalene is a diaromatic compound. To achieve group-type separation between saturates and diaromatics, all saturates would elute before all diaromatics. Therefore, if docosane elutes after naphthalene, the group-type resolution would be less than zero even if the two compounds were baseline resolved.

The order of elution on all columns tested had the saturate compound elute later than monoaromatics. In some cases the saturate also eluted later than the diaromatic compound. Therefore, the resolutions

were calculated assuming an elution order of monoaromatics, saturates, diaromatics and finally tri/polyaromatics. This is not necessarily an accurate representation of the resolution between monoaromatics and saturates, as smaller saturate compounds would overlap the monoaromatic region, but it allows for direct comparison of all of the columns studied. With these guidelines, the resolution between monoaromatics and saturates was determined by tetralin and docosane, saturates versus diaromatics was determined by docosane and naphthalene, diaromatics and polyaromatics resolution was calculated based on dibenzothiophene and anthracene, and finally triaromatics versus polyaromatics was determined by anthracene and pyrene. However, the resolution for monoaromatics versus saturates is represented as a negative resolution, because ideally the saturates would elute before the monoaromatics, so the greater the resolution between the two groups, the worse result it actually is. This same logic was followed for saturates versus diaromatics on columns where the saturates eluted between the diaromatics. Using this method, the more negative the resolution the worse overlap there is between the two groups.

4.2.3 Results and Discussion

To determine which column would give the best group-type resolution initial testing was completed on six different IL columns, where

each column was run with a start temperature of 60°C, an initial hold time of 3 minutes, and a ramp rate of 3°C/min, to directly compare their results. To ensure that a different start temperature, ramp rate, or initial hold time, would not allow significantly better group-type separation, a number of combinations were tested. Different columns were compared on the basis of their group-type resolution. Determining the resolution between latest eluting model compound of one group-type versus the earliest eluting model compound of the next group-type is one way of quantifying the degree of separation between two group-types, using Equation 4-1. Where, for example the diaromatic versus triaromatic resolution is calculated using the earliest eluting triaromatic and the latest eluting diaromatic model compound. A resolution of zero or less than zero indicates that model compounds from different group-types are eluting the in the wrong order. For example, docosane is a saturate model compound and napthalene is a diaromatic compound. Therefore, if docosane elutes after napthalene, the group-type resolution would be zero or less than zero even if the two compound were baseline resolved.

Since docosane eluted later than monoaromatics on all columns, and overlap with saturates and diaromatics was observed on some columns, the resolutions were calculated assuming an elution order of monoaromatics, saturates, diaromatics and finally tri/polyaromatics. This is not necessarily an accurate representation of the resolution between monoaromatics and

saturates, as smaller saturate compounds would overlap the monoaromatic region, but it allows for direct comparison of all of the columns studied. With these guidelines the resolution between monoaromatics and saturates is determined by tetralin and docosane, saturates versus diaromatics is determined by docosane and naphthalene, diaromatics and triaromatics resolution is calculated based on dibenzothiophene and anthracene, and finally triaromatics versus polyaromatics is determined by anthracene and pyrene. Using this method, the more negative the resolution the worse overlap there is between the two groups.

In comparing six different IL columns, it was found that only IL-100 and IL-111 were able to separate the saturate compounds from the diaromatic compounds, using any feasible separation conditions. Figure 1 shows the direct comparison of group-type resolution on the six different columns. It is clear in this figure that SLBIL-59, SLBIL-61, SLBIL-76 and SLBIL-82 are not capable of separating the saturate compounds from the diaromatic compounds. The negative resolutions for this group-type separation occur because on these columns docosane (saturate) elutes between naphthalene (diaromatic) and dibenzothiophene (diaromatic). When compared to SLBIL-100 and SLBIL-111 which show significant resolution between the saturates and diaromatics, it becomes readily apparent that SLBIL-100 and SLBIL-111 would make much better choices for group-type separation of saturates and

aromatics. This is a promising result as Krupcik et al., also found that these two IL columns were useful for quantitative analysis of BTEX samples [143].

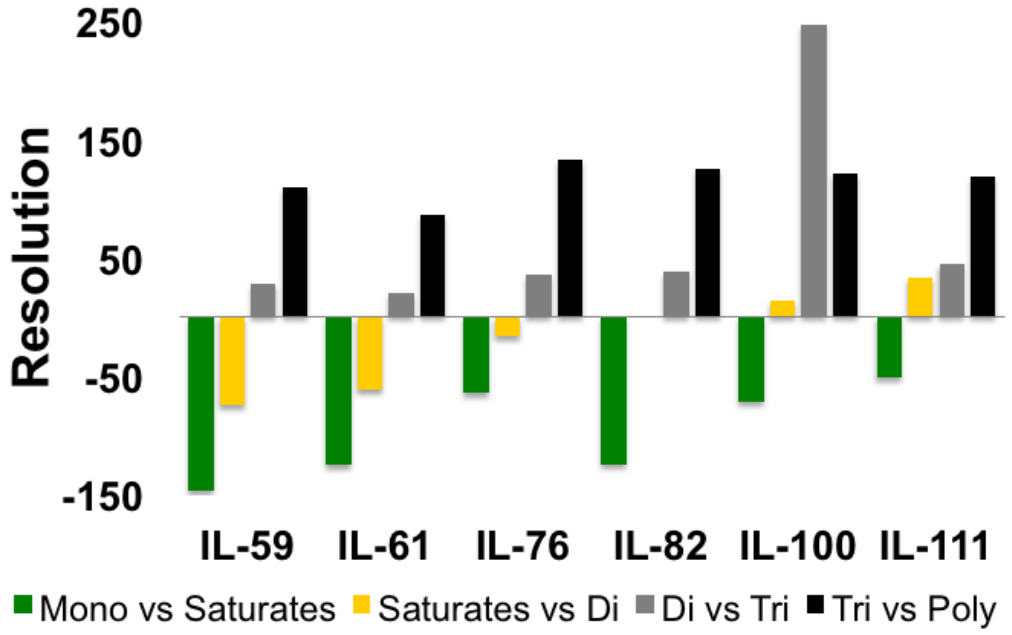

Figure 4-1. Comparison of group-type resolution on a number of ionic liquid columns.

Comparing only SLBIL-100 and SLBIL-111 in Figure 1, it becomes apparent that SLBIL-111 is capable of the best resolution for saturate versus diaromatic compounds. This is the crucial group-type and requires the best resolution, as long as there is still sufficient resolution between the remainder of the group types. Another promising result is that the closer the monoaromatic versus saturate is to zero the better progress there is towards reducing the degree of overlap of these two groups; and it can be seen in this

figure that SLBIL-111 is closer to zero for monoaromatic versus saturates than SLBIL-100. Therefore, further experiments were done using SLBIL-111, to determine the optimal method for this group-type separation. A Box-Behnken design of experiment was used to determine the necessary twelve experiments outlined in Table 4-1 [141,142]. Once these experiments were carried out, the data were analyzed to find the optimal conditions for three parameters: ramp rate, hold time and start temperature. Table 4-2 shows the three parameters that were chosen for each variable.

Table 4-3. Test parameters for variables in method optimization.

	Low	Medium	High
Ramp Rate (°C/min)	3	10	20
Start Temperature (°C)	60	90	120
Hold Time (min)	0	3	6

Once the results from these experiments were collected, Box-Behnken design calculations were completed, yielding three surface plots for each group-type separation (e.g. three surface plots for monoaromatics versus saturates). Figure 4-2 shows the resulting surface plots.

A) Ramp rate vs Start T (M v S)

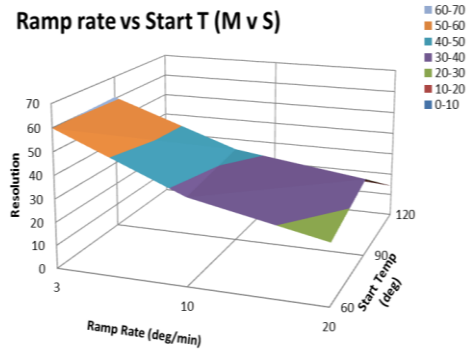

B) Ramp rate vs Hold time (M v S)

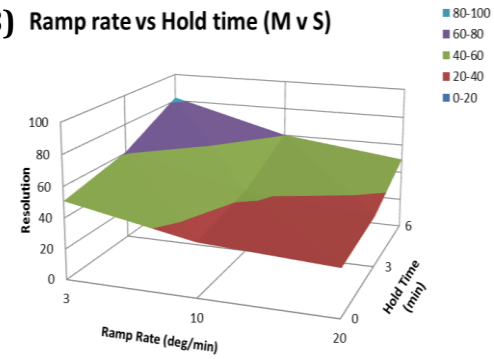

C) Start Temp vs Hold Time (M v S)

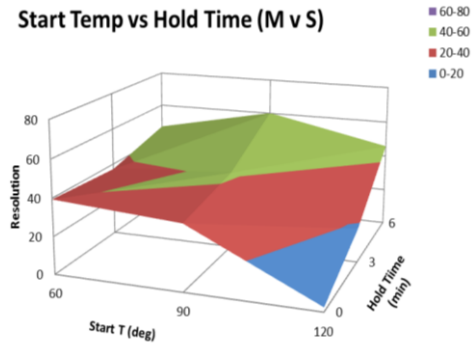

D) Ramp Rate vs Start Temp (S v D)

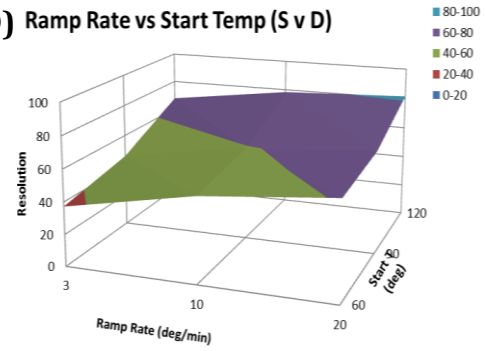

E) Ramp Rate vs Hold Time (S v D)

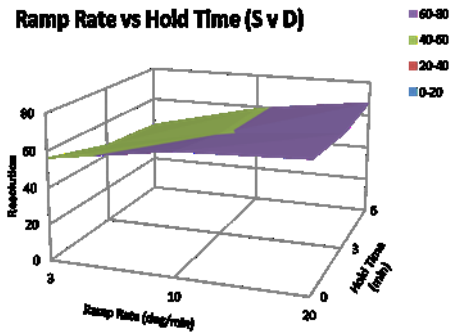

F) Start T vs Hold Time (S v D)

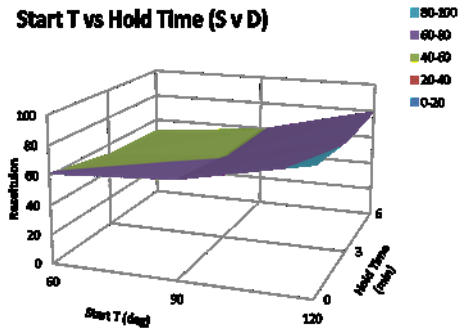

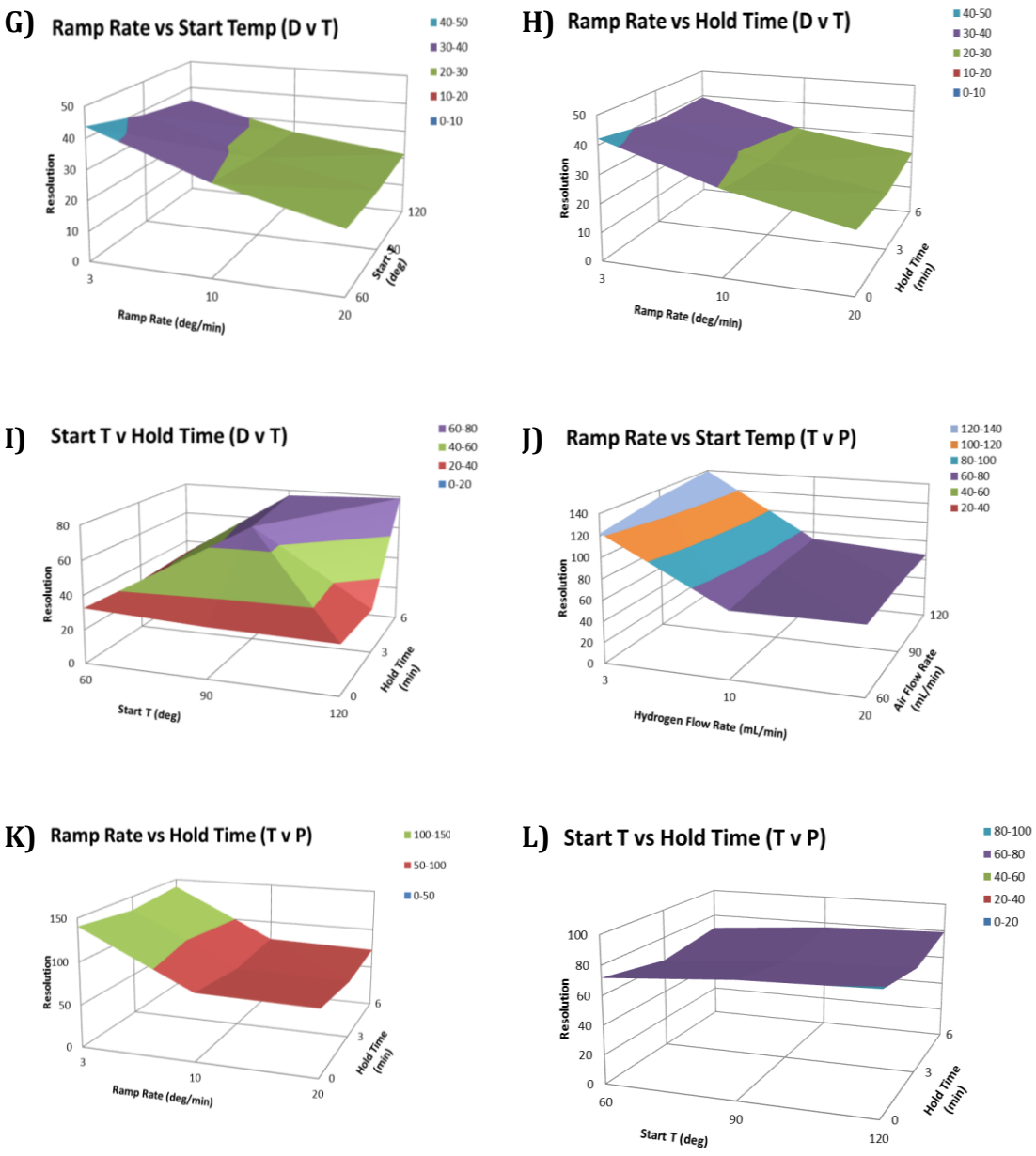

Figure 4-2. Box-Behnken surface plots, testing ramp rate, start temperature and hold time. (A – C) Monoaromatics (M) vs Saturates (S), (D – F) Saturates vs Diaromatics (D), (G – I) Diaromatics vs Triaromatics (T), (J – L) Triaromatics vs Polyaromatics (P).

By finding the maxima on the surface plot, the optimal conditions for each parameter can be determined. For instance in Figure 4-2A the maximum is located in the front left quadrant, with a resolution around 60. At this point the surface plot suggests an optimal ramp rate of 3 °C/min and an optimal start temperature of 120 °C. This process is then repeated for each plot as summarized in Table 4-4.

Table 4-4. Optimal parameters based on Box-Behnken surface plots. Monoaromatics (M) vs Saturates (S), Saturates vs Diaromatics (D), Diaromatics vs Triaromatics (T), and Triaromatics vs Polyaromatics (P).

Surface Plot	Optimal Ramp Rate (°C/min)	Optimal Start Temp (°C)	Optimal Hold Time (min)
A (M v S)	3	120	-
B (M v S)	3	-	6
C (M v S)	-	90	6
D (S v D)	20	120	-
E (S v D)	20	-	0 or 6
F (S v D)	-	120	0
G (D v T)	3	60	-
H (D v T)	3	-	0
I (D v T)	-	120	6
J (T v P)	3	120	-
K (T v P)	3	-	0 or 6
L (T v P)	-	120	0

In examining each of the four group-type parameters separately it is determined that for monoaromatics (M) vs. saturates (S), diaromatics (D) vs. triaromatics (T) and T vs. polaromatics (P) while S vs. D had an optimal ramp rate would be 3°C/min with S v D being the outlier with the optimal ramp rate of 20°C/min. For start temperature all group type results indicate that a temperature of 120°C would be optimal. In the case of hold time M v S is the only group that does not match the hold time of 0 minutes, but rather has an optimal hold of 6 minutes. Based on these results a start temperature of 120°C should be used with a 0 minute hold time. However, the results of the ramp rate are not as clear cut, because the critical group-type separation is for saturates versus the diaromatics. Since we want to optimize the group-type separations it is important to look at the consequences of using both the 3°C/min and the 20°C/min ramp rate.

First we will consider the effect of using a 20°C/min ramp on the resolution of the other group types by locating the resolution in the plots located at 20°C/min, 120°C and 0 minute hold time. Second we will consider the effect of using a 3°C/min ramp rate, with 120°C start temperature and 0 min hold on saturate versus diaromatic resolution. If the second route is taken the lowest resolution observed is still quite large, where we preserve the maximum resolutions from other group types, while still having a minimum resolution of 56 for saturate vs diaromatic compounds. Therefore, based on these model compounds the final optimized conditions chosen

were; start temperature of 120 °C, 0 minute hold time and a ramp rate of 3 °C/min.

4.2.4 Conclusions

Comparison of numerous ionic liquid capillary columns demonstrates the ability of the very polar ionic liquid phases IL-100 and IL-111 to selectively retain aromatic hydrocarbons. This selectivity for aromatic hydrocarbons over saturates will allow the group-type separation of petroleum products. These columns are also capable of group-type separation of polyaromatic hydrocarbons, which is an extremely important step in replacing the current ASTM D5186 method. In the optimized GC-FID method developed in this work; more than sufficient resolution is achieved for saturates vs diaromatics, diaromatics vs triaromatics, and triaromatic vs polyaromatics, using the model compounds tested. The best results were seen using a start temperature of 120 °C with a 0 minute hold time and a ramp rate of 3 °C/min. Unfortunately, this current set-up will only allow for separation of aromatics that are diaromatic and larger to be separated from saturates. To make this technique a plausible replacement for the current ASTM method, the saturates must also be separated from the monoaromatic compounds. To accomplish this, further work in Chapter 5 will be undertaken to study a selective detector for separation of the monoaromatics from saturates.

4.3 Use of an ultraviolet absorption detector in conjunction with a flame ionization detector

4.3.1 Overview

Using a one-dimensional gas chromatograph allows for the simplest instrumentation to replace the current SFC method ASTM D5186; this is of utmost importance since this GC is readily available in industrial laboratories. Based on the results in Section 4.2.3, use of an ionic liquid column will only allow separation of aromatics that are diaromatic and larger to be separated from saturates. This necessitates a secondary method of separating the saturates from the monoaromatics. One relatively simple way to do this is by selective detection. As discussed in Section 1.3.4, the typical FID detector employed in GC responds to all analytes containing a carbon-hydrogen bond, while a UV detector only responds to compounds that absorb UV light. Conveniently, aromatic compounds absorb UV light and saturate compounds cannot. Therefore, by combining FID and UV detectors at the end of the GC column it will be possible to differentiate the signal at the FID that is due to the saturates and the portion due to monoaromatics. This set-up may be accomplished by having a flow cell UV detector at the end of the GC column, so that the column effluent leaves the column, enters the UV flow cell for detection, and then enters the FID. Using UV detection in GC is fairly new and there are not many instruments currently equipped with this detector. SRI (Torrance,

CA, USA) introduced a GC with the capability of using UV and FID in series as is depicted in Figure 4-3.

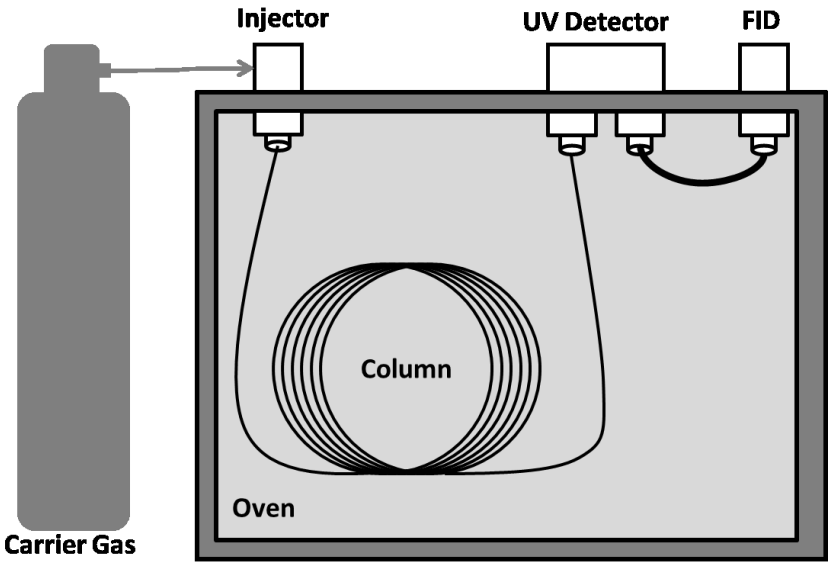

Figure 4-3. Schematic of GC-UV-FID instrument.

This setup works well because the UV detector is non-destructive and responds to compounds with Pi-electrons (aromatics), and then the sample is transferred to the FID where all hydrocarbon compounds are detected. By comparing the UV and FID signals it will be possible to determine how much of the FID response is due to saturates and how much is due to aromatics.

4.3.2 Experimental

4.3.2.1 Chemicals

Initial testing was performed using a mixture of four monoaromatics: toluene (Fisher Scientific), ethyl benzene (Fisher Scientific), para-xylene (Fisher Scientific) and ethyl toluene (Sigma Aldrich). Further testing was completed using ten model compounds: docosane (Sigma Aldrich), ethyl toluene (Sigma Aldrich), tetralin (Caledon), naphthalene (Fisher Scientific), dibenzothiophene (Sigma Aldrich), anthracene (Eastman), pyrene (Sigma Aldrich), toluene (Fisher Scientific), ethyl benzene (Fisher Scientific), and para-xylene (Fisher Scientific). Model compound samples were prepared by dissolving each compound in ACS grade carbon disulfide (Fisher Scientific) to 1000 μg/mL.

4.3.2.2 Instrumentation

The GC used for this portion of the research was an SRI 8619C (Torrance, CA, USA) equipped with UV and FID detectors. Running in constant pressure mode helium carrier gas was used at a linear velocity of ~30 cm/s at the highest column temperature. The injector and detector temperatures were set to 10 °C below the maximum temperature for the column used. Initial testing was completed using a 5% phenyl column Rtx-5 (Restek) with dimensions of 30 m × 250 μm with 0.25 μm and 15 m ×

530 µm with 0.5 µm film thickness, followed by studies conducted on the IL-111 (Supelco) 30 m × 250 µm with 0.2 µm film thickness.

4.3.2.3 Procedure

Initially the four compound mix was used to make sure peaks were visible on both detectors. Based on the results different parameters and columns were then tested to see if performance could be improved for either detector. All separations were performed under constant pressure conditions, where the pressure was set so that at the highest oven temperature the linear velocity was ~30 cm/s. The separations were started at 40 °C (5 min), with a temperature programmed rate of 10 °C/min to a final temperature of 200 °C. Previously determined instrument settings were then used with our ten component mixture in conjunction with the IL-111 column, using the column conditions that were shown to work best in Section 4.2.3 (start temperature of 120 °C, 0 minute hold time and a ramp rate of 3 °C/min).

4.3.3 Results and Discussion

Initially the system was configured as the manufacturer of the GC recommended, with a 0.53 mm inner diameter column. Initial testing was

completed using a 5% phenyl phase. The column was connected directly to the FID by passing the UV detector, as outlined in Figure 4-4.

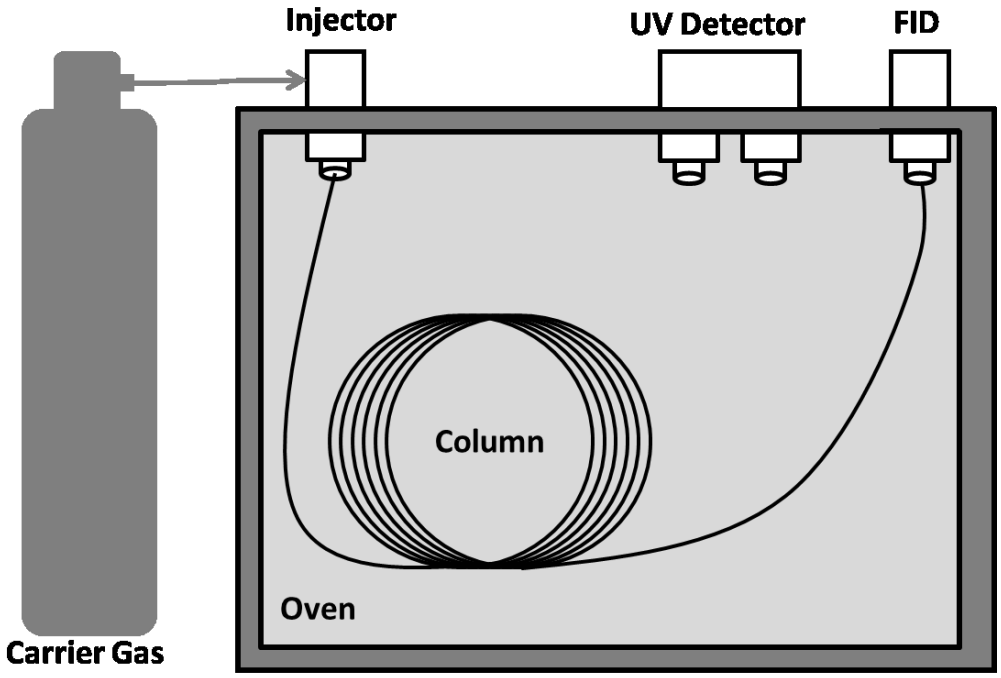

Figure 4-4. Schematic diagram of initial configuration of GC-UV-FID, bypassing the UV detector.

In this configuration the test mixture was run at two different concentrations, 1000 and 100 μg/mL. Figure 4-5 indicates that the instrument (i.e. injector, column, detector) was performing well with sharp, well-resolved peaks at both concentrations, with an expected intensity decrease from 1000 to 100 μg/mL.

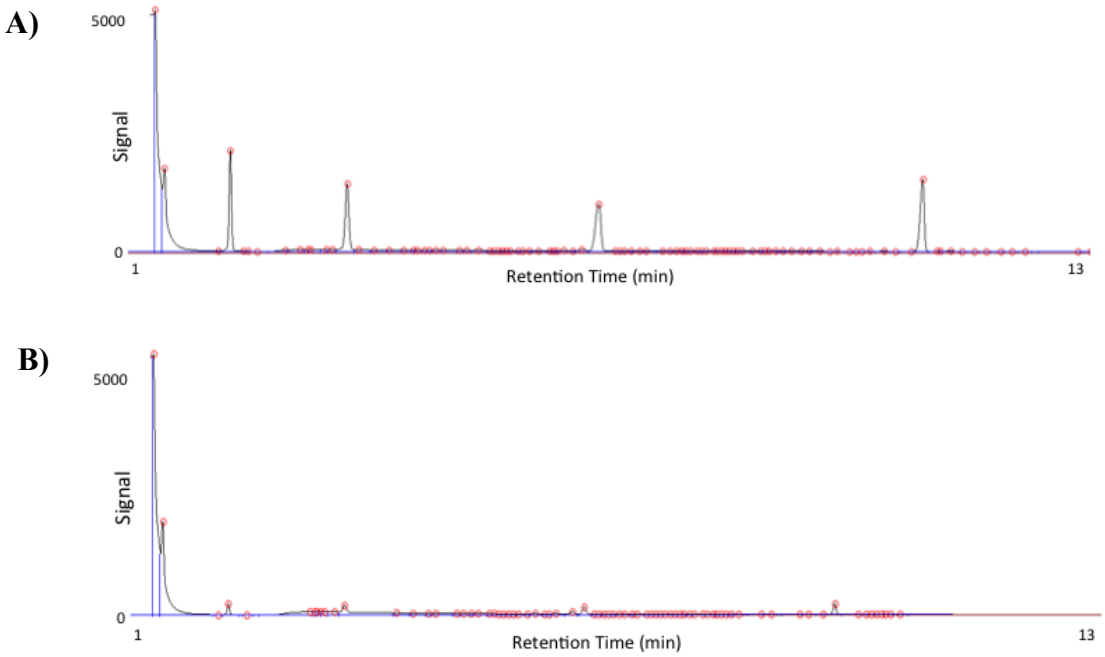

Figure 4-5. FID traces for 0.53 mm inner diameter column. A) 1000 µg/mL B) 100 µg/mL.

The instrument was then reconfigured to use both the UV and FID detectors as intended by the manufacturer. When this was completed the peaks in the FID became small and broad at 1000 µg/mL and undetectable at 100 µg/mL (Figure 4-6).

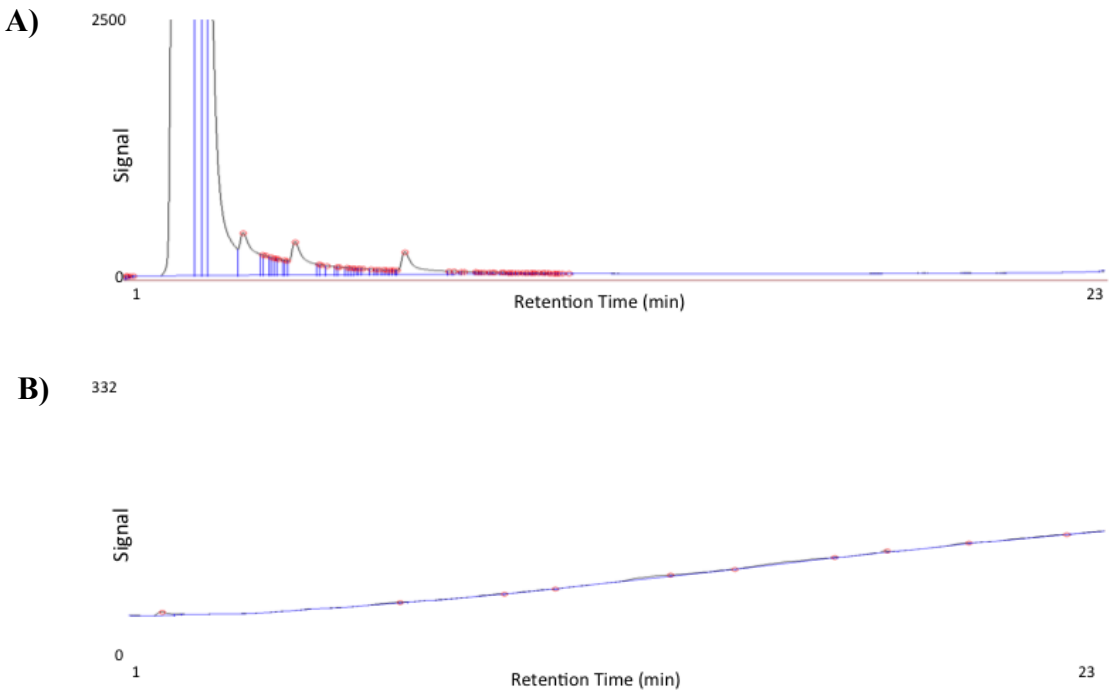

Figure 4-6. UV and FID trace of text mixture at 1000 **µ**g/mL using SRI GC-UV-FID. A) FID at 1000 **µ**g/mL B) UV at 1000 **µ**g/mL.

Not only were the peaks small and broad in the FID, they were undetectable in the UV even at this relatively high concentration. After careful consideration of the situation it was surmised that the broad peaks may be due to a large dead volume in the UV detector. Examining the instrument, we determined that the transfer tubing leading from the outlet of the column into the UV and from the UV to the FID had an inner diameter larger than our column. This instrument faces some challenges since the dead volume of this tubing as well as the dead volume of the UV flow cell leads to broad and even undetectable peaks. To mitigate this

problem we reconfigured the instrument by adding a T-piece before the UV detector as shown in Figure 4-7.

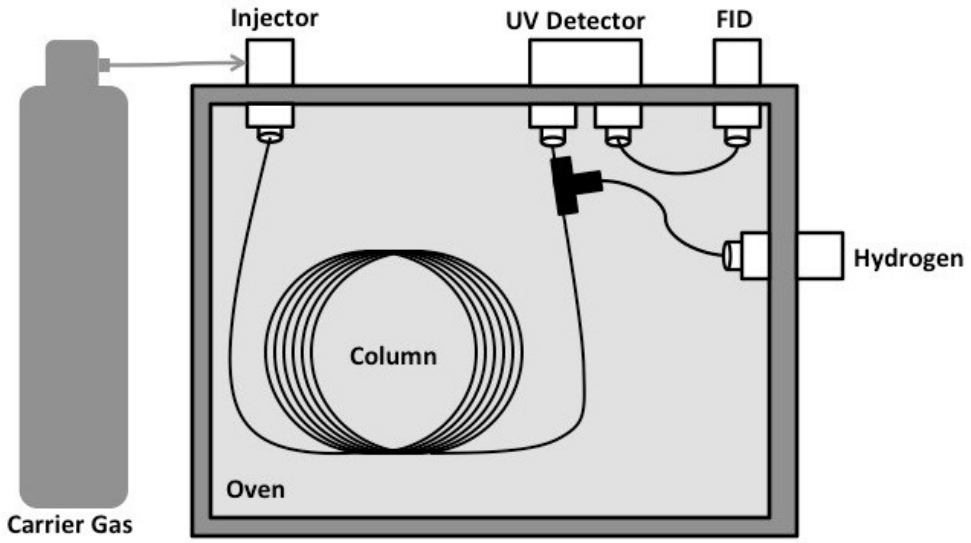

Figure 4-7. Modified schematic of the SRI GC-UV-FID including the addition of T-piece before UV detector, diverting hydrogen flow from FID detector.

In this setup the column was connected again through the UV and FID system but the flow through the detectors and tubing was increased by ~30 mL/min by diverting the hydrogen gas for the FID through the T-piece, shown as the separate hydrogen on the schematic diagram. This resulted in much sharper FID peaks, and the UV peaks were visible as seen in Figure 4-8.

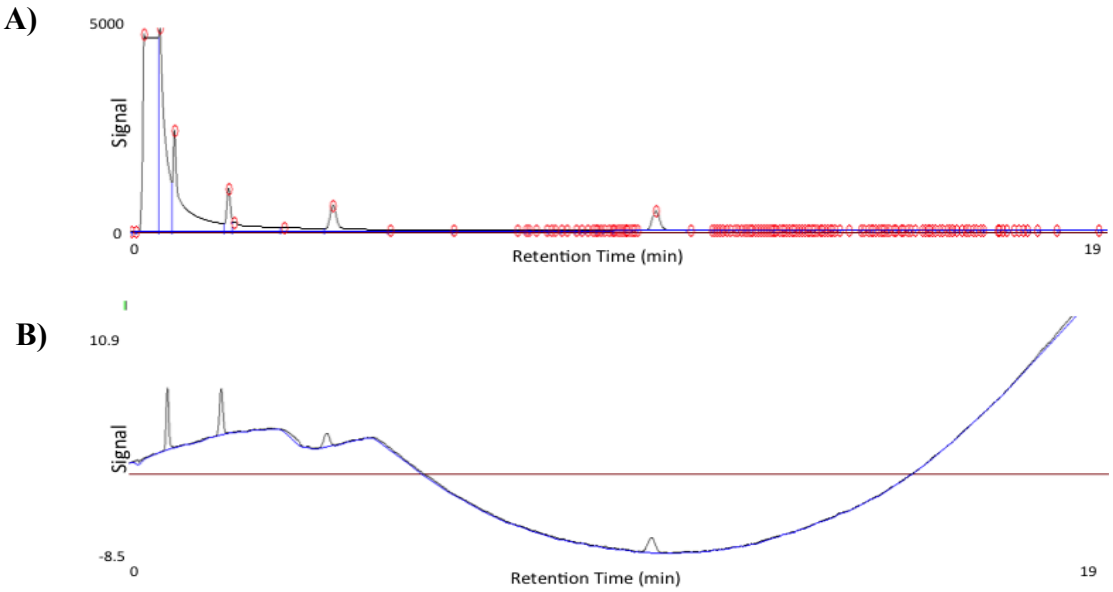

Figure 4-8. FID and UV traces with reconfigured system. A) FID at 1000 **µ**g/mL B) UV at 1000 **µ**g/mL.

This modified setup achieves sharper FID peaks, while still observing UV peaks. However, IL columns are currently only commercially available with 0.25 mm inner diameters.

An ionic liquid column was then installed into the system for initial testing. Figure 4-9 A demonstrates that when the column inner diameter was decreased to 0.25 mm the UV peaks became indistinguishable, and the FID peaks were small compared to runs completed at the same concentration on the 0.53 i.d. column. Since the peaks were so small at 1000 µg/mL, the concentration of the sample components were increased to 10,000 µg/mL to see if the instrument would respond to this concentration. The results of this experiment are shown in part C and D of Figure 4-9.

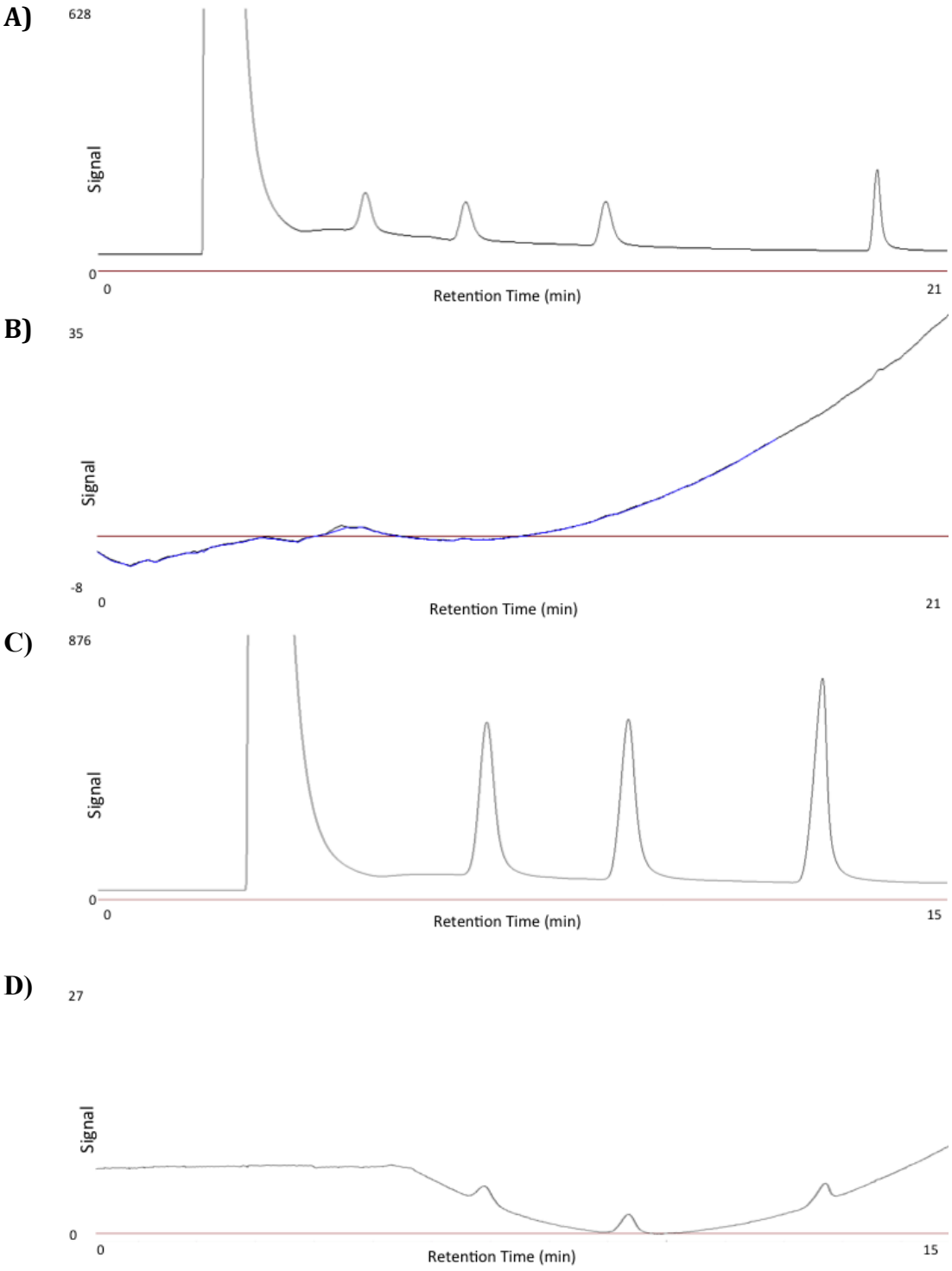

Figure 4-9. FID and UV traces using a 0.25 i.d. column. A) FID at 1000 µg/mL B) UV at 1000 µg/mL C) FID at 10,000 µg/mL D) UV at 10,000 µg/mL.

Although these results were less than ideal, we went ahead with calibrating the instrument for proof-of-concept of UV and FID calibration. In doing so four different concentrations, of our four different monoaromatics were examined for linearity. For all of the curves, the analyte of interest was normalized against naphthalene, and analyzed in triplicate. Figure 4-10 shows the resulting monoaromatic calibration curves for both the FID and UV detectors.

A)

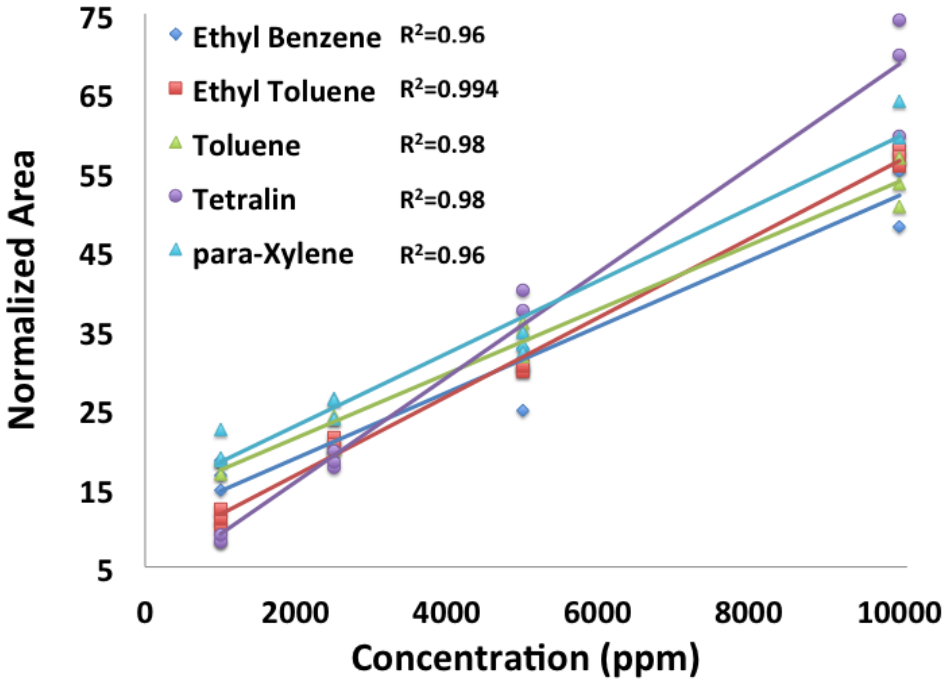

B)

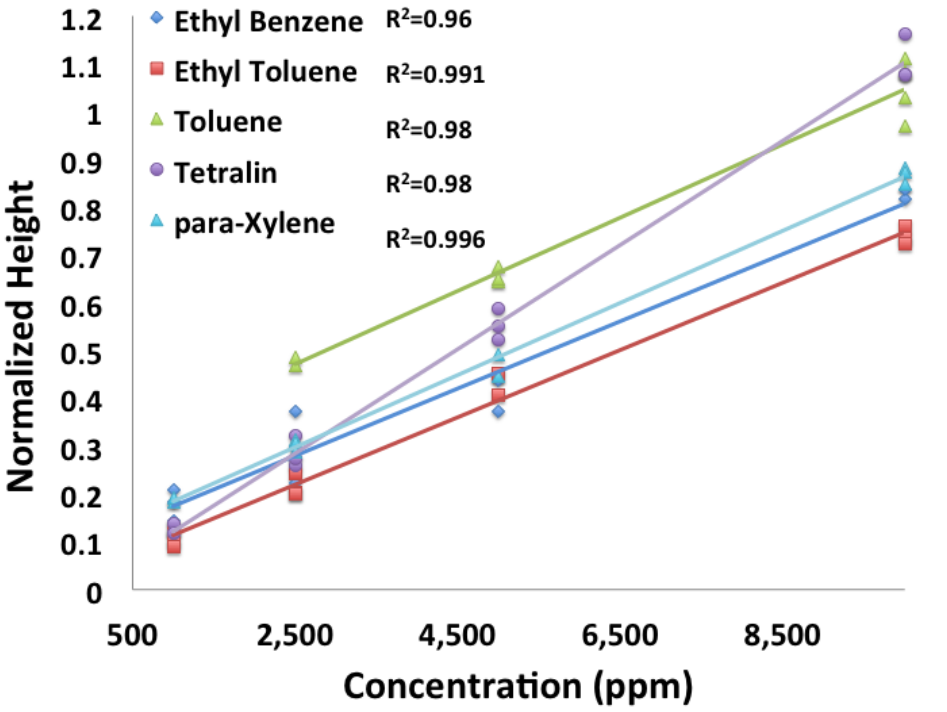

Figure 4-10. Calibration curves for monoaromatic standards run in triplicate. A) FID calibrations B) UV calibrations.

These experiments show that linear calibrations can be achieved in both the UV and FID, even though it requires high concentrations. FID calibration curves showed R^2 values higher than 0.95 in all cases, and the UV showed R^2 values greater than 0.96. However, in the case of UV analysis detecting 1000 μg/mL was difficult for most compounds, and could not be accomplished for toluene. The FID and UV calibrations had to be performed in a slightly separate manner as the FID calibration performs well using normalized area, and the UV calibration performs better with the use of normalized height instead. This difference is due to the fact that the FID is a mass-sensitive detector, and the UV is a concentration-dependent detector [144]. This distinction is important because the FID signal is dependent on the rate at which solute molecules enter the detector. Response of such detectors is not affected by gas flow rate changes. However, for concentration dependent detectors, the detector generates a specific peak height dependent on the concentration within the detector at a specific point in time, and dilution of sample with makeup gas will lower the detector response. The UV calibration curves have slopes that are very similar, so even with co-elution we can obtain quantifiable numbers and use total response, such as quantifying all monoaromatics together.

4.3.4 Conclusions

Monoaromatic compounds can be detected with both FID and UV detectors. These compounds have linear calibration curves showing that they can be calibrated. These linear calibrations indicate proof-of-concept as we can calibrate these aromatic compounds. However, operating at such high concentrations (i.e. > 1000 ppm) is unreasonable in real samples. However, we believe that this type of selective detection would be very useful for this type of analysis if it could be configured in a way that could detect much lower concentrations.

CHAPTER FIVE. Vacuum Ultraviolet Detection for Selective Determination of Aromatic and Biodiesel Content in Diesel

5.1 Introduction

In this chapter major analytical challenges surrounding the chemical analysis of diesel-range fuels will be addressed. Middle-distillate fuels, including diesel and jet fuels, provide the bulk of the energy requirements for commercial transportation (i.e., trucking, rail and aviation), construction and agriculture. There are two basic types of diesel: petroleum-based diesel (petrodiesel) and diesel fuels derived from biological fats and oils (biodiesel) [35]. There are analytical challenges facing the measurement of both of these fuel supplies. As outlined in Chapter 4, the first challenge pertains to the development of a method for group-type separation for diesel samples. The second challenge pertains to the development of a method for determination of biodiesel content in diesel samples. The group-type separation of diesel fuel relies on SFC, instrumentation that is becoming difficult to access, while biodiesel fouls SFC columns. Industrial determination of biodiesel content is of utmost importance due to government regulations on addition of an average of 2% biodiesel to petrodiesel. The overall goal of this chapter will be the

development of methods that deliver reliable results for both group-type and biodiesel content with the simplest instrumentation possible.

Based on Chapter 4, selective detection will be required to develop the specified methods. A bench top vacuum ultraviolet detector (VUV) for gas chromatography has been recently developed and tested [145,146,147,148,149]. This detector allows collection of absorption spectra in the range of 125 – 240 nm, giving much more information than a typical UV detector. In using this range of wavelengths it is possible to probe all compounds, not just the ones traditionally probed by UV absorption, such as those containing π-bonds. Almost every chemical compound absorbs in the VUV spectral range (115-185 nm) [145]. An added benefit of this type of system is that it also provides the user with full absorption spectra at every point in time, leading to useful qualitative data. Figure 5-1 outlines the general schematic of how the VUV detector is coupled to the gas chromatograph and how it operates. All compounds eluted from the GC are transferred to the VUV detector where they enter a flow cell. The flow cell has a set path length of 10 cm and an internal volume of 80 μL, and has an argon make-up gas flow introduced before the flow cell, which is responsible for altering the residence time of the sample, to optimize detection. A charged coupled device (CCD) is used to simultaneously collect absorption features for the whole spectrum as peaks elute from the GC column.

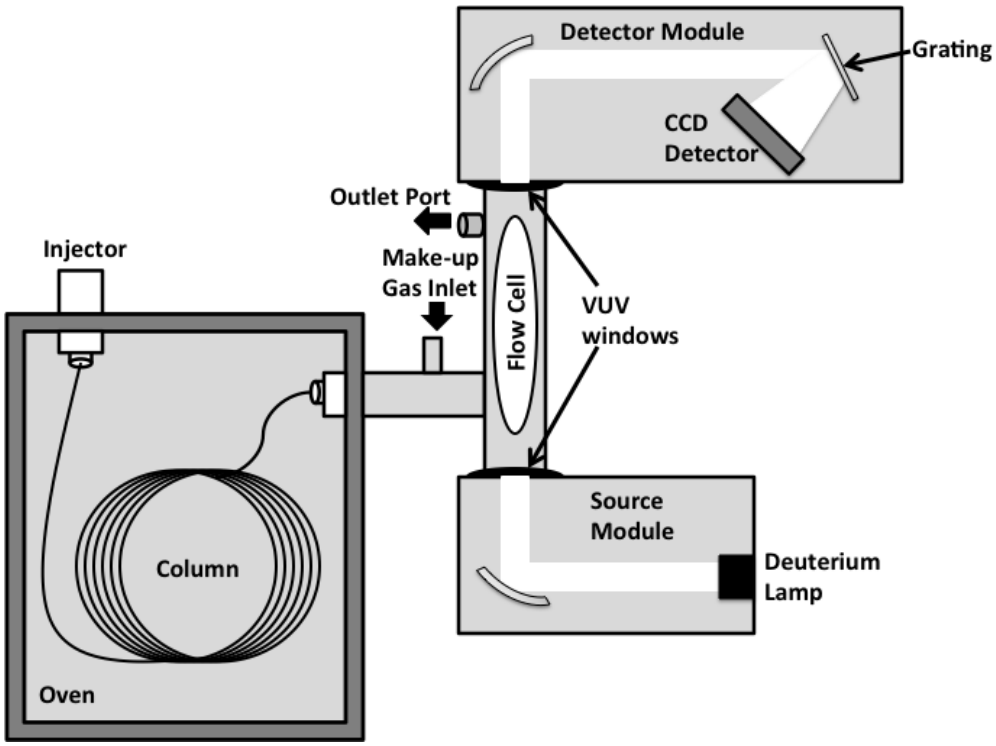

Figure 5-1. Schematic Diagram of VGA-100. Instrument adapted from [145].

This detector will be a useful tool for the analytical challenges faced in diesel and biodiesel analysis, providing both quantitative and qualitative information simultaneously. VUV is a powerful detection method that can detect volatile and semi-volatile compounds. Each compound has unique and highly featured spectra in the VUV. Figure 5-2 depicts an example of the differences in VUV spectra for water, nitrogen, and oxygen.

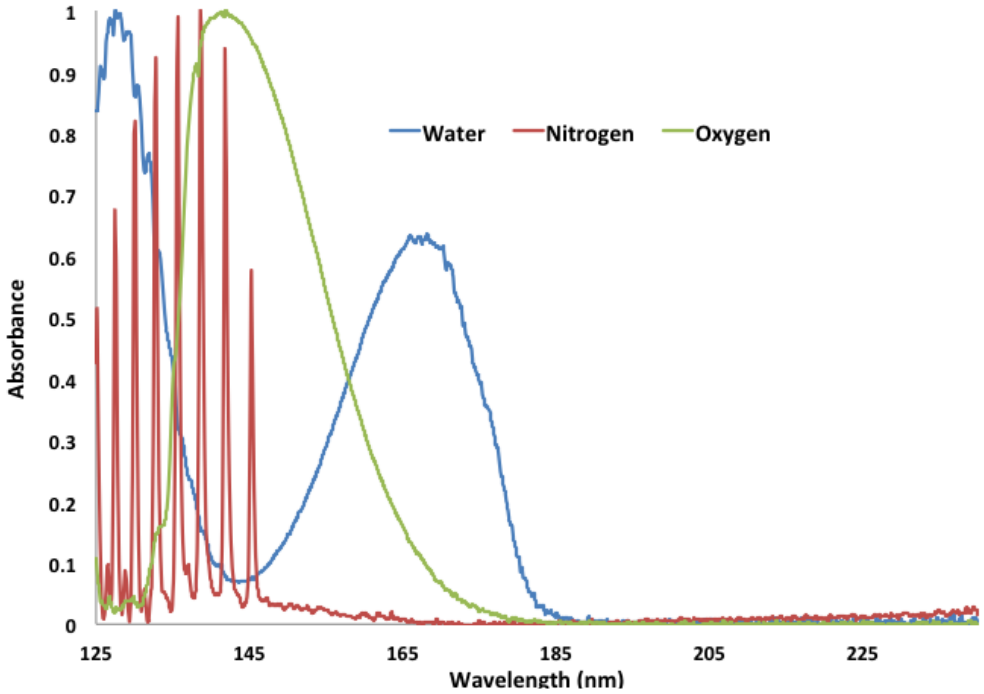

Figure 5-2. VGA-100 library absorbance spectra for water, nitrogen, and oxygen from 125-240 nm.

In this work the VUV system will be used to differentiate multiple overlapping signals and provide an enhanced dimension of separation based on absorption spectra. Candidate methods will be tested on actual diesel samples for both petrodiesel and biodiesel. Section 5.2 will discuss the development of a group-type aromatic separation for petrodiesel, while Section 5.3 will focus on the development of biodiesel determination in petrodiesel samples.

5.2 VUV Aromatics

5.2.1 Overview

Properties of petrodiesel such as cetane number and exhaust emissions are linked to the total aromatic and polycyclic aromatic content of the fuel, and the aromatic content of diesel is regulated in some jurisdictions. Thus the measurement and characterization of aromatic content is necessary for quality control of diesel and to meet regulatory limits. The current method is used to measure the non-aromatic (saturates) content, as well as mono-, di- and polyaromatic content of diesel samples. ASTM D5186 relies on SFC separation [33]. However, the SFC instrumentation that is required for this technique is now increasingly difficult to access. As a result, a replacement method is required. Since the simplest instrumentation (GC and GC-UV-FID) discussed in Chapter 4 was incapable of completing this determination, a VUV detector will be employed.

5.2.2 Experimental

5.2.2.1 Chemicals

Initial testing was completed using five model compounds dissolved in ACS grade carbon disulfide (Fisher Scientific): ethyl toluene (Sigma Aldrich), tetralin (Caledon), naphthalene (Fisher Scientific), toluene (Fisher

Scientific), ethyl benzene (Fisher Scientific), and para-xylene (Fisher Scientific).

A ten-compound mix was used in method development consisting of: docosane (Sigma Aldrich), ethyl toluene (Sigma Aldrich), tetralin (Caledon), naphthalene (Fisher Scientific), dibenzothiophene (Sigma Aldrich), anthracene (Eastman), pyrene (Sigma Aldrich), toluene (Fisher Scientific), ethyl benzene (Fisher Scientific), and para-xylene (Fisher Scientific). Model compound samples were prepared by dissolving each compound in ACS grade carbon disulfide (Fisher Scientific) to 1000 μg/mL.

A collection of Syncrude diesel samples with varying aromatic content were also used for method development and validation: FUEL 2, FUEL 6, FUEL 9, FUEL 8, FUEL 1, FUEL 12, FUEL 13, FUEL 11, FUEL 7 and FUEL 4. A few Syncrude light gas oil samples were also tested: FUEL 3, FUEL 4 and FUEL 5. Syncrude quality control (QC) sample, which is a well characterized diesel, was also tested. All samples were analyzed without dilution.

Standard addition was completed using FUEL 7 as the sample of interest. Varying masses of monoaromatic, diaromatic and polyaromatic standard compounds were added to the diesel matrix.

5.2.2.2 Instrumentation

Experiments were conducted on an HP6890 GC (Agilent Technologies, Mississauga, ON, Canada) using helium as carrier gas at a linear velocity of ~30 cm/s. This instrument was equipped with an Agilent 7683 auto sampler (Agilent Technologies). All studies were conducted on the IL-111 (Supelco) 30 m × 250 μm with 0.2 μm film thickness. The injector temperature was set to 250 °C. For calibration curves of standard compounds, a 1 μL injection was used with a 20:1 split ratio. For all neat diesel samples an injector volume of 0.2 μL was used, with a split ratio of 60:1. A VGA-100 VUV detector (VUV Analytics, Inc., Austin, TX, USA), was coupled to the Agilent GC. The VUV and accompanying transfer line and flow cell were kept at 300 °C. The VUV instrument collects the absorbance across all wavelengths (125-240 nm) for each time point of the run.

5.2.2.3 Procedure

Calibration curves for the monoaromatic compounds were first constructed to test the linearity of the detector, and the detector response as compared to the GC-UV-FID studied in Chapter 4. This was accomplished by completing triplicate measurements of 100, 200, 500, 1000, 1500 and 2000 μg/mL for each compound. Further calibration was completed using neat diesel samples, which had previously collected SFC data for their aromatic content. VGA-100 software, which contains a library of UV

absorbance spectra for approximately 500 compounds, was used for identification of peaks.

5.2.3 Results and Discussion

Initially, the instrument was set up using an ionic liquid column, with a 120 °C start temperature, 0 min hold time and a ramp rate of 20°C/min. The first step in testing the performance of this VGA-100 detector was to complete calibration using the same standards as in Section 4.3. The results of this calibration are depicted in Figure 5-3.

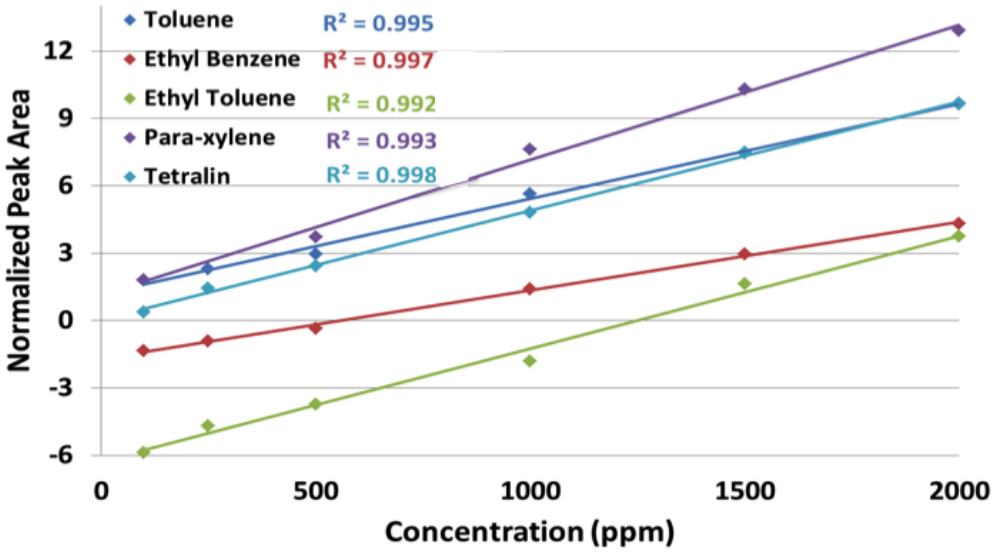

Figure 5-3. Monoaromatic compound calibration using VUV detector.

The calibrations for the monoaromatic compounds tested all had R^2 values greater than 0.99. These results are promising, especially considering that they were collected using a split ratio of 20:1 and were still able to easily quantify

down to 100 µg/mL. This is a drastic difference from the difficulty in quantifying at 1000 µg/mL in Section 4.3, with the previous GC-UV-FID instrument. These curves were collected by integrating across all wavelengths while some have negative peak areas this is due to the method of background subtraction. With this success the next step was to determine whether or not the monoaromatic compounds could be differentiated from the saturate compounds. Specific absorbance filtering of collected chromatograms will be done to differentiate the different compounds. This is an appropriate way to distinguish saturates and aromatics because the saturate compounds have very little absorbance above ~170 nm while the aromatic compounds have their maximum absorbance above 170 nm as shown in Figure 5-4.

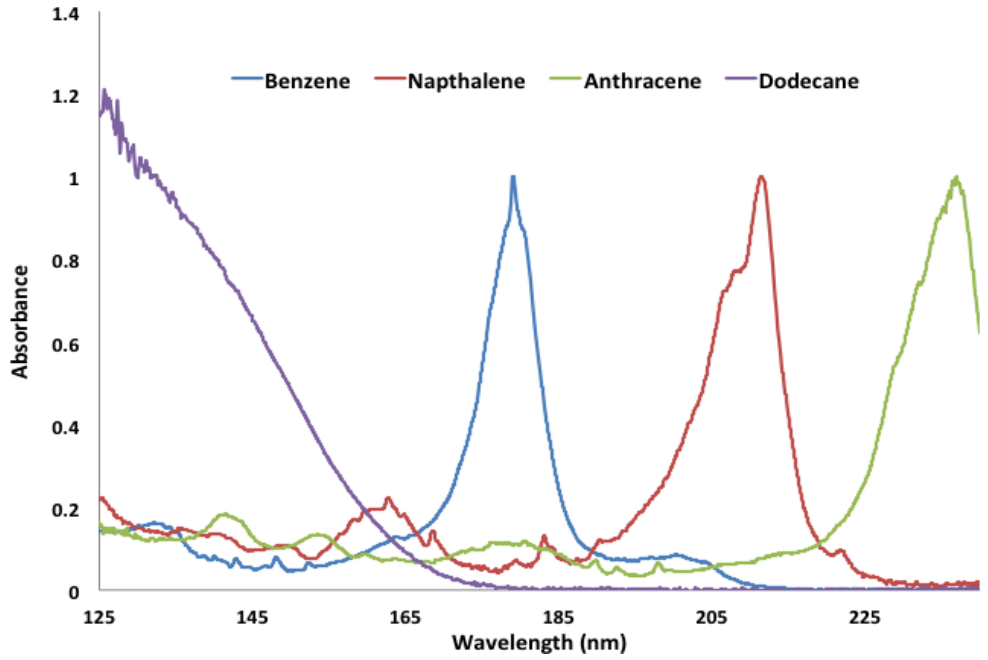

Figure 5-4. VGA-100 library absorbance spectra for benzene, naphthalene, anthracene and dodecane from 125-240 nm.

To test the filtering technique the SFC 10 standard mix was run and resulting spectra using different wavelength filters were examined. Figure 5-5 displays two different filters applied to the same data. The blue trace shows the so called 'aromatics' filter, generated by averaging the absorbance spectra over the wavelength region 170 – 200 nm, while the red shows the 'saturates' filter using the wavelengths from 125 – 160 nm. The expanded region depicted in Figure 5-5B, shows the docosane peak around 4 minutes in red and it is noted that the blue trace (aromatic) does not contribute to this peak. This is a general property exhibited by saturates and aromatics, allowing us to easily distinguish between these two compound classes simply by comparing chromatogram responses. Note that while saturates do not contribute significantly to the 'aromatics' filter, all of the compounds in the standard mix contribute to the 'saturates' filter, since the aromatic compounds do absorb in this region. This fact will need to be taken into account when generating quantitative results from the chromatogram responses.

A)

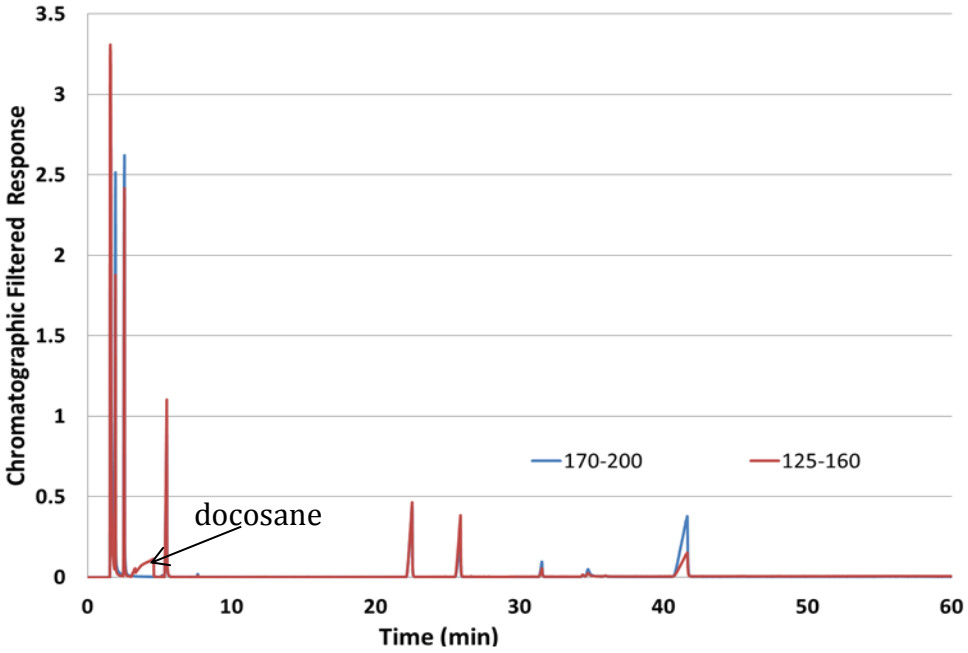

B)

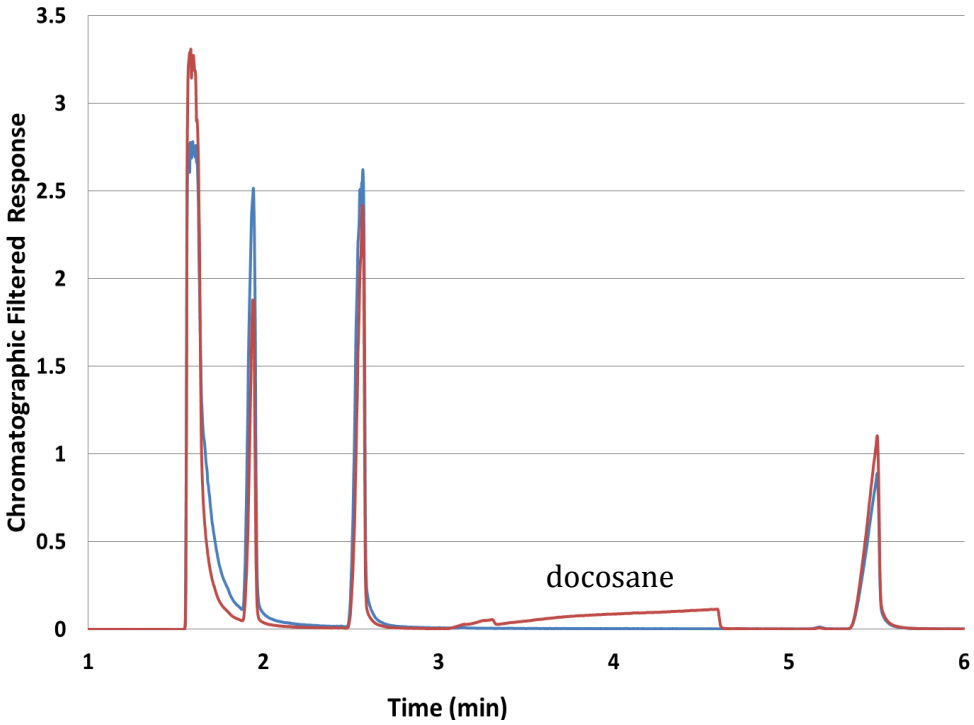

Figure 5-5. VUV Response of SFC Standard Mix**.** A) Full Spectra B) Expanded Version from 1 – 6 minutes. Blue trace is from filter 170-200 nm, Red trace is filter from 125-160 nm.

Unfortunately, it was found that running real diesel samples using the same GC conditions caused the detector response to saturate at the beginning of the chromatogram. This can be seen in Figure 5-6 where large amounts of noise are observed in the 125-160 nm region of the absorbance spectra. This occurs because of the large amount of compound eluting off of the column quickly with the high start temperature. In order to spread out this early region of the chromatogram and to avoid saturation of the detector, new conditions were tested with the results shown in Figure 5-6B. The first method (Method 1) used the original optimized method with a ramp rate of 3°C/min, start temperature at 120°C (0 minute hold) and a 5 minute hold at the final temperature to ensure all compounds came off of the column. The second method (Method 2) used a start temperature of 60°C/min with a 3 minute hold time, while increasing the ramp rate at 20°C/min to keep the run time lower. Both methods have the same final temperature of 210°C. The blue trace for Method 2, with the lower start temperature, is very successful at spreading out the beginning area of this chromatogram.

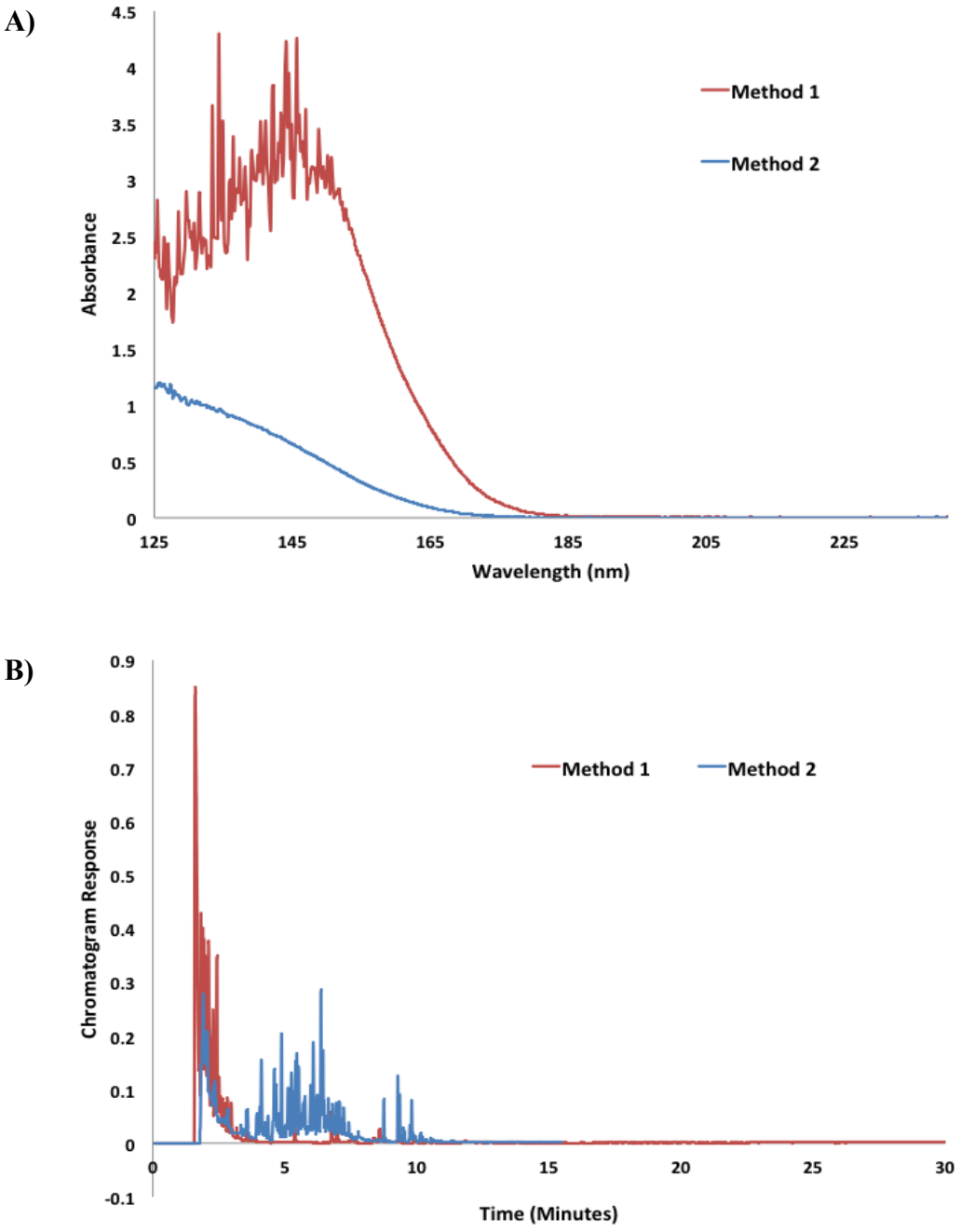

Figure 5-6. Diesel samples run using two different methods. A) Absorbance spectra collected at 2.2 minutes from chromatograms in (B) B) Chromatograms of diesel samples. Red trace is 120 °C (0 minute hold), 3 °C/minute to 210 °C (5 minute hold), blue trace is 60 °C (3 minute hold), 20 °C/minute to 210 °C (0 minute hold).

Testing of real diesel samples was done using these new conditions of 60°C (3 minute hold time), ramp rate of 20°C/minute to 210°C (0 minute hold). The first step was to determine which regions of the chromatogram belong to which group type. The start of the naphthalene peak determines the start of the diaromatic region and end of the monoaromatic/saturate region, while the start of the anthracene peak marks the end of the diaromatic region and the beginning of the polyaromatic region. These peaks can be easily identified using the corresponding VUV library absorbance spectra. At the point in time where characteristic spectra for naphthalene is found, marks the end of the monoaromatics/saturate region and the beginning of the diaromatic region. Time regions corresponding to the other major groupings are identified similarly. Once the regions are selected, the total response areas for each grouping along with the group relative response factors are used to calculate the mass percentages for each group type.

Since a full range absorbance spectrum is obtained during each detector scan, a chromatogram response can be generated using any number of spectral range filters. It is simplest to work with a full-range response, consisting of average absorbance over 125-240nm, although as shown later this does not have to be the case. Using the time regions as determined above, the total area responses for polyaromatics, $AP_{125\text{-}240}$, diaromatics, $AD_{125\text{-}240}$, and monoaromatics/saturates, $AMN_{125\text{-}240}$ are recorded. Here we note that it is permissible to compute response 'area' that simply consists of the summed

response over each of the group regions, provided the scan rate remains constant. The relationship between this total response and an integrated area is a multiplicative factor (the time between scans) that does not affect any of the determined mass % results reported in this paper. In the monoaromatic/saturate region, both monoaromatics and saturates contribute to the 125-240nm response area. However, as pointed out earlier, monoaromatics absorb strongly in the 170-200nm region while saturated hydrocarbons absorb very little in that region. In fact, by moving the filter 5nm longer in wavelength to 175-205nm, the contribution from saturates becomes negligible. Therefore, in the monoaromatic/saturate region a monoaromatics-only response, $AM_{175\text{-}205}$, can be determined from a 175-205nm filter. Figure depicts the different filters used.

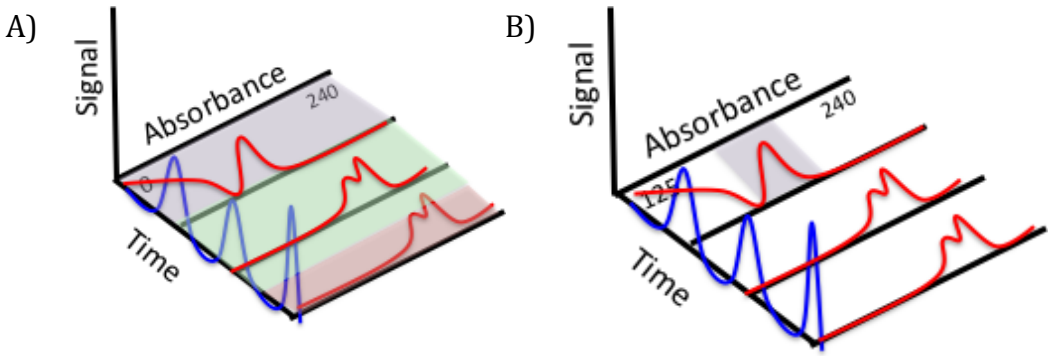

Figure 5-7. Three-dimensional plot showing signal on the z-axis, time on the x-axis and absorbance on the y-axis A) Indicates filtering over entire range (125-240 nm), color coded by group-type region, monoaromatic/saturate (purple), diaromatic (green) and polyaromatic (pink) B) Filtering monoaromatic range (175-205 nm) in monoaromatic/saturate region (purple)

Further, if the full 125-240nm response for monoaromatics, $AM_{125\text{-}240}$, can be predicted from the 175-205nm response, then the saturates response, $AN_{125\text{-}240}$, can be determined by subtracting $AM_{125\text{-}240}$ from $AMN_{125\text{-}240}$. Based on a range of monoaromatic spectra from the VUV spectral library, the two monoaromatics filters are related by:

$$AM_{125\text{-}240} \approx AM_{175\text{-}205}/2 \qquad \text{(Equation 5-1)}$$

This relationship can be used to predict the full 125-240nm monoaromatics response from the 175-205nm response, which can be measured without interference from coeluting saturates. When implementing the method we found that a factor of 1.8 between $AM_{125\text{-}240}$ and $AM_{175\text{-}205}$ resulted in better agreement to the available SFC data. The reason for this may be due to the distribution and types of monoaromatics in diesel compared to monoaromatics currently available in the VUV library, which is still relatively small. Saturate content ($AN_{125\text{-}240}$) is calculated by subtracting the calculated monoaromatic response ($AM_{125\text{-}240}$) from the total response in this region ($AMN_{125\text{-}240}$).

Once the response areas for all of the compound groups are determined the mass percent for each group type is calculated:

(Equation 5-2)

$$M\% = \frac{AM_{125-240} \times RRF_M}{\left(AM_{125-240} \times RRF_M\right) + \left(AD_{125-240} \times RRF_D\right) + \left(AP_{125-240} \times RRF_P\right) + \left(AN_{125-240} \times RRF_N\right)}$$

(Equation 5-3)

$$D\% = \frac{AD_{125-240} \times RRF_D}{\left(AM_{125-240} \times RRF_M\right) + \left(AD_{125-240} \times RRF_D\right) + \left(AP_{125-240} \times RRF_P\right) + \left(AN_{125-240} \times RRF_N\right)}$$

(Equation 5-4)

$$P\% = \frac{AP_{125-240} \times RRF_P}{\left(AM_{125-240} \times RRF_M\right) + \left(AD_{125-240} \times RRF_D\right) + \left(AP_{125-240} \times RRF_P\right) + \left(AN_{125-240} \times RRF_N\right)}$$

(Equation 5-5)

$$N\% = \frac{AN_{125-240} \times RRF_N}{\left(AM_{125-240} \times RRF_M\right) + \left(AD_{125-240} \times RRF_D\right) + \left(AP_{125-240} \times RRF_P\right) + \left(AN_{125-240} \times RRF_N\right)}$$

where RRF is the relative response factor for the corresponding group type, RRf_M is 0.275, RRf_D is 0.275, RRf_P is 0.275 and RRf_N is 0.775, which are the response factors for monoaromatics (%M), diaromatics (%D), polyaromatics (%P) and non-aromatics (%N) respectively. These relative response factors were obtained from prior studies of gasoline-range samples. This determination was then performed on a number of diesel and light gas oil samples, the results of this are shown in Table 5-1.

Table 5-1. Absolute calculated mass percent difference between aromatic determinations of diesel samples by VUV compared to original SFC results.

SFC vs VUV	Sat %	Mono %	Di %	Poly %
FUEL 1	-2.9	3.9	-2.6	0.0
FUEL 2	-2.5	3.5	-1.0	0.0
FUEL 3	-3.3	14.4	-9.9	1.6
FUEL 5	-4.0	12.6	-8.4	0.6
FUEL 5	3.4	1.1	-4.4	0.0
FUEL 6	-2.9	4.2	-1.4	0.0
FUEL 7	-2.9	4.4	-1.5	0.0
FUEL 8	-3.8	6.0	-2.0	0.8
FUEL 9	-1.4	7.6	-5.1	0.0
FUEL 10	-4.6	5.7	-1.1	0.0
FUEL 11	-3.3	4.6	-1.3	0.0
FUEL 12	-1.4	4.0	2.7	0.0

This table shows the difference between SFC values which were collected by Syncrude versus the VUV technique. There are a few samples that stand out with large amounts of variance (FUEL 3-FUEL 5, FUEL 8 and FUEL 9).

Upon closer examination of the VUV data for these samples it was noted that FUEL 3 had large amounts of overlap between the monoaromatics and diaromatics, while FUEL 8 had moderate amounts of overlap between these same groups, which lead to poor determination of the relative amounts using our VUV method, compared to the other samples. To improve the separation between group types the ramp rate was decreased from 20°C/min to 5°C/min to account for the decreased start temperature, which is what originally moved these two group-types closer together. Additionally, in order to further optimize the method one of the samples, Fuel 7, was spiked with various amounts of known compounds in order to perform standard addition measurements.

Standard addition was done by spiking known percent amounts of the group-type of interest into the diesel sample at four different percent values, depending on solubility of the compounds. The curves generated by this data were then used to determine the original percent amount of each group-type in the Fuel 7 sample. Figure 5-8 shows the results of our standard addition calibrations, along with the slopes and intercepts which were used to calculate the original percent amounts. The results of these standard addition experiments along with our results based on VUV determination are summarized in Table 5-2.

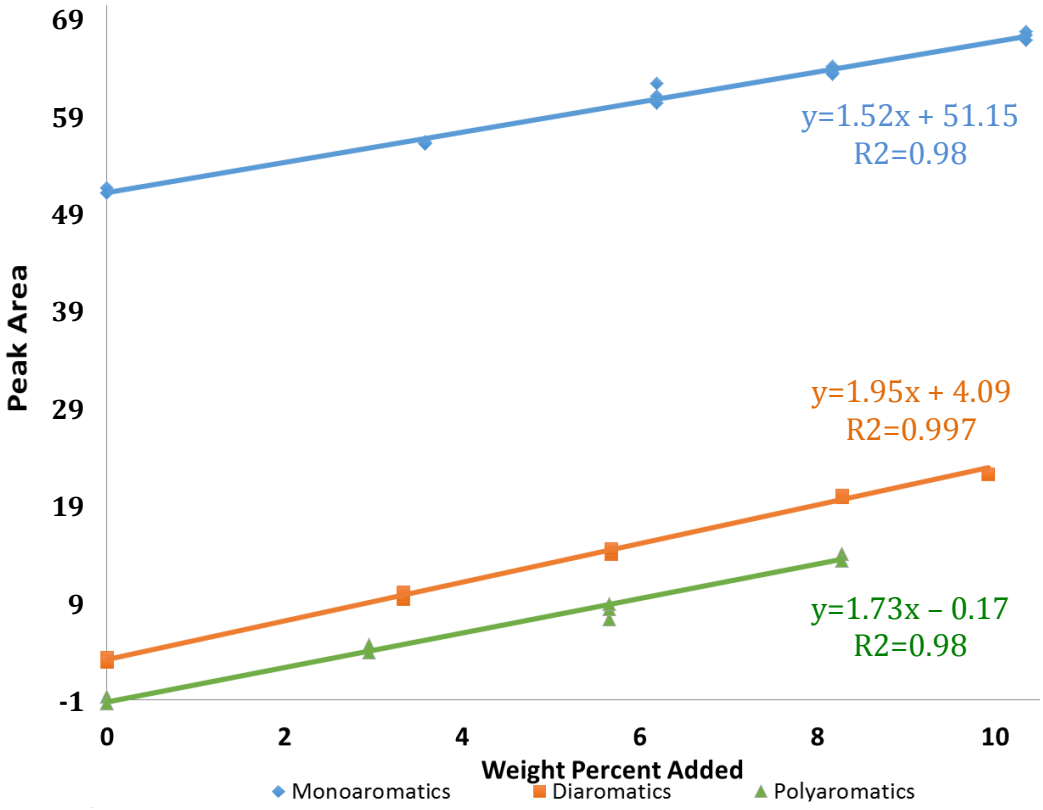

Figure 5-8. Standard addition data for monoaromatic, diaromatic and polyaromatics in Fuel 7.

Table 5-2. FUEL 7 group-type weight percent determinations, using different ramp rates and standard addition.

Technique	Saturate %	Monoaromatic %	Diaromatic %	Polyaromatic %
SFC	64.6	32.4	3	0
VUV (20°C/min)	67.6	28.0	4.5	0
VUV (5°C/min) Run 1	63.4	34.2	2.6	0.2
VUV (5°C/min) Run 2	64.2	33.8	2.9	0.2
Standard Addition	64.2	33.5	2.1	0.09

In Table 5-2 it can be noted that the runs completed using the 5°C/min ramp rate matched much better with the SFC data than the results from the 20°C/min ramp rate run. It is also positive that the standard addition results matched well with the SFC data, indicating that the SFC results are accurate, at least for this sample.

In an attempt to further improve the aromatic characterization of these samples different filters were tested for their performance. The current filters were considered static filters whereby they selected a specific region of

wavelengths, e.g. average absorbance over 125-240 nm. To have better specificity, improve signal-to-noise, and decrease sensitivity to background variations a dynamic filter was generated. The dynamic filter selects a specific region of wavelengths, e.g. 200-240 nm. Within this region the filter selects the apex of the largest absorbance peak and collects the average absorbance within a ±2 nm window around the apex. This dynamic filter will be used for determination of the response in diaromatic and polyaromatic regions. The equations for determining group mass % given earlier is modified accordingly:

(Equation 5-6)

$$M\% = \frac{100 \times AM_{125-240} \times RRf_M}{AN_{125-240} \times RRf_N + AM_{125-240} \times RRf_M + AD_{Max,200-240} \times RRf_D + AP_{Max,200-240} \times RRf_P}$$

(Equation 5-7)

$$D\% = \frac{100 \times AD_{Max,200-240} \times RRf_D}{AN_{125-240} \times RRf_N + AM_{125-240} \times RRf_M + AD_{Max,200-240} \times RRf_D + AP_{Max,200-240} \times RRf_P}$$

(Equation 5-8)

$$P\% = \frac{100 \times AP_{Max,200-240} \times RRf_P}{AN_{125-240} \times RRf_N + AM_{125-240} \times RRf_M + AD_{Max,200-240} \times RRf_D + AP_{Max,200-240} \times RRf_P}$$

(Equation 5-9)

$$N\% = \frac{100 \times AN_{125-240} \times RRf_N}{AN_{125-240} \times RRf_N + AM_{125-240} \times RRf_M + AD_{Max,200-240} \times RRf_D + AP_{Max,200-240} \times RRf_P}$$

where $AD_{max,200\text{-}240}$ and $AP_{max,200\text{-}240}$ are the response areas determined from the dynamic filters. Since the response areas for di- and polyaromatics are no longer determined from a full-range response, the relative response factors for these groups must be modified as well. Based on the standard addition data, the relative response factors were replaced by 0.045 for diaromatics and 0.09 for polyaromatics when using the dynamic filters.

Table 5-3. Dynamic filtering results for group-type determination of FUEL 7.

Technique	Saturate %	Monoaromatic %	Diaromatic %	Polyaromatic %
SFC	64.6	32.4	3	0
VUV Dynamic Processing Replicate 1	63.6	34.2	2.2	0
VUV Dynamic Processing Replicate 2	64.6	32.4	3.0	0

By altering our filtering technique the results were improved, and compared better with the SFC data as shown in Tables 5-3, 5-4, and 5-5. Table 5-4 shows the refined method applied to Fuel 7. Table 5-4 shows the results of applying the refined method to determine aromatic content of diesel and light gas oil samples. Table 5 shows the difference between the refined GC-VUV method and SFC results for the same samples.

Table 5-4. VUV detector dynamic filtering results for weight percent group-type determination of diesel samples. Samples were run in triplicate.

	Saturates %	Monoaromatics %	Diaromatics %	Polyaromatics %
FUEL 1	69.8±0.7	27.9±1.0	1.7±0.4	0.6±1.3
FUEL 2	67.6±0.4	28.7±0.5	2.4±0.1	1.4±0.7
FUEL 3	65.8±0.5	30.9±0.5	2.6±0.3	0.6±0.7
FUEL 5	69.5±0.8	19.1±0.4	9.5±0.1	1.9±1.3
FUEL 5	90.5±1.2	4.6±1.4	3.7±0.5	1.2±3.0
FUEL 6	64.9±0.2	31.2±0.4	2.9±0.2	0.9±0.4
FUEL 7	64.6±0.3	32.6±0.3	2.7±0.1	0.2±0.2
FUEL 8	69.0±1.2	24.6±1.4	5.8±0.6	0.6±2.0
FUEL 9	72.6±1.9	20.7±2.3	6.0±0.3	0.7±4.1
FUEL 10	63.6±0.2	33.1±0.2	3.0±0.2	0.4±0.2
FUEL 11	67.2±0.5	30.1±0.4	2.5±0.2	0.3±0.6
FUEL 12	65.8±0.4	31.6±0.1	2.1±0.2	0.5±0.4
FUEL 13	67.0±0.1	29.6±0.2	2.9±0.2	0.4±0.2

Table 5-5. Comparison of VUV-dynamic filtering and SFC data for group-type weight percent determination in diesel and light gas oil samples.

SFC vs VUV	Saturates %	Monoaromatics %	Diaromatics %	Polyaromatics %
FUEL 1	-0.1	-0.7	1.7	0.6
FUEL 2	-1.8	-0.6	1.0	1.4
FUEL 3	12.6	2.8	-14.5	-1.0
FUEL 4	4.8	-9.5	3.4	1.3
FUEL 5	-4.1	-0.2	3.1	1.2
FUEL 6	-1.1	-0.4	0.5	0.9
FUEL 7	0.0	0.2	-0.3	0.2
FUEL 8	3.4	-2.3	-1.0	-0.2
FUEL 9	1.7	-4.5	2.0	0.7
FUEL 10	1.0	-1.3	0.0	0.4
FUEL 11	0.1	-0.8	0.5	0.3
FUEL 12	-1.2	0.2	0.5	0.5
FUEL 13	-4.8	12.1	-7.8	0.4

There are still a few samples with large differences when compared to the SFC data; Fuel 3, Fuel 4 and Fuel 13. Upon closer examination we noted that the SFC results for Fuel 13 did not make sense. The measured absorbance data for this sample was very similar to the absorbance data for Fuel 6 as seen in Figure 5-7, while the SFC results for these two samples differ significantly. The VUV absorbance spectra and chromatograms for these two samples (Fuel 6 and Fuel 13) are very similar, and the GC-VUV mass % results for these samples are consequently very similar, as expected. However, the SFC data suggested that they would be very different as outlined in Table 5-6.

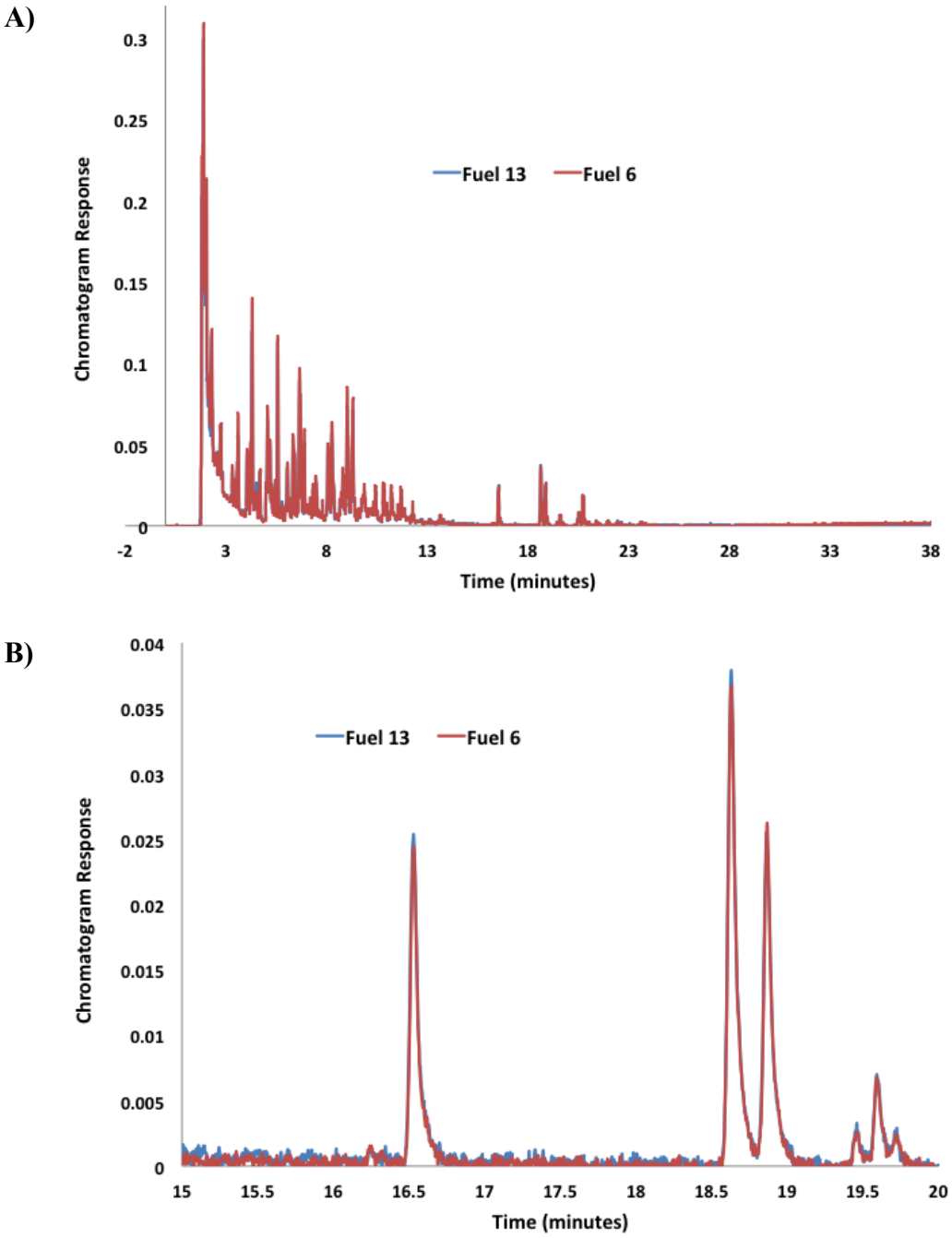

Figure 5-9. Chromatogram Comparison of Fuel 6 and Fuel 13 A) Full overlaid chromatograms B) Expanded region between 15 and 20 minutes

Table 5-6. Comparison of VUV and SFC data for samples Fuel 6 and Fuel 13.

Technique	Saturate %	Monoaromatic %	Diaromatic %	Polyaromatic %
SFC FUEL 6	66.0	31.6	2.4	0
VUV FUEL 6	64.9	31.2	2.9	0.9
SFC FUEL 13	71.8	17.5	10.7	0.0
VUV FUEL 13	67.0	29.6	2.9	0.4

Based on this finding we surmise that the SFC data was incorrect. This is entirely possible, as the SFC method in use did not always achieve baseline resolution for the samples of interest. We looked at a couple other samples more closely and noted errors in SFC data as well. For instance SFC data for FUEL 1 indicated that there was no diaromatic content, but as shown by the GC-VUV data in Figure 5-10 it becomes clear that diaromatics are in fact present. In this figure the two peaks past ~16.5 minutes have been identified as naphthalene and 2-methylnapthalene, indicating that there is definitely diaromatic content in this sample.

A)

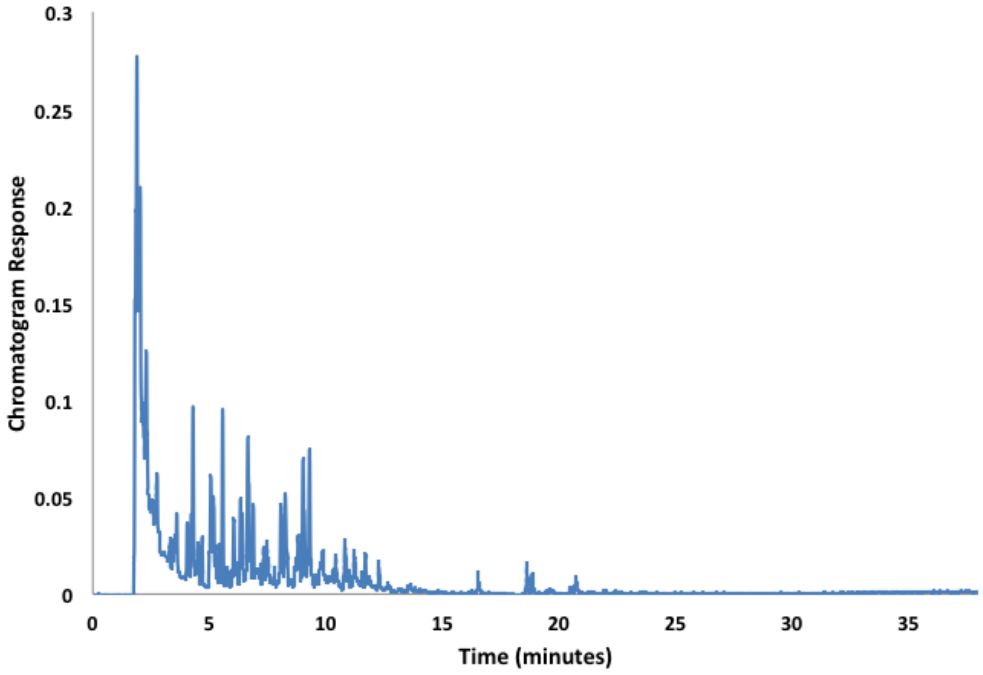
Chromatogram Response
0.3
0.25
0.2
0.15
0.1
0.05
0
0
5
10
15
20
25
30
35
Time (minutes)

B)

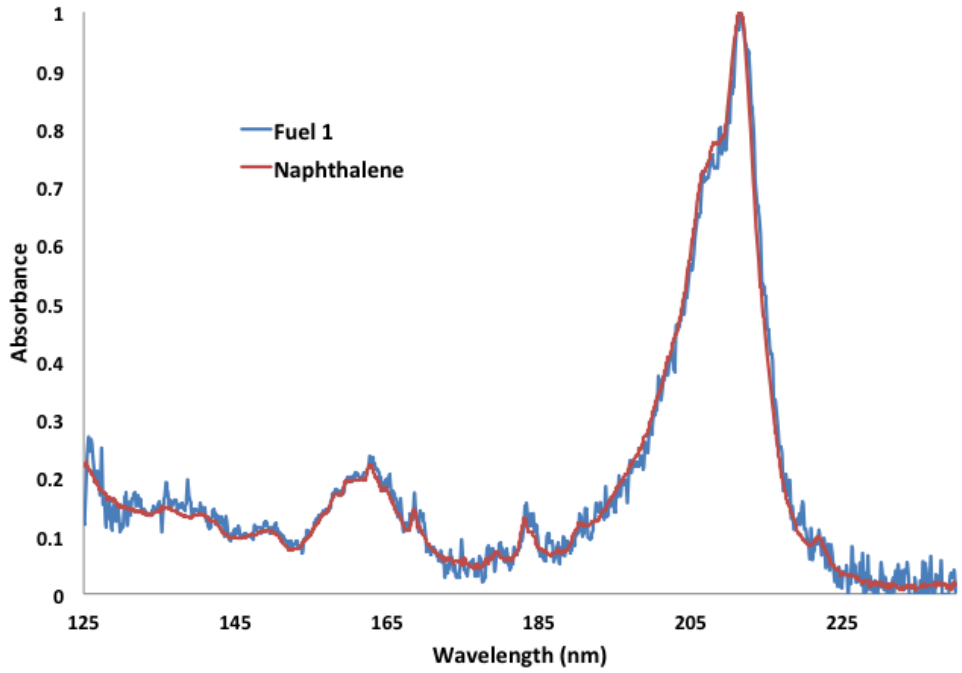
Absorbance
1
0.9
0.8
0.7
0.6
0.5
0.4
0.3
0.2
0.1
0
Fuel 1
Naphthalene
125
145
165
185
205
225
Wavelength (nm)

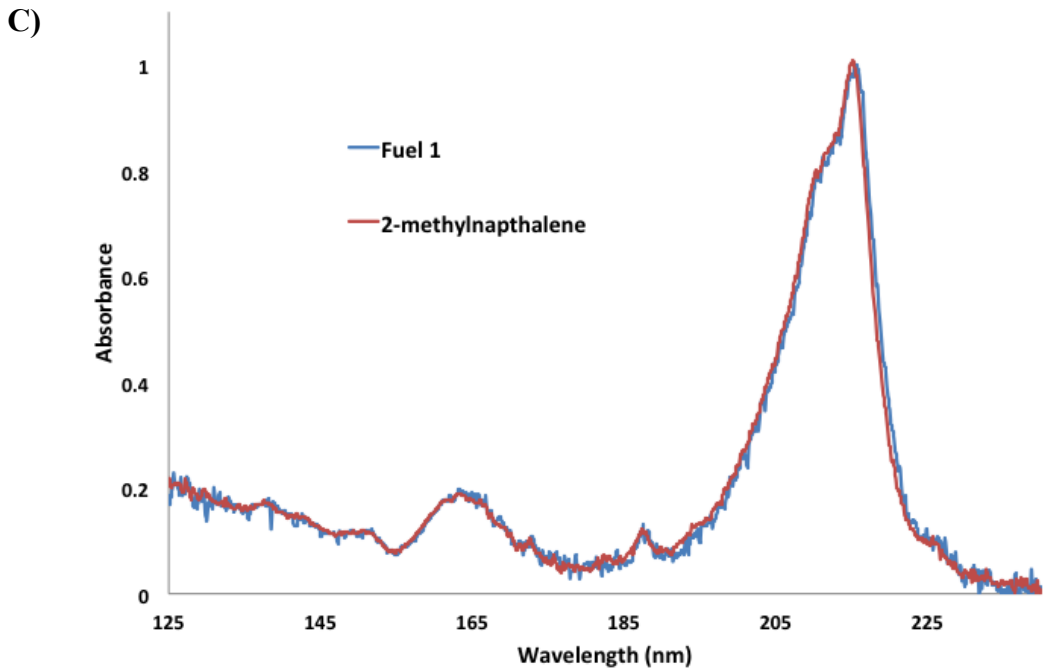

Figure 5-10. VGA-100 chromatographic and selected absorbance data for Fuel 1. Indicating the presence of diaromatic content A) Full chromatogram B) Absorbance spectra at ~ 16.5 minutes C) Absorbance spectra at ~18.5 minutes

The relatively poor repeatability of results for polyaromatics was caused by the low polyaromatic contribution to these samples, combined with the relatively large time region and baseline variation over the polyaromatics regions of the chromatograms. Visual inspection of the chromatograms suggested that an automated peak integration routine would provide more robust determination of polyaromatic response areas, especially since such routines are able to better account for local baseline variation. Future work can be done to refine this portion of the model.

As a further test of the new method, a Syncrude quality control sample was measured. Syncrude uses a quality control sample for which data was collected from 2010 – 2012. A comparison of the SFC and VUV method results for this sample are presented in Table 5-7.

Table 5-7. Comparison of VUV and SFC data for QC sample, including standard deviation.

Technique	Saturate %	Monoaromatic %	Diaromatic %	Polyaromatic %
SFC - QC	66.6 ± 0.4	31.3 ± 0.4	2.1 ± 0.2	0
VUV - QC	66.5 ± 0.2	31.2 ± 0.1	2.6 ± 0.0	0.0 ± 0.2

The VUV data agrees within error for saturates, monoaromatics and polyaromatics, providing further evidence that the new VUV method is capable of providing group-type composition results for diesel fuels.

5.2.4 Conclusions

Comparison of numerous ionic liquid capillary columns demonstrates the ability of the very polar ionic liquid phas-es IL-100 and IL-111 to selectively retain aromatic hydrocarbons. This selectivity for aromatic hydrocarbons over saturates will allow the separation of petroleum

products. These columns are also capable of group-type separation of polyaromatic hydrocarbons, which is an extremely important step in replacing the current ASTM and CGSB methods. In the optimal GC-FID method determined in this work, more than sufficient resolution is possible for saturates vs diaromatics, diaromatics vs triaromatics, and tri-aromatic vs polyaromatics. The best results were seen using a start temperature of 120°C with a 0 minute hold time and a ramp rate of 3°C/min. Unfortunately, this set-up will not allow for separation of saturates and monoaromatics. In order to make this technique a plausible re-placement for the current ASTM/CGSB methods the saturates must also be separated from the monoaromatic compounds. In order to accomplish this, a selective detector will be used for separation of the monoaromatics from saturates.

A new vacuum ultra-violet absorption spectroscopy detector was tested for this purpose. The VUV detector is capable of simultaneously collecting quantitative and qualitative data, and along with carefully selected integration filters, allows for selective detection of monoaromatics and saturate compounds. With fine-tuning of the filtering methods, the VUV detector is able to provide results that agree well with previously collected SFC data. Undiluted real diesel samples can be run on this instrument, and the resulting data can be used for aromatic group type determination.

5.3 Biodiesel

5.3.1 Overview

Biodiesels are increasingly important biologically derived sources of fuel that may be used on their own or blended with conventional petroleum diesel fuels (petrodiesel). The blends of fatty acid methyl and ethyl esters (FAMEs/FAEEs) used in biodiesel are produced by trans esterification of tri-glycosides derived from biological sources [150]. The Canadian requirement to add 2% biodiesel content to diesel fuel in 2011 has further complicated the ASTM D5186 protocol [5] as the biodiesel component does not readily elute from the SFC column. This leads to incorrect analytical results and fouling of the SFC column, and is another reason a replacement method is required.

Previous research has shown that FAMEs and FAEEs can be measured in biodiesel using comprehensive multidimensional gas chromatography (GC×GC), and there has also been research showing excellent separations of FAME/FAEE using GC×GC with an IL column in one of the two dimensions [151, 152, 153, 154]. It is proposed to investigate the chromatographic behavior of biodiesel on IL columns in the hopes that 1D GC group-type separation can be developed to perform routine quantification of percent biodiesel in biodiesel blends. A VUV detector will be employed to selectively detect percent biodiesel.

5.3.2 Experimental

5.3.2.1 Chemicals

Syncrude synfuel samples Fuel 7, Fuel 11, Fuel 2, Fuel 14, and Fuel 15 were used for this portion of research. 100% Biodiesel from Syncrude was also used. Mixtures of percent diesel were prepared by adding a specified weight percent of 100% biodiesel to the diesel samples. Two samples, Fuel 16 and Fuel 17, were also used. These samples are diesel samples that have been previously blended with approximately 4-5% biodiesel onsite at Syncrude Research.

5.3.2.2 Instrumentation

Experiments were conducted on an HP6890 GC (HP Agilent Technologies) Mississauga, ON, Canada) using helium as a carrier gas at a linear velocity of ~30 cm s^{-1}. This instrument was equipped with an Agilent 7683 auto sampler (Agilent Technologies). All studies were conducted on the IL-111 column (Supelco) with dimensions of 30 m × 250 μm with 0.2 μm film. The injector temperature was set to 250 °C. An injector volume of 0.2 μL was used with a split ratio of 60:1. A VGA-100 VUV detector (VUV Analytics, Inc., Austin TX), was coupled to the Agilent GC. The VUV and accompanying transfer line and flow cell were kept at 300 °C.

5.3.3 Results and Discussion

Since biodiesel fouls the SFC column, finding a new method for the determination of percent biodiesel was of utmost importance. Successful use of filters in Section 5.2 led to trying to find a selective filter for biodiesel in diesel samples. The first step in determining a useful filter was to run a few diesel samples as well as a 100% biodiesel sample in the whole wavelength range, as shown in Figure 5-11.

Both Fuel 13 and Fuel 14 are Syncrude reference diesel samples, while both Fuel 15 and Fuel 16 samples are Syncrude diesel samples, and the biodiesel is a 100% biodiesel. The interesting features of biodiesel occur in the diaromatic region. When looking closer at the peaks observed in biodiesel, the peaks are much different than those of the diaromatics presented in Section 5.2. Figure 5-12 shows the resultant biodiesel chromatogram and the absorbance for one of the peaks. This compound was identified as a fatty acid methyl ester and has characteristic absorption spectra for FAME/FAEEs.

A)

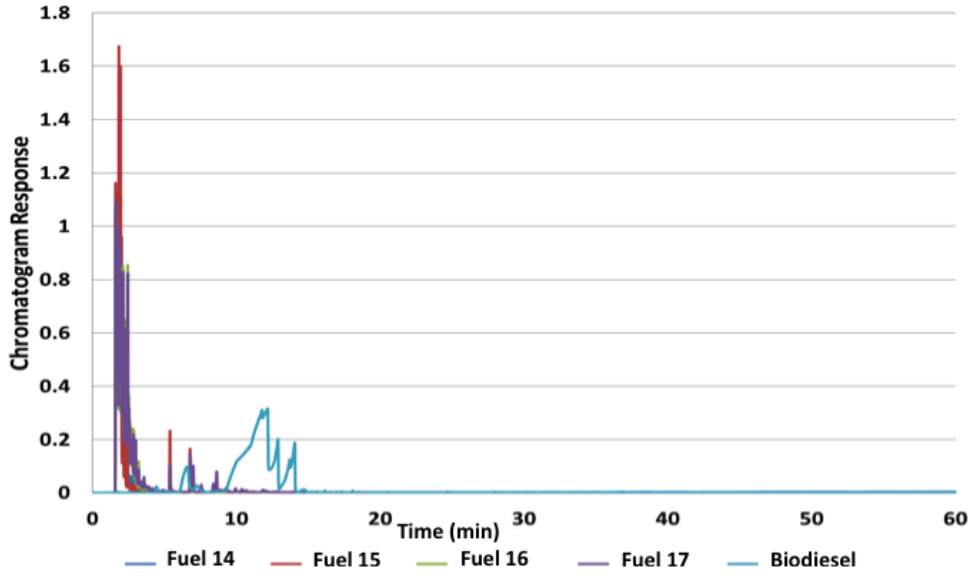
Chromatogram Response
1.8
1.6
1.4
1.2
1
0.8
0.6
0.4
0.2
0
0
10
20
30
40
50
60
Time (min)
Fuel 14
Fuel 15
Fuel 16
Fuel 17
Biodiesel

B)

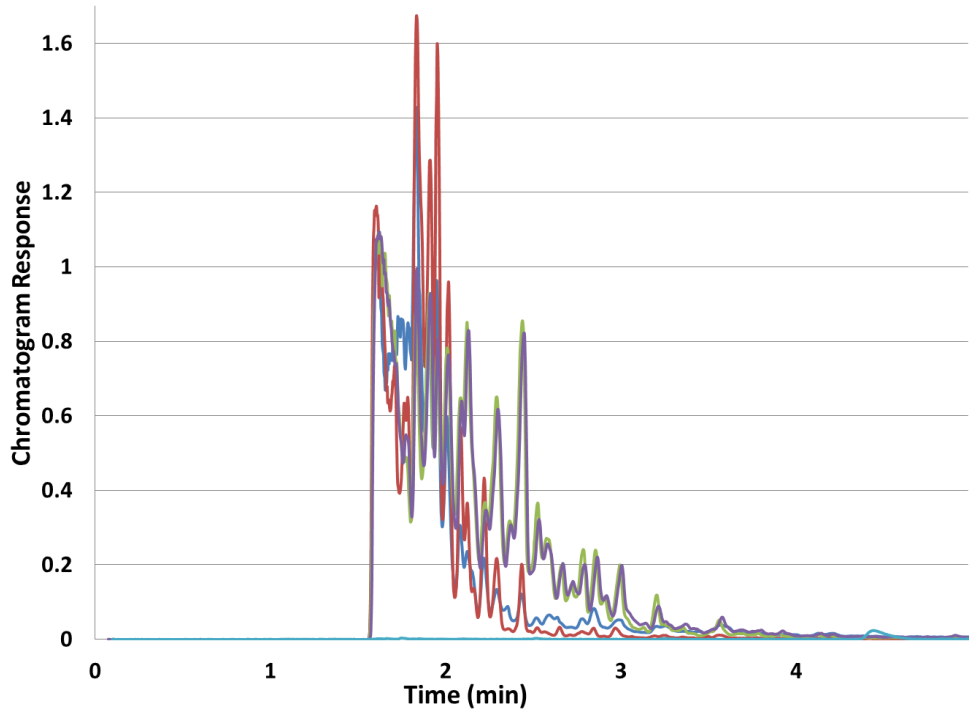
Chromatogram Response
1.6
1.4
1.2
1
0.8
0.6
0.4
0.2
0
0
1
2
3
4
Time (min)

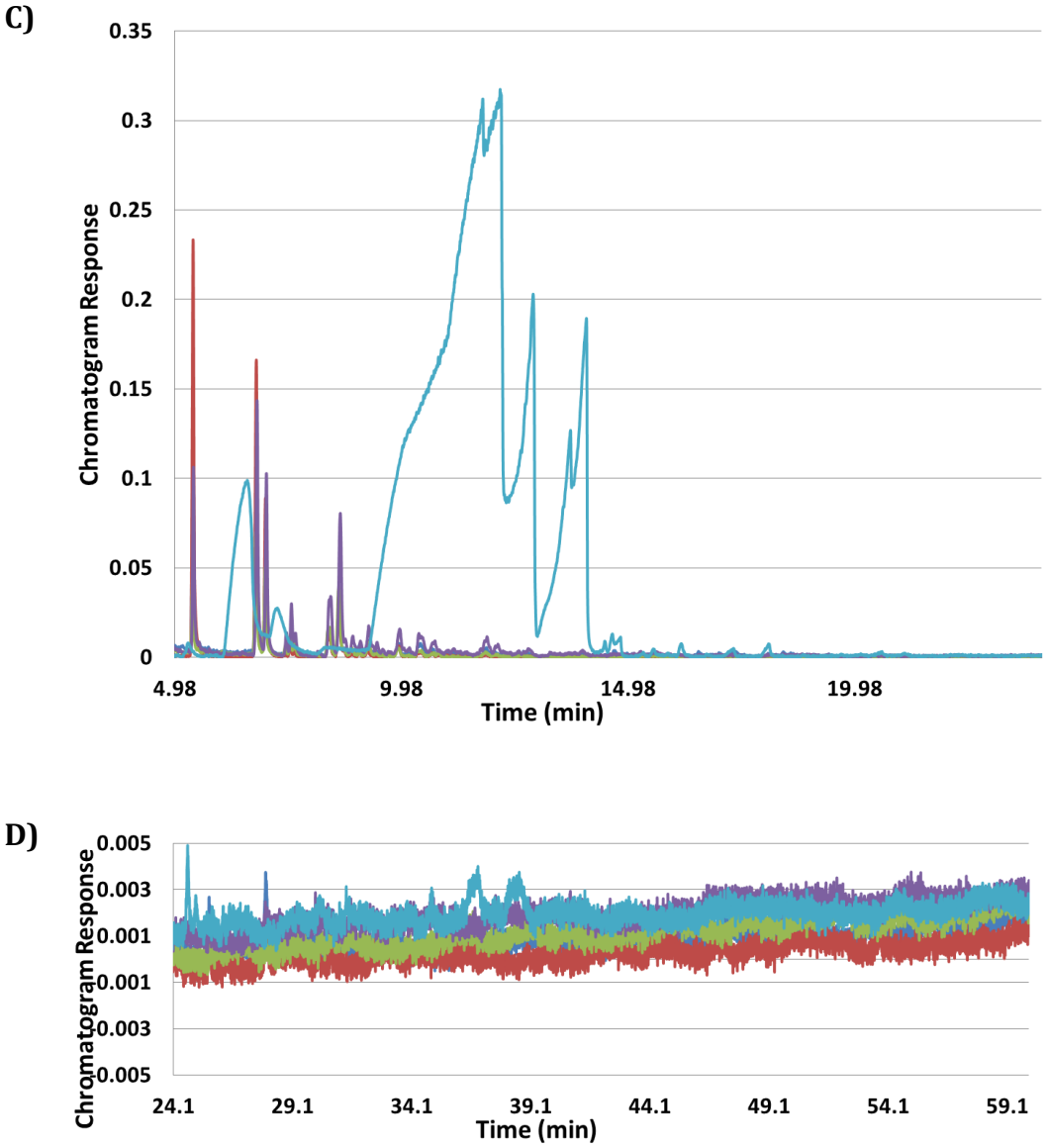

Figure 5-11. Diesel and Biodiesel Samples Collected on VUV using a 125-240 nm filter. A) Full Chromatogram B) Monoaromatic region C) Diaromatic Region D) Polyaromatic Region. Fuel 14 (Blue), Fuel 15 (Red), Fuel 16 (Green), Fuel 17 (Purple) and Biodiesel (Teal)

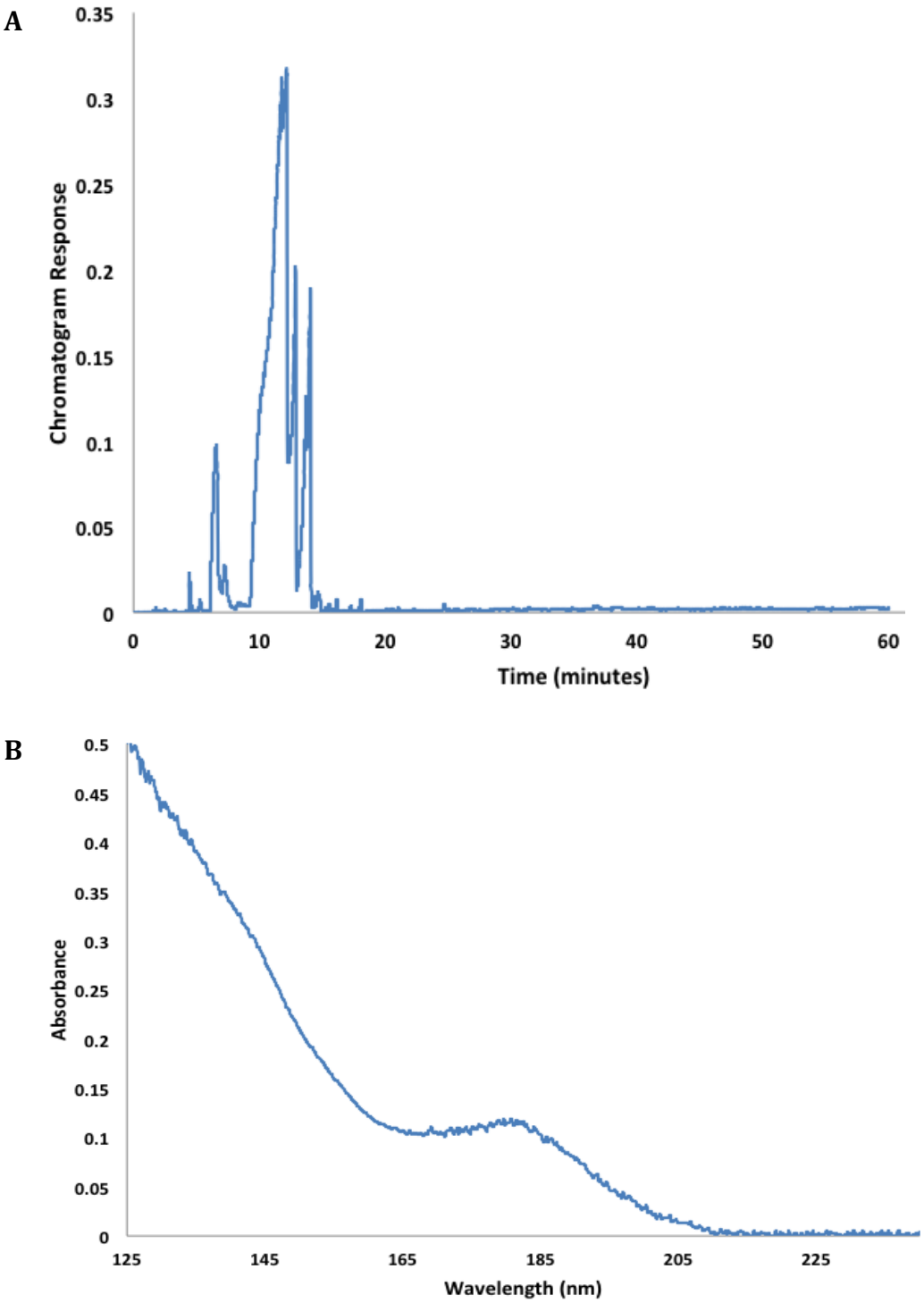

Figure 5-12. VUV Data of 100% Biodiesel. A) Full Chromatogram B) Average absorbance spectra collected between 12-13 minutes.

The absorbance spectrum is representative of the absorbance spectra across the chromatogram for FAME/FAEE peaks. What is interesting about these spectra as shown in Figure 5-12, is that they have the majority of their absorbance below 200 nm, which is the opposite of the diaromatic compounds of diesel found in this region, that have the majority of their absorbance above 200 nm.

With the success of using selective wavelength filters to determine monoaromatic and saturate content in the first region of the chromatogram in Section 5.2, a similar strategy was applied to biodiesel. In this case the diaromatic content was determined ($AD_{200-240)}$, followed by determination of the whole range including diesel and biodiesel content ($ADB_{125-240)}$. Therefore, leaving the 'bio' content ($AB_{125-240}$)to be determined by subtracting ($AD_{125-240}$)from ($ADB_{125-240.}$) In order to do this ($AD_{200-240}$) was correlated to ($AD_{125-240}$), which was accomplished by multiplying ($AD_{200-240}$) by 0.163, which was determined to be the correction factor for diaromatics as described in Section 4.3.

Experiments were conducted using samples containing approximately 1, 5, 10, 20 and 30% biodiesel in diesel by weight, and run in duplicate. When the percentages of biodiesel were plotted against the $AB_{125-240}$ linear calibration curves were achieved, as depicted in Figure 5-13.

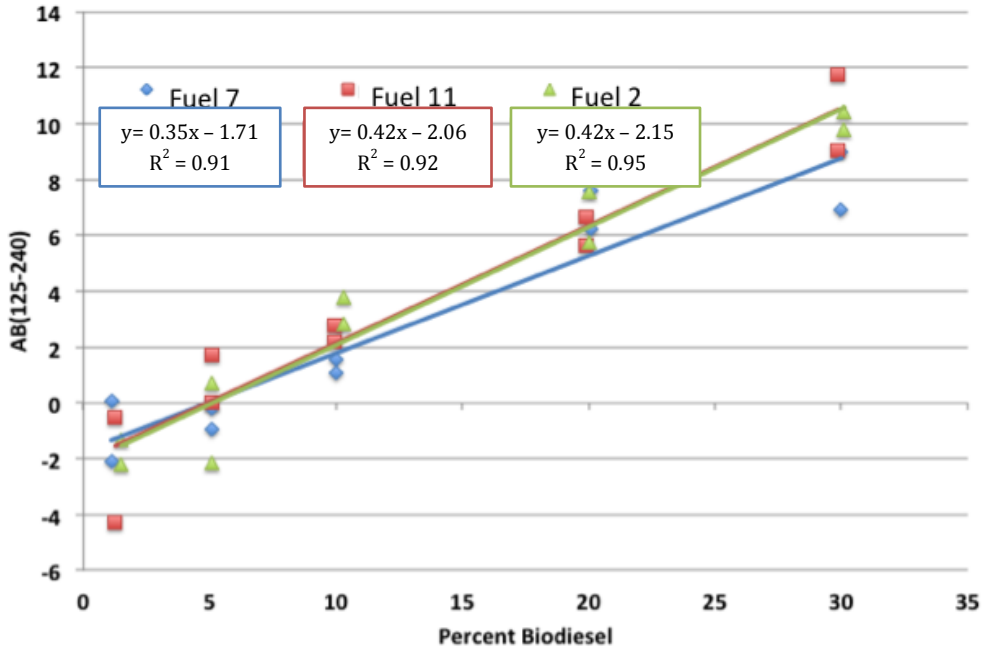

Figure 5-13. Percent biodiesel calibrations curves completed in three different diesel samples (FUEL 7, FUEL 11 and FUEL 2).

These calibration curves show that in all three sample matrices the biodiesel content still achieves a linear calibration with acceptable R^2 values. To validate this calibration, each calibration curve was used to predict the concentration in the other samples. Each sample's weight percent biodiesel was calculated from each calibration curve, giving a total of 90 runs, where 30 were projected onto their own calibration curve. The percent difference was then taken for each run, and the absolute percent error for the 90 runs was 1.03%; this information is found in Table 5-8.

Table 5-8. Comparison of calculated biodiesel percentage using calibration curves from all samples.

			% Calculated Based on Calibration Curve		
Sample Name	Biodiesel %	$AB_{125-240}$	FUEL 7	FUEL 11	FUEL 2
FUEL 7	1.10	0.72	0.05	1.09	1.40
	1.10	1.64	2.34	3.19	3.56
	5.06	2.81	5.26	5.87	6.31
	5.06	2.44	4.33	5.02	5.43
	10.00	4.59	9.72	9.95	10.50
	10.00	4.76	10.14	10.34	10.90
	20.10	8.88	20.42	19.75	20.56
	20.10	9.05	20.86	20.15	20.98
	30.00	12.79	30.19	28.70	29.75
	30.00	12.40	29.22	27.81	28.84
FUEL 11	1.27	-1.06	-4.40	-2.98	-2.78
	1.27	1.63	2.33	3.18	3.55
	5.10	3.34	6.58	7.08	7.55
	5.10	2.50	4.50	5.17	5.59
	9.93	4.94	10.57	10.73	11.30
	9.93	4.63	9.81	10.04	10.59
	19.91	9.24	21.33	20.58	21.42
	19.91	8.55	19.60	19.00	19.80
	29.86	13.90	32.94	31.22	32.35
	29.86	12.52	29.52	28.09	29.12
FUEL 2	1.50	0.16	-1.34	-0.18	0.10
	1.50	0.58	-0.31	0.77	1.06
	5.10	2.62	4.78	5.43	5.86
	5.10	2.25	3.87	4.59	5.00
	10.30	4.64	9.83	10.05	10.60
	10.30	4.99	10.72	10.87	11.44
	20.00	9.29	21.44	20.69	21.52
	20.00	8.32	19.01	18.46	19.24
	30.12	12.76	30.11	28.63	29.68
	30.12	12.70	29.97	28.50	29.55

Although these results are promising, an error of 3% is still quite high for this application. Referring back to the absorption spectra of FAME/FAEE content in Figure 5-12 B, there is some absorption in the region of 200-210 nm. To remedy this the dynamic filter for diaromatic content was adjusted to 210-240 nm, as the FAME compounds show basically no spectra over 210 nm, and is as long of a wavelength that can be used without losing diaromatic signal. When using our adjusted filter (210-240 nm) the calibration perform better as shown in Figure 5-14, and the absolute percent error decreases to 0.9 %.

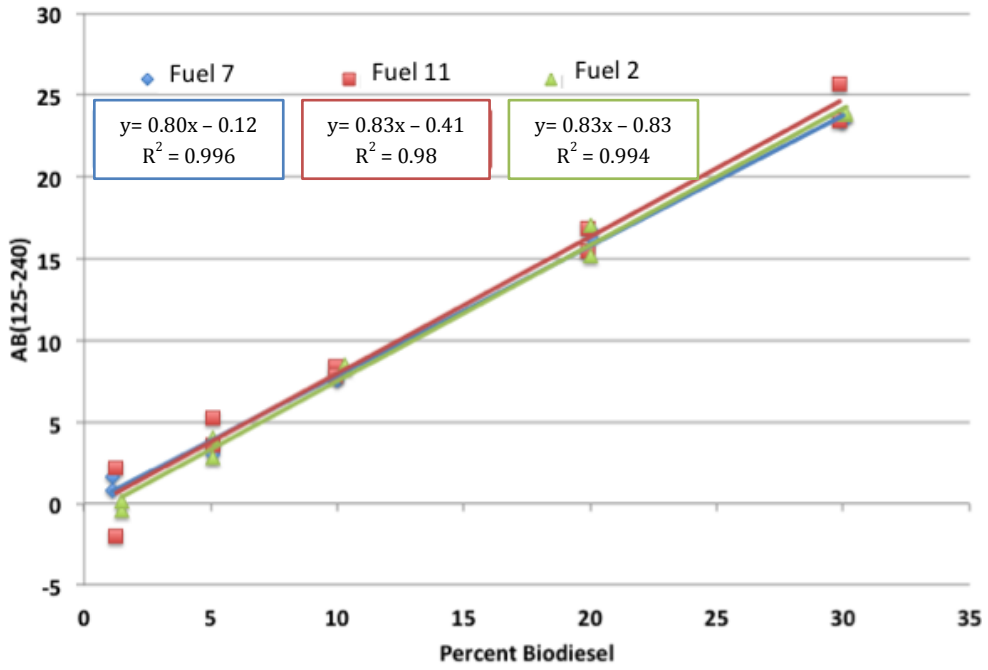

Figure 5-14. Percent biodiesel calibrations curves completed in three different diesel samples (FUEL 7, FUEL 11 and FUEL 2), using 210-240 filtering.

While the results for correlation to biodiesel seem promising, it is also important that our aromatic and saturate content determinations are unchanged. Therefore, saturate, monoaromatic, diaromatic and polyaromatic content were determined a second time in the samples with biodiesel added. To do this the same group-type analysis completed in Section 5.2 was done across all samples, while ignoring the biodiesel content. Table 5-9 shows the group-type percentages originally determined (Section 5.2) as well as the amounts in the spiked samples without correction for biodiesel contribution.

Table 5-9. Determination of aromatic and saturate group-type content by VUV with (Biodiesel) and without (Original) biodiesel content added.

	Saturates %	Monoaromatics %	Diaromatics %	Polyaromatics %
Fuel 2 Original	67.6±0.4	28.7±0.5	2.4±0.1	1.4±0.7
Fuel 2 Biodiesel	69.5±0.3	29.0±0.2	1.0±0.2	0.5±0.3
Fuel 7 Original	64.6±0.3	32.6±0.3	2.7±0.1	0.2±0.2
Fuel 7 Biodiesel	64.8±0.5	32.2±0.3	2.4±0.3	0.7±0.6
Fuel 11 Original	67.2±0.5	30.1±0.4	2.5±0.2	0.3±0.6
Fuel 11 Biodiesel	67.7±0.2	29.9±0.1	1.9±0.2	0.5±0.2

The group-type amounts determined from samples spiked with biodiesel and those without biodiesel spiked in give results that agree within error for fuel 7 and fuel 11, and are similar for fuel 2. This indicates that our group-type analysis can be done even in the presence of biodiesel. When this analysis is completed both the biodiesel content and the resulting calculated group-type percentages should be reported. When biodiesel is added to the sample it contributes to the total weight of the sample, which will effectively decrease the group-type percentages. Table 5-10 shows the data collected for both biodiesel and group-type determination for Fuel 11.

Table 5-10. Aromatic and biodiesel percent determination for fuel 11.

	Biodiesel %	Saturates %	Mono Aromatics %	Di aromatics %	Poly Aromatics %
Fuel 11 Original	0.0	67.2±0.5	30.1±0.4	2.5±0.2	0.3±0.6
Fuel 11 Biodiesel	1.1	66.5	29.8	2.5	0.3
Fuel 11 Biodiesel	5.1	63.7	28.6	2.4	0.3
Fuel 11 Biodiesel	10.0	60.5	27.1	2.2	0.3
Fuel 11 Biodiesel	20.1	53.1	23.8	2.0	0.2
Fuel 11 Biodiesel	30.0	47.0	21.1	1.7	0.2

As shown in Table 5-10 the group-type percentages decrease as biodiesel content increase. Adding biodiesel dilutes the sample. So it is important to take this dilution into account when reporting the aromatic and saturate percentages.

5.3.4 Conclusions

Determining the amount of biodiesel in a diesel sample is of great importance for government regulations and quality control. Using selective wavelength filtering on our VUV instrument in conjunction with an ionic liquid column it is possible to detect biodiesel content with diaromatic content present with an average error of 0.9%. However, it is important that we can still determine the relative percent contribution of all group-types simultaneously. With our current filtering methodology the group-type percent results continue to perform well, as indicated by their agreement with the valued determined in Section 5.2.3. Therefore, VUV our method is capable of determining aromatic and saturate content, while simultaneously determining biodiesel content.

CHAPTER SIX. Conclusions and Future Work

6.1 Conclusions

This thesis explored the use of ionic liquid capillary columns in gas chromatography for separation of petroleum samples. This work was completed in two different areas. The first focusing on separation of a single contaminant from the complex matrix, while the second focused on group-type separation of petroleum samples.

6.1.1 Alkyl Phosphate Contaminants

In Chapter 2 a number of ionic liquid capillary columns were studied for use in gas chromatography. Seven alkyl phosphate standards representing possible contaminants in petroleum products were used to compare the retention on each phase. Ionic liquids provide a host of interesting selectivities to address challenging separations. Although, the retention behavior of compounds of interest on ionic liquid columns may not be as expected as demonstrated in Chapter 2. For the alkyl phosphate standards tested, it was observed that the retention behavior of the entire suite of compounds could not be easily rationalized, and may be difficult even in the case of a homologous series. Despite these obstacles, it was still possible to reliably predict retention using a thermodynamic model.

Method development can be guided in a logical manner by using retention studies such as those presented in Chapter 2. IL-100 proved to be

highly selective for alkyl phosphate compounds in this research, meaning that this column would be a likely choice for selective separation of these compounds from petroleum hydrocarbons in 1D GC. This stationary phase may also be very useful in multidimensional GC analysis for alkyl phosphates.

Chapter 3 continued the studies of alkyl phosphate retention on ionic liquid columns, but was expanded to two-dimensional gas chromatography. Seven alkyl phosphate standards representing possible contaminants in petroleum products were used to test prediction models for these compounds. Prediction of alkyl phosphate standards in GC can be useful for identifying unknown alkyl phosphates in complex samples. Using a selective ionic liquid column in conjunction with a prediction model can improve challenging separations and allow for identification of unknown compounds. Caution must be used with prediction models, and extra care taken to be sure that the chromatographic data is reliable. If chromatography is performing well predictions work extremely well. Unknown compounds can also be predicted using the method presented in Chapter 3, but improved use of parameters will lead to more accurate results. Determination of unknowns using a predictive model in complex samples would be a useful tool for both GC and GC×GC.

During testing of our predicted models it was noted that there was significant retention time drift for our alkyl phosphates. Drifting retention

times made it more difficult to predict our retention times and made the model unreliable. The alkyl phosphates did not quantitatively elute from ionic liquid columns that used imidizolium rings as part of their cation. Using this information it was inferred that reactions were happening between the phosphate compounds and the column.

6.1.2 Group-Type Separations

The latter half of this thesis focused on the development of methods to analyze diesel samples by group-type. IL-111 selectively retained aromatic hydrocarbons over saturates, while providing group-type aromatic separation better than the other five ionic liquid columns tested. These characteristics lend the IL-111 column to be as a possible replacement for the current SFC method which does group-type separation of saturates and polyaromatic hydrocarbons. Unfortunately, this column is only capable of fully separating diaromatic and larger compounds from saturates in diesel samples. Therefore, selective detection is necessary to separate the monoaromatic compounds from the saturates. A simple monochromatic GC-UV-FID is capable of selectively detecting these group types, but does not have low enough detection limits for practical use.

Therefore, a VUV detector was used for the detection of saturates and aromatic compounds, using selective filters. This allows the user to determine the weight percent of each group type in diesel samples, with

results similar to the current SFC. The advantages of this method are two-fold. Not only does the VUV detector provide both quantitative and qualitative information simultaneously, but the column used does not suffer from column fouling due to biodiesel content.

The VUV detector was also employed for determining the biodiesel content in diesel samples. Since biodiesels sample foul traditional SFC columns for group-type analysis of diesel samples, an alternate technique was necessary for this determination. While we have only tested our method on one biodiesel sample, I believe that it is proof of concept for this selective filtering method, which could potentially work well for all biodiesel samples. With this method being based on selective filtering that differentiates between diaromatics and FAME/FAEE compounds the changing profile of the FAME/FAEE should not affect the ability to deconvolve our signal. This method is also advantageous because it allows the determination of biodiesel content while simultaneously determining the group-type content of the diesel portion.

6.2 Future Work

6.2.1 Improved Characterization of Ionic Liquid Columns

Ionic liquid columns provide unique retention for alkyl phosphates, based on the standard compounds analyzed. IL-100 specifically has a very high affinity for alkyl phosphates, which may help separate them from

complex samples. The problem with developing further separations with the IL-100 column is the lack of understanding of the retention mechanism on the column. It is unclear why one phase is more selective than the rest for these compounds, but of greater concern is whether or not there is a reaction happening with the capillary column.

To determine what, why and how these reactions are happening, in-depth studies of these column materials and alkyl phosphate standards will be necessary. This can include stability studies, further NMR determination (including P NMR) as well as computer modeling and simulation of the structures of these columns and how they change with temperature. Knowledge of the nature of the interaction occurring between the imidizolium rings on the ionic liquid cation and the alkyl phosphate standards would benefit future synthetic design of columns. Understanding the reaction may also allow for purposeful modification and design of future stationary phases, in order to make them less reactive.

Another general challenge for this type of predictive work is the lack of available analytical standards to predict the retention of compounds on our stationary phases. We also need to add more molecular descriptors for the standards that we do have to improve our predictive modeling. As shown in Chapter 3 it is difficult to predict the behavior of compounds without reliable chromatography, and with a small number of standards to build a successful model.

6.2.2 Industrial Use of VUV Determinations

While flame ionization detection provides reliable mass quantification of hydrocarbon samples for GC, FID is not capable of selective detection. Since an ionic liquid stationary phase does not currently exist that is capable of separating saturates from mono-, di- and polyaromatics, it is necessary to use a selective detector. Traditional UV absorbance detection does not provide a response for analytes that lack a chromophore. As a result, saturated compounds cannot be detected. Therefore, VUV detection must be used to detect all of our group-types of interest.

UV response factors for aromatic compounds can vary significantly, depending on chemical structure [155,156,157]. Even though this is also true in VUV, the relative response factors for each group-type are on average the same, and work well for determining group-type percentages as evidenced in Chapter 5. However, this does make the analysis slightly more cumbersome than using an FID. To make this process user friendly it would be helpful to have a function for determining response factor, and possibly even to determine the relative weight percent built into the VGA-100 software. This will not be a difficult change as the software is already set up to automatically create calibration curves, and has library database of absorbance spectra to easily determine relative response factor.

A function for baseline fitting of our di- and polyaromatic region would also be helpful to improve our analysis. Especially in the

polyaromatic region where we have such low concentrations it is important to properly identify the peaks in the background signal. This type of fitting is currently being implemented in the software and will only improve the results of our analysis.

Finally, a challenge facing industry and consumers who operate in cold climates should be addressed. Government regulations mandate that industry use 2% biodiesel in their operations in order to lessen the reliance on fossil fuels and decrease emissions of carbon dioxide. Therefore, there is a need to have a reliable commonly available method to measure the percentage of biodiesel in diesel fuel, as reported in Chapter 5. However, even though the percentage of biodiesel may be the same, the molecular profiles may be different, leading to differences in performance.

In cold weather, biodiesel fuels have an issue where solids form in the fuel if the ambient temperature gets too low [158]. This causes fouling of engines and equipment. Compounding this problem, this issue can arise at two completely different temperatures for a pair of fuels with same percent biodiesel content. These differences in performance are due to differences in the molecular profile of biodiesel. A routine method for the detailed profiling of biodiesel fuel blends and reliable mathematical models of fuel performance based on these profiles should be developed. There is not yet a good model that can be used to predict cloud point or cold filter plugging point of a biodiesel. With this knowledge, it would be possible to

fine-tune biodiesel blends based on current temperature and the profiles of feedstock. Thus maximizing biodiesel content while avoiding problems associated with particulate formation. Developing a method by which cloud point and cold filter plugging point could be accurately predicted when a fuel is being blended would be valuable for industrial operators blending biodiesel for use in cold climates.

References

[1] R.O Dunn, *Trans ASAT,* 44 (2001) 1155.

[2] J.M. Carpentier, Our Energy Heritage Oil and Gas, Meridian Press, Montreal (1989) 73.

[3] S.C. Lawrence, A.C. Kalenchuck, K. Ranicar, S. Dhillon, A. Baig, *SPE Prod. Oper.* (2009) 556.

[4] R.S. Tayor, P.S. Stemler, A. Lemieux, G.C. Fyten, A. Cheng, *J. Can. Petro. Technol.* 46 (2007) 16.

[5] *Method D 5186-03, Annual Book of ASTM Standards,* American Society for Testing and Materials, West Conshohoken, PA, USA, 2009.

[6] N. Šegudovic, T. Tomic, L. Škrobonja, L. Konitc. *J. Sep. Sci.,* 27 (2004) 65.

[7] C.W. Skink, D.R. Hardy. *Anal. Chem.* 66 (1994) 1334.

[8] D.J. Cookson, P. Iliopoulos, B.E. Smith. *Fuel* 4(1995) 70.

[9] S. Sato, Y. Sugimoto, K. Sakanishi, I. Saito, S. Yui. *Fuel* 3 (2004) 1915.

[10] A. Karonis, E. Lois, F. Zannikos, A. Alexandridis, H. Sarimveis. *Energy & Fuels* 17 (2003) 1259.

[11] D.T. Hountalas, S.I. Raptotasios, T.C. Zannis. *Energy & Fuels* 27 (2013) 4910.

[12] A. Ohtsuka, K. Hashimoto, Y. Akutsu, M. Arai, M. Tamura. *J. Jpn. Petrol. Inst.* 45 (2002) 24.

[13] B.L. Valle-Hernández, O. Amador-Muñoz, A. Jazcilevich-Diamant, A. E. Hernández-López, R. Villalobos-Pietrini, R. González-Oropeza. *Combustion Science and Technology* 185 (2013) 420.

[14] R. Sitko, B. Zawisza, K. Kowaleska, K. Kocot, M. Polowniak, *Talanta* 85 (2011) 2000.

[15] K.D. Nizio, T.M. McGinitie, J.J. Harynuk. *J. Chromatogr. A.* 1255 (2012) 12.

[16] B.N. Barman, V.L. Membrado. *Crit. Rev. Anal. Chem.* 30 (2000) 75.

[17] J. Blomberg, E.P.C. Mes, P.J. Schoenmakers, J.J.B. van der Does, *J. High Resol. Chromatogr*. 20 (1997) 125.

[18] S.Schubarth, D. Milton-Tayler, SPE Annual Technical Conference and Exhibition, Houston, Texas, 26-29 September 2004, Paper 90562-MS.

[19] W.M. Harms in: J.K. Borchard, T.F. Yen (Eds.), Oil-Field Chemistry: Enhanced Recovery and Production Stimulation, American Chemical Society, Washington DC, 1989, p. 55.

[20] J.I. DiStasio (Ed.), Chemicals for Oil Field Operations, Noyes Data Corportation, New Jersey, 1981, p.141.

[21] L.J. Maberry, S.B. McConnell, K.V. Tanner, J.J. Hinkel, *SPE Prod. Facil.* 13 (1998) 236.

[22] S.H. Rose, B.P. Block, J. Am. Chem. Soc. 87 (1965) 2076.

[23] J.I. Fukasawa, H. Tsutsumi, *J. Colloid Interface Sci*. 143 (1991) 69.

[24] M.G. Page, G.G. Warr, *J. Phys. Chem.* B 108 (2004) 16983.

[25] M.G. Page, G.G. Warr, *Langmuir* 25 (2009) 8810.

[26] National Northeast British Columbia's Ultimate Potention for Conventional Natural Gas Fact Sheet 2006, available online at http://www.neb-one.gc.ca/clf-nsi/rnrgynfmtn/nrgyrprt/ntrlgs/nbcltmtptntl2006/fctsht0609-eng.html, accessed December 1, 2014.

[27] R.S. Taylor, P.S. Stemler, A. Lemieux, G.C. Fyten, A. Cheng, J. Can. *Petro. Technol*. 46 (2007) 16.

[28] A. Lemieux, *Crude Quality Concern, Phosphorus in Light Sweet Canadian Crude.* Canadian Crude Quality Technical Association, Ontario. 1999, p. 1-7.

[29] The Canadian Crude Quality Technical Association (CCQTA), Phosphorus in Crude Oil, available online at http://www.ccqta.com/projects.php?project_id=6, accessed on May 27, 2014.

[30] G.P. Funkhouser, US Patent 7066262 B2 (2006).

[31] L.J. Maberry, S.B. McConnell, K.V. Tanner, J.J. Hinkel, *SPE Production & Facilities* 13 (1998) 236.

[32] B.N. Barman, V.L. Cebolla, L. Membrando, *Crit. Rev. Anal. Chem.* 30 (2000) 75.

[33] F. Adam, F. Bertoncini, V. Coupard, N. Charon, D. Thiebaut, D. Espinat, M.C. Hennion, *J. Chromatogr. A,* 1186 (2008) 236.

[34] A. Demirbas, *Energy Convers. Manag.* 43 (2002) 2349.

[35] Y.H. Tan, M.O. Abdullah, C. Nolasco-Hipolito, *Renewable and Sustainable Energy Reviews,* 47 (2015) 589.

[36] G. Arzamendi, E. Arguinarena, I. Campo, L.M. Gandia, *Chem. Eng. J.* 122 (2006) 31.

[37] Environment Canada, Renewable Fuels Regulations (SOR/2010-189), available online at http://ec.gc.ca accessed on June 17, 2015.

[38] H.H. Strain, J. Sherma. *J. Chem. Edu.* 44 (1967) 235.

[39] A.J.P. Martin, R.L.M. Synge. *Biochem J.* 35 (1941) 1358.

[40] A.T. James, A.J.P. Martin. *Biochem. J.* 50 (1952) 679.

[41] K.D. Bartle, P. Myers. *Trends Anal. Chem.* 21 (2002) 547.

[42] Z. Liu, J.B. Phillips. *J. Chromatogr. Sci.* 29 (1991) 227.

[43] H.J. de Geus, J. de Boer, J.B. Phillips, E.B. Ledford Jr., U.A.T. Brinkman. *J. High Resol. Chromatogr.* 21 (1998) 411.

[44] A.L. Lee, K.D. Bartle, A.C. Lewis. *Anal. Chem.* 73 (2001) 1330.

[45] J.B. Phillips, E.B. Ledford, *Field Anal. Chem. Technol.* 1 (1996) 23.

[46] J.B. Phillips, R.B. Gaines, J. Blomberg, F.W.M. van der Wielen, J.M. Dimandja, V. Green, J. Granger, D. Patterson, L. Racovalis, H.J. de Gues, J. de Boer, P. Haglund, J. Lipsky, V. Sinha, E.B. Ledford. *J. High Resol. Chromatogr.* 22 (1999) 3.

[47] R.M. Kinghorn, P.J. Marriott. *J. High Resol. Chromatogr.* 21 (1998) 620.

[48] J. Beens, M. Adachour, R.J.J. Vreuls, K. van Altena, U.A.T. Brinkman. *J. Chromatogr. A.* 919 (2001) 127.

[49] M. Adahchour, J. Beens, U.A.T. Brinkman. *Analyst* 128 (2003) 213.

[50] J.J. Harynuk, T. Górecki. *J. Chromatogr. A* 1019 (2003) 53.

[51] P.A. Bueno Jr., J.V. Seeley. *J. Chromatogr. A* 1027 (2004) 3.

[52] C. von Muhlen, W. Khummueng, C.A. Zini, E.B. Caramao, P.J. Marriott, *J. Sep. Sci.* 29 (2006) 1909.

[53] L. Mondello (Ed.), Comprehensive Chromatography in Combination with Mass Spectrometry (1st Ed.), John Wiley & Sons, Inc., Hoboken, New Jersey (2011).

[54] M. Adahchour, J. Beens, R.J.J. Vreuls, U.A.Th.Brinkman, *Trends Anal. Chem.* 25 (2006) 726.

[55] M. Kallio, T. Hyotylainen, M. Lehtonen, M. Jussila, K. Hartonen, M. Shimmo, M.I. Riekkola, J. Chromatogr. A 1019 (2003) 251.

[56] O. Panic, T. Gorecki, *Anal. Bioanal. Chem*. 386 (2006) 1013.

[57] A. Casilli, E. Decorzant, A. Jaquier, E. Delort, *J. Chromatogr. A* 1375 (2014) 169.

[58] H.P. Tan, T.S. Wan, C.L. Min, M. Osborne, K.H. Ng, *J. Chromatogr. A* 1333 (2014) 106.

[59] G.S. Frysinger, R.B. Gaines, *J. Forensic Sci.* 47 (2002) 27.

[60] G.S. Frystinger, R.B. Gaines, C.M. Reddy, *Environ. Forenics* 3 (2002) 27.

[61] R.K. Nelson, B.M. Kile, D.I. Plata, S.P. Sylva, L.Xu, C.M. Reddy, R.B. Gaines, G.S. Frysinger, S.E. Reichenbach, *Environ. Forenics* 7 (2006) 33.

[62] S. Maity, A. Jannasch, J. Adamec, T. Nalepa, T.O. Hook, M.S. Sepulveda, *Comp Biochem. Physiol. B Biochem. Mol. Biol.* 161 (2012) 348.

[63] K. Ralston-Hooper, A. Hopf, C. Oh, X. Zhang, J. Adamec, M.S. Sepulveda, *Aquat Toxicol.* 88 (2008) 48.

[64] C. Lledo-Fernandez, C.E. Banks. *Anal. Methods.* 3 (2011) 1227.

[65] N.H. Snow. *Adv. in Chromatogr.* 45 (2007) 215.

[66] A.D. Pert, M.G. Baron, J.W. Birkett. *J. Forensic Sci.* 51 (2006) 1033.

[67] J. Seeley. *J. Chromatogr. A* 1255 (2012) 24.

[68] S.P.J. van Leeuwen, J. de Boer. *J. Chromatogr. A* 1186 (2008) 161.

[69] M.F. Almstetter, P.J. Oefner, K. Dettmer. *Anal. Bioanal. Chem.* 6 (2012) 1993.

[70] W. Kaye, *Anal. Chem.* 34 (1962) 287.

[71] T. Cedron-Fernandez, C. Saenz-Barrio, S. Cabredo-Pinillos, I. Sanz-Vicente, *Talanta* 57 (2002) 555.

[72] H.V. Lagesson, A. Nilsson, C. Tagesson, *Chromatographia* 52 (2000) 621.

[73] V. Lagesson, L. Lagesson-Andrasko, J. Andrasko, F. Baco, *J. Chromatogr. A* 867 (2000) 187.

[74] P. Straka, M. Havelcova, *Acta geodynamica et geomaterialia* 9 (2012) 481.

[75] K.A. Schug, I. Sawicki, D.D. Carlton, Jr., H. Fan, H.M. McNair, J.P. Nimmo, P. Kroll, J. Smuts, P. Walsh, D. Harrison. *Anal. Chem.* 86 (2014) 8329.

[76] K. Huang, X. Han, X. Zhang, D.W. Armstrong, R.E. Synovec. *Anal. Bioanal. Chem*. 389 (2007) 2265.

[77] P. Sun, D.W. Armstong, *Anal. Chim. Acta* 661 (2010) 1.

[78] D.W. Armstrong, T. Payagala, L.M. Sidisky. *LCGC North Am.* 27(2009) 596.

[79] http://www.sigmaalrich.com/analytical-chromatography/gas-chromatography/columns/ionic-liquid-literature.html (accessed Feb. 11/13)

[80] P. Delmonte, A.R.F. Kia, J.K.G. Kramer, M.M. Mossoba, L. Sidisky, J.I. Rader, *J. Chromatogr. A* 1218 (2011) 545.

[81] L. Mahe, T. Dutriez, M. Courtaid, D. Thiebaut, H. Dulot, F. Bertoncini, *J. Chromatogr. A.* 1218 (2011) 534.

[82] E.Kováts, *Helv. Chim. Acta.* 41 (7) (1958)1915.

[83] H. van Den Dool, P. Kratz, *J. Chromatogr. A* 11 (1963) 463.

[84] J.V. Seeley, S.K. Seeley, *J. Chromatogr. .* 1172 (2007) 72.

[85] Y.P. Zhao et al. *J. Chromatogr. A* 1218 (2011) 2577.

[86] C. von Muhlen, P.J. Marriott, *Anal. Bioanal. Chem*. 401 (2011) 2351.

[87] F.R. Gonzalez, A.M. Nardillo. *J. Chromatogr. A* 842 (1999) 29.

[88] Y. Thewalim, F. Aldaeus, A. Colmsjo, *Anal. Bioanal. Chem.* 393 (2009) 327.

[89] F. Aldaeus, Y. Thewalim, , A. Colmsjo, *Anal. Bioanal. Chem.* 389 (2007) 941.

[90] K. Herberger, T. Kowalska, *Chromatographia* 48 (1998) 89.

[91] R.C. Castells, E.I. Arancibia, A.M. Nardillo, *J. Chromatogr.* 504 (1990) 45.

[92] T.M. McGinitie, J.J. Harynuk, *J. Chromatogr. A* 1255 (2012) 184.

[93] B. Karolat, J.J. Harynuk, *J. Chromatogr. A* 1217 (2010) 4862.

[94] H. Snijders, H.G. Janssen, Cramers, *J. Chromatogr. A* 718 (1995) 339.

[95] K.D. Nizio, J.J. Harynuk, *J. Chromatogr. A* 1252(2012) 171.

[96] G.P. Funkhouser, Gelled liquid hydrocarbon treatment fluids having reduced phosphorus volatility and their associated method of use and preparation, US Patent 7066262 B2 (2006).

[97] B. Lukocs, S. Mesher, T.P. Wilson Jr., T. Garza, W. Mueller, F. Zamora, L.W. Gatlin, Non-volatile phosphorus hydrocarbon gelling agent, US Patent 2007/0173413 A1 (2007).

[98] J.J. Harynuk, A.D. Rossé, G.B. McGarvery, *Anal. Bioanal. Chem.* 401 (2011) 2415.

[99] F.R. Gonzalez, A.M. Nardillo, *J. Chromatogr. A* 842 (1999) 29.

[100] K. Huang, X. Han, X. Zhang, D.W. Armstrong, *Anal. Bioanal. Chem.* 389 (2007) 2265.

[101] V.R. Ried, J.A. Crank, D.W. Armstrong, R.E. Synovec, *J. Sep. Sci.* 31 (2008) 3429.

[102] L.J. Maberry, S.B. McConnell, K.V. Tanner, J.J. Hinkel, *SPE Production and Facilities,* vol. 13, 1998, p. 236.

[103] M. Mehran, W.J. Cooper, N. Golkar, M.G. Nickelsen, *J. High Resol. Chromatogr.* 14 (1991) 745.

[104] P. Delmonte, A.R. Fardin-Kia, J.K.G. Kramer, M.M. Mossoba, L. Sidiisky, C. Tyburczy, J.I. Rader, *J. Chromatogr. A* 133 (2012) 137.

[105] P. Delmonte, A.R. Fardin-Kia, J.K.G. Kramer, M.M. Mossoba, L. Sidiisky, J.I. Rader, *J. Chromatogr. A* 1218 (2011) 545.

[106] Sigma-Aldrich specification sheet for product 29486-U, http://www.sigmaaldrich.com/catalog/product/supelco/29486U accessed September 21, 2012.

[107] B.M. Weber, J.J. Harynuk, *J. Chromatogr. A* 1271 (2013) 170.

[108] F.R. Gonzalez, A.M. Nardillo, *J. Chromatogr. A* 842 (1999) 29.

[109] Y. Thewalim, F. Aldaeus, A. Colmsjo, *Anal. Bioanal. Chem.* 393 (2009) 327.

[110] F. Aldaeus, Y. Thewalim, A. Colmsjo, *Anal. Bioanal. Chem.* 389 (2007) 941.

[111] R.C. Castells, E.L. Arancibia, A.M. Nardillo, *J. Chromatogr.* 504 (1990) 45.

[112] N.J. Micyus, S.K. Seeley, J.V. Seeley, *J. Chromatogr. A* 1086 (2005) 171.

[113] T.M. McGinitie H. Ebrahimi-Najafabadi, J.J. Harynuk, *J. Chromatogr. A* 1325 (2014) 204.

[114] S.M.I. Al-Rafia, A.C. Malcolm, S.K. Liew, M.J. Ferguson, R. McDonald, E. Rivard, *Chem. Commun.* 47 (2011) 6987.

[115] S.M.I. Al-Rafia, M.J. Ferguson, E. Rivard, *Inorg. Chem*. 50 (2011) 10543.

[116] S.M.I. Al-Rafia, M.R. Momeni, R. McDonald, M.J. Ferguson, A. Brown, E. Rivard, *Angew. Chem. Int. Ed.* 52 (2013) 6390.

[117] C.J. Berger, G. He, C. Merten, R. McDonald, M.J. Ferguson, E. Rivard, *Inorg. Chem*. 53 (2014) 1475.

[118] *Method D 5186-03, Annual Book of ASTM Standards,* American Society for Testing and Materials, West Conshocken, PA, USA, 2009.

[119] F. Adam, F. Bertoncini, V. Coupard, N. Charon, D. Thiébaut, D. Espinat, M.C. Hennion, *J. Chromatogr. A* 1186 (2008) 236.

[120] B.N. Barman, *Anal. Chem.* 73 (2001) 2791.

[121] F.C.Y. Want, K. Qian, L.A. Green, *Anal. Chem.* 77 (2005) 2777.

[122] Y. Briker, Z. Ring, A. Iacchelli, N. McLean, P.M. Rahimi, C. Fairbridge, R. Malhotra, M.A. Coggiola, S.E. Young, *Energy & Fuels* 15 (2001) 23.

[123] R.E. Paproski, J. Cooley, C.A. Lucy, *J. Chromatogr. A* 1095 (2005) 156.

[124] D.M. Qiang, W.Z. Lu, *J. Petroleum Sci. and Eng.* 22 (1999) 31.

[125] N. Šegudovic, T. Tomic, L. Škrobonja, L. Kontic, *J. Sep. Sci.* 27 (2004) 65.

[126] C.W. Sink, D.R. Hardy, *Anal. Chem.* 66 (1994) 1334.

[127] E.H. McKerrell, *Fuel 7*2 (1993) 1403.

[128] A. Trisciani, F. Munari, *J. High Resol. Chromatogr.* 17 (1994) 452.

[129] I.L. Davies, K.D. Bartle, G.E. Andrews, P.T. Williams, *J. Chromatogr. Sci.* 26 (1988) 125.

[130] R. Pál, M. Juhász, Á. Stumpf, *J. Chromatogr. A* 819 (1998) 249.

[131] K. Qian, J.W. Diehl, J.G. Decher, F.P. DiSanzo, *Eur. J. Mass Spectrom.* 10 (2004) 187.

[132] D. Thiebaut, *J. Chromatogr. A* 1252 (2012) 177.

[133] H. Potgieter, R. van der Westhuizen, E. Rohwer, D. Malan, *J. Chromatogr. A* 1294 (2013) 137.

[134] K.D. Nizio, T.M. McGinitie, J.J. Harynuk, *J. Chromatogr. A* 1255 (2012) 12.

[135] D.R.P. Thiébaut, E.C. Robert, *Analusis* 27 (1999) 681.

[136] F.P. DiSanzo, R.E. Yoder, *J. Chromatogr. Sci.* 29 (1991) 4.

[137] R. M'Hamdi, D. Thiébaut, M. Caude, *J. High Resol. Chromatogr.* 20 (1997) 545.

[138] http://www.sigmaalrdrich.com/analytical-chromatography/gas-chromatography/columns/ionic-liquid-literature.html (accessed Feb. 11/13)

[139] P. Delmonte, A-R.F. Kia, J.K.G. Kramer, M.M. Mossoba, L. Sidisky, J.I. Rader, *J. Chromatogr. A* 1218 (2011) 545.

[140] L. Mahe, T. Dutriez, M. Courtiade, D. Thiebaut, H. Dulot, F. Bertoncini, *J. Chromatogr. A* 1218 (2011) 534.

[141] S.L.C. Ferreria, R.E. Bruns, H.S. Ferreira, G.D. Matos, J.M. David, G.C. Brandão, E.G.P. da Silva, L.A. Portugal, P.S. dos Reis, A.S. Souza, W.N.L. dos Santos, *Anal. Chim. Acta,* 597 (2007) 179.

[142] G.E.P. Box and D.W. Behnken, *Technometrics*, 2 (1960) 455.

[143] J. Krupcik, R. Gorovenko, I. Spanik, I. Bockova, P. Sandra, D.W. Armstong. *J. Chromatogr. A* 1301 (2013) 225-236.

[144] D.A.. Skoog, F.J. Holler, S.R. Crouch, Principles of Instrumental Analysis (2007) Australia: Brooks/Cole.

[145] K.A. Schug, I. Sawicki, D.D. Carlton, Jr., H. Fan, H.M. McNair, J.P. Nimmo, P. Kroll, J. Smuts, P. Walsh, D. Harrison. *Anal. Chem.* 86 (2014) 8329-8335

[146] M. Wilkonson, *American Laboratory*, 47 (2015) 28.

[147] H. Fan, J. Smuts, P. Walsh, D. Harrison, K.A. Schug, *J. Chromatogr. A* 1389 (2015) 120.

[148] L. Bai, J. Smuts, P. Walsh, H. Fan, Z. Hildenbrand, D. Wong, D. Wetz, K.A. Schug, *J. Chromatogr. A* 1388 (2015) 244.

[149] K.A. Schug, H.M. McNair, J.V. Hinshaw, *LC GC Europe* 28 (2015) 45.

[150] R. Sitko, B. Zawisza, Z. Kowalewska, K. Kocot, M. Polowniak, *Talanta* 85 (2011) 2000.

[151] J.V. Seeley, C.T.Bates, J.D. McCurry, S.K. Seely, *J. Chromatogr. A* 1226 (2012) 103.

[152] K.M. Pierce, S.P. Schale, *Talanta* 83 (2011) 1254.

[153] P. Delmonte, A.R.Fardin-Kia, J.K.G. Kramer, M.M. Mossoba, L. Sidisky, C. Tyburczy, J.I. Rader, *J. Chromatogr. A* 1233 (2012) 137.

[154] A.X. Zeng, S.T. Chin, P.J. Marriott, *J. Sep. Sci.* 00 (2013) 1.

[155] B.N. Barman, V.L. Cebolla, L. Membrado., *Crit. Rev. Anal. Chem.* 30 (2000) 75.

[156] K. Thurbide, Z. Xia, *Anal. Chem.* 74 (2002) 5459.

[157] M. Kaminiski, R. Kartanowicz, E. Gilgenast, J. Namiesnik, *J. Crit. Rev. Anal. Chem.* 35 (2005) 193.

[158] J.H. Lee, Y.Z. Lee, Journal of Automotive Technology, 16 (2015) 807.